

**FINITE ELEMENT MODELING OF SUCTION CAISSON AND  
LARGE DIAMETER MONOPILE IN DENSE SAND UNDER  
OBLIQUE AND LATERAL LOAD**

by

© **SHEIKH SHARIF AHMED**

A thesis submitted to the

School of Graduate Studies

in partial fulfillment of the requirements for the degree of

**Master of Engineering (Civil Engineering)**

**Faculty of Engineering and Applied Sciences**

Memorial University of Newfoundland

**August, 2015**

St. John's

Newfoundland and Labrador

# ABSTRACT

Pile foundations have various kinds of applications in both onshore and offshore environments. The use of large-diameter piles with smaller length-to-diameter ratio installed in both sand and clay in offshore environments has increased significantly in last few decades. This thesis concentrates on the numerical modeling of large diameter suction caisson and monopile foundation systems installed in dense sand subjected to oblique pullout and eccentric lateral loading, respectively.

In the first part of this thesis, three-dimensional finite element (FE) analyses have been performed to evaluate the inclined loading pullout capacity of suction caisson in dense sand. The numerical issues due to mesh distortion at large displacement have been reduced by the use of Arbitrary Lagrangian Eulerian (ALE) method offered by the commercially available Abaqus/Explicit FE software. The first set of the analyses has been conducted using the built-in Mohr-Coulomb (MC) soil model in Abaqus; however, it is unable to address the post-peak softening behavior of dense sand. In the next set, a modified form of Mohr-Coulomb (MMC) model has been employed by the aid of user-subroutine to capture the pre-peak hardening and post-peak softening behavior of dense sand. FE analyses results are compared with the centrifuge test results available in literature. The MMC model has been found to simulate better the soil behavior around the caisson.

In the second part of the thesis, FE analyses have been performed to estimate the

lateral load-carrying capacity of large diameter monopile in dense sand for different load eccentricities. The above mentioned MMC model has been employed in the simulations. The simulation results are compared with available centrifuge test results and a good match has been found. A parametric study has also been performed and a simplified method to estimate the capacity of monopile has been proposed. Analyses have also been conducted with the MC model. The comparison between the results obtained with the MMC and the MC models have been presented. The response of soil surrounding the monopile during loading is also examined.

## **ACKNOWLEDGEMENT**

I would like to thank Dr. Bipul Hawlader for his constant guidance and support during this research work. It has been a great pleasure working with him. A great deal of inspiration was provided by my friends and colleagues in Memorial University during my stay at St. John's. I am especially grateful to Md. Iftekharuzzaman for his help associated with the development of the initial finite element models. Also, the support associated with the implementation of the modified Mohr-Coulomb model in Abaqus from Kshama Roy is greatly appreciated.

My parents and family members inspired me a lot to carry out this research work. They were always beside me while conducting the research works and advised me throughout.

I would like to thank the School of Graduate Studies (SGS) of Memorial University, MITACS and NSERC for providing financial support for this research work.

# Table of Contents

<b>ABSTRACT</b>	<b>i</b>
<b>ACKNOWLEDGEMENT</b>	<b>iii</b>
<b>Table of Contents</b>	<b>iv</b>
<b>List of Tables</b>	<b>ix</b>
<b>List of Figures</b>	<b>x</b>
<b>List of Symbols</b>	<b>xiii</b>
<b>1 Introduction</b>	<b>1</b>
1.1 General . . . . .	1
1.2 Scope of the Work . . . . .	3
1.3 Objectives . . . . .	3
1.4 Organization of Thesis . . . . .	4
1.5 Contributions . . . . .	5
<b>2 Literature Review</b>	<b>7</b>
2.1 Introduction . . . . .	7
2.2 Suction Caisson: An Overview . . . . .	8

2.2.1	Research on Suction Caisson . . . . .	11
2.2.1.1	Field Trials . . . . .	11
2.2.1.2	Laboratory Model Tests . . . . .	14
2.2.1.3	Centrifuge Tests . . . . .	18
2.2.1.4	Finite Element (FE) Analysis . . . . .	21
2.3	Large Diameter Monopiles as Offshore Wind Turbine Foundation System: An Overview . . . . .	25
2.3.1	Capacity of Laterally Loaded Rigid Piles . . . . .	26
2.3.1.1	$p$ - $y$ Curve Method for Sand . . . . .	26
2.3.1.2	Limitations of $p - y$ Curve Method for Large-Diameter Pile . . . . .	29
2.3.2	Research on Large Diameter Monopiles . . . . .	30
2.3.2.1	Field Trials on Laterally Loaded Rigid Piles . . . . .	31
2.3.2.2	Laboratory Model Tests . . . . .	32
2.3.2.3	Centrifuge Tests . . . . .	34
2.3.2.4	Finite Element (FE) Analyses . . . . .	36
2.4	Summary . . . . .	39
	<b>Bibliography</b>	<b>41</b>
<b>3</b>	<b>Numerical Analysis of Inclined Uplift Capacity of Suction Caisson in Sand</b>	<b>59</b>
3.1	Abstract . . . . .	60

3.2	Introduction . . . . .	61
3.3	Problem Definition . . . . .	63
3.4	Finite Element Model . . . . .	64
3.4.1	Modeling of Suction Caisson . . . . .	66
3.4.2	Modeling of Mooring Line . . . . .	67
3.4.3	Modeling of Sand . . . . .	67
3.4.4	Interface Behavior . . . . .	67
3.4.5	Modulus of Elasticity of Sand . . . . .	68
3.4.6	Mooring Positions and Load Inclination Angles . . . . .	69
3.5	Results . . . . .	69
3.5.1	Mesh Sensitivity Analysis . . . . .	69
3.5.2	Force-displacement Curves . . . . .	70
3.5.3	Pullout Capacity . . . . .	73
3.5.4	Rotation . . . . .	75
3.5.5	Lateral Displacement . . . . .	79
3.5.6	Shape of Soil Failure Wedge . . . . .	82
3.6	Effect of Aspect Ratio ( $L/D$ ) . . . . .	85
3.7	Analyses Using Modified Mohr-Coulomb Model . . . . .	88
3.8	Conclusions . . . . .	93
3.9	Acknowledgements . . . . .	94
	<b>Bibliography</b>	<b>95</b>

<b>4</b>	<b>Numerical Analysis of Large-Diameter Monopiles in Dense Sand Supporting Offshore Wind Turbines</b>	<b>100</b>
4.1	Abstract . . . . .	101
4.2	Introduction . . . . .	101
4.3	Finite Element Model . . . . .	105
4.3.1	Modeling of the Monopile . . . . .	107
4.3.2	Modeling of Sand . . . . .	108
4.3.3	Model Parameters . . . . .	110
4.4	Model Test Simulation Results . . . . .	112
4.4.1	Simulation of Klinkvort and Hededal (2014) Centrifuge Test Results	112
4.4.2	Effects of Vertical Load . . . . .	115
4.4.3	FE Simulation with Mohr-Coulomb Model . . . . .	117
4.4.4	Soil Failure Mechanism . . . . .	118
4.5	FE Simulations for Different Aspect Ratios . . . . .	121
4.5.1	Force–displacement and Moment–rotation Curves . . . . .	122
4.5.2	Point of Rotation . . . . .	124
4.5.3	Force–moment Interaction Diagram . . . . .	126
4.5.4	Horizontal Stress Around The Pile . . . . .	126
4.5.5	Effects of $\eta$ and $e$ on initial stiffness . . . . .	128
4.6	Proposed Equation for Lateral Load-carrying Capacity and Moment . . . .	129
4.7	Lateral Force-Moment Interaction . . . . .	132

4.8	Conclusions . . . . .	134
4.9	Acknowledgements . . . . .	135
	<b>Bibliography</b>	<b>136</b>
<b>5</b>	<b>Conclusions and Future Recommendations</b>	<b>145</b>
5.1	Conclusions . . . . .	145
5.2	Future Recommendations . . . . .	148
	<b>Appendix A</b>	<b>149</b>
	<b>Appendix B</b>	<b>157</b>

## List of Tables

2.1	Major field applications of suction caissons (modified from Tran, 2005) . . .	10
2.2	Large scale field tests on suction caissons installed in clay . . . . .	13
2.3	Centrifuge tests on suction caissons installed in clay . . . . .	21
2.4	Summary of finite element analyses of suction caissons in clay . . . . .	24
3.1	Geometry and mechanical properties in FE modeling . . . . .	68
3.2	Geometric parameters for different aspect ratios . . . . .	86
3.3	Equations for Modified Mohr-Coulomb Model (MMC) (after Roy et al., 2014a) . . . . .	89
4.1	Equations for Modified Mohr-Coulomb model (MMC) (summarized from Roy et al., 2014a,b) . . . . .	110
4.2	Soil parameters used in FE analyses . . . . .	113
4.3	Dimensions used for varying aspect ratio . . . . .	122

## List of Figures

2.1	Schematic of a typical suction caisson . . . . .	9
2.2	Use of suction caisson (redrawn after Maniar, 2004) . . . . .	9
2.3	Schematic of a monopile supporting offshore wind turbine (redrawn after Malhotra, 2011) . . . . .	25
2.4	$p - y$ curves generated by the Reese et al. (1974) approach . . . . .	28
3.1	Problem definition . . . . .	64
3.2	FE mesh used in the analysis . . . . .	65
3.3	Mesh sensitivity analysis . . . . .	70
3.4	Force-displacement curve for 5% mooring position . . . . .	71
3.5	Force-displacement curve for 25% mooring position . . . . .	71
3.6	Force-displacement curve for 50% mooring position . . . . .	72
3.7	Force-displacement curve for 75% mooring position . . . . .	73
3.8	Force-displacement curve for 95% mooring position . . . . .	73
3.9	Comparison of pullout capacity between FE and centrifuge tests . . . . .	74
3.10	Rotation-displacement curve for 5% mooring position . . . . .	75
3.11	Rotation-displacement curve for 25% mooring position . . . . .	76
3.12	Rotation-displacement curve for 50% mooring position . . . . .	76
3.13	Rotation-displacement curve for 75% mooring position . . . . .	77

3.14	Rotation-displacement curve for 95% mooring position . . . . .	78
3.15	Force-rotation curve for 5% mooring position . . . . .	78
3.16	Force-rotation curve for 25% mooring position . . . . .	79
3.17	Force-rotation curve for 50% mooring position . . . . .	79
3.18	Force-rotation curve for 75% mooring position . . . . .	80
3.19	Force-rotation curve for 95% mooring position . . . . .	80
3.20	Rotation of caisson at pullout capacity . . . . .	81
3.21	Lateral displacement of caisson for $\theta = 0^\circ$ . . . . .	81
3.22	Maximum principal plastic strain and total displacement profile for 75% mooring position and 1.5 m displacement at $\theta = 0^\circ$ . . . . .	83
3.23	Maximum principal plastic strain and total displacement profile for 25% mooring position and 1.5 m displacement at $\theta = 0^\circ$ . . . . .	84
3.24	Failure wedge for $\theta = 67.5^\circ$ and $90^\circ$ and all mooring positions . . . . .	84
3.25	Failure wedge for $\theta = 0^\circ, 22.5^\circ$ and $45^\circ$ : (a) mooring positions 5%, 25% and 50%, (b) mooring positions 75% and 95% . . . . .	85
3.26	Normalized Force-displacement curves for 50% mooring position . . . . .	87
3.27	Normalized pullout capacity for $\theta = 0^\circ$ for different mooring positions . . . .	87
3.28	Force-displacement curve for 75% mooring position with MC and MMC model . . . . .	90
3.29	Development of plastic shear strain at $0.1D$ and $0.3D$ pad eye displacement	91
3.30	Mobilized $\phi'$ and $\psi$ using MMC for $0.1D$ and $0.3D$ pad eye displacement .	92

4.1	Problem statement: (a) loading and sign convention, (b) assumed pressure distribution, (c) mode of shearing of soil elements . . . . .	105
4.2	FE mesh used in this study . . . . .	107
4.3	Comparison between FE simulation and centrifuge test results by Klinkvort and Hededal (2014) . . . . .	114
4.4	Effects of vertical load and eccentricity on: (a) ultimate capacity and (b) initial stiffness . . . . .	116
4.5	Development of plastic shear zone around the monopile . . . . .	119
4.6	Mobilized $\phi'$ and $\psi$ around the monopile . . . . .	120
4.7	Analysis for $L = 12$ m and $D = 3$ m: (a) lateral force–displacement, (b) moment–rotation . . . . .	124
4.8	Lateral displacement for different length-to diameter ratios and eccentricities	125
4.9	Lateral load–moment interaction diagrams: (a) for $\theta = 0.5^\circ$ , (b) for $\theta = 1^\circ$ , (c) for $\theta = 5^\circ$ . . . . .	127
4.10	Development of soil horizontal stress at ultimate state ( $\theta = 5^\circ$ ) in the plane of symmetry . . . . .	128
4.11	Effects of length-to-diameter ratio and eccentricity on initial stiffness . . . . .	129
4.12	Comparison between lateral loads calculated from proposed simplified equation and FE analyses . . . . .	131
4.13	Normalized force–moment interaction diagram for $\theta = 0.5^\circ$ , $1^\circ$ and $5^\circ$ . . . . .	133

## List of Symbols

$L$	length of pile
$D$	diameter of pile
$t$	thickness of pile
$I_p$	moment of inertia of the pile section
$\mu$	pile/soil interaction properties
$\phi_\mu$	pile/soil interface friction angle
$H$	lateral load capacity
$M$	moment capacity
$K_0$	lateral earth pressure coefficient at rest
$k$	coefficient of initial modulus of horizontal subgrade reaction
$p$	soil reaction per unit length of pile
$p_u$	ultimate soil reaction per unit length of pile
$y$	lateral deflection of pile
$E_0$	initial stiffness
$\phi'$	effective internal friction angle of soil
$\phi'_p$	peak friction angle of soil
$\phi'_c$	critical state friction angle of soil
$\phi'_{in}$	$\phi'$ at the start of plastic deformation

$\psi$	dilation angle of soil
$\psi_p$	peak dilation angle of soil
$D_r$	relative density of soil
$I_D$	relative density index of soil
$\gamma^p$	engineering plastic shear strain
$E_s$	Young's modulus of soil
$E_p$	Young's modulus of pile
$\nu_s$	Poisson's ratio of soil
$\nu_p$	Poisson's ratio of pile
$\gamma'$	submerged unit weight of soil
$p_{atm}$	atmospheric pressure
$\theta$	load inclination angle
$\sigma'_v$	initial vertical effective stress
$g$	gravitational acceleration
$R$	rigidity parameter of pile
$e$	load eccentricity
$p'$	mean stress
$\sigma'_c$	confining pressure
$\dot{\gamma}^p$	plastic shear strain increment
$\dot{\epsilon}_{ij}^p$	plastic strain increment tensor

# Chapter 1

## Introduction

### 1.1 General

Various are the applications of pile foundations in both onshore and offshore environments. In last few decades, the use of large-diameter piles installed in both sand and clay has been expanded significantly for diverse applications under different loading conditions. The increased use of large-diameter piles in different forms such as suction caisson and monopile foundation systems under oblique and lateral loading, respectively, has earned great attention of the researchers around the world. The behavior of suction caissons and monopiles in sand under such loading conditions is not well understood.

An innovative foundation system widely used in the offshore to resist both axial and lateral loading as well as oblique loading is the suction caisson (also known as suction anchors, suction piles or suction buckets). A suction caisson is a large-diameter hollow cylinder, usually made of steel having top end closed and bottom end opened that is installed in soil by applying suction with pumping water out of caisson interior. The advantages of suction caissons over traditional pile foundations and anchors include fast installation, elimination of the pile driving process, reduction in material costs and reusability. Suction caissons are now widely being used in offshore industries for anchoring large offshore floating facilities

to the seafloor. The use of suction caisson as a foundation system to support offshore wind turbines is also gaining popularity.

Although suction caisson is now a widespread anchorage option for offshore floating facilities, the behavior of caisson under oblique pullout loading is yet to be investigated further. The pullout capacity of suction caisson under inclined load is one of the main design concerns. Suction caisson is now being preferred to other conventional foundation systems such as long pile and embedded anchors in deep water oil and gas development projects because of its inherent advantages as stated earlier. The necessity of better understanding of the behavior of suction caisson has, therefore, increased significantly.

Another foundation system which is being extensively used to support offshore wind turbine is the large-diameter monopile. The current design practice of monopile is based on the  $p-y$  curve method, which has originally been developed from the field test data on long and flexible piles with small load eccentricity and having relatively small diameters compared to monopiles. Since large moment and lateral load are anticipated on offshore wind turbine supporting monopiles, the design of these monopiles based on so called  $p-y$  curve method requires significant extrapolation. Thus, the need of an appropriate design approach for large-diameter monopiles is essential.

## **1.2 Scope of the Work**

The advancement of computing power in last few decades has expedited the significant improvement of finite element (FE) modeling techniques. With today's computing facilities, FE simulation can be performed with greater accuracy and reliability. In this study, three-dimensional FE analyses have been performed to simulate the behavior of suction caisson as mooring system for offshore floating facilities as well as the behavior of monopile foundation for supporting offshore wind turbines in dense sand. The FE analyses have been conducted using FE software package Abaqus 6.13-1. Very limited studies of FE modeling of large-diameter pile foundations are available in the literature. Most of the available FE analyses were conducted using the built-in elastic-perfectly plastic Mohr-Coulomb model available in commercial software packages. However, post-peak softening of stress–strain behavior of dense sand is a well-known phenomenon. These characteristics, including other features of stress–strain behavior, need to be incorporated in the soil model for successful simulation of response of suction caisson and monopiles.

## **1.3 Objectives**

The main objectives of this study are:

- i) evaluation of the pullout capacity of suction caisson anchors in dense sand for offshore floating facilities under oblique loading; and
- ii) estimation of the load-carrying capacity of large-diameter monopile foundations

installed in dense sand for offshore wind turbines subjected to lateral loading at different load eccentricities.

In order to achieve the above mentioned objectives, FE analyses have been performed using the built-in Mohr-Coulomb model and also by implementing a better soil model that can capture many features of dense sand behavior. In addition, simplified methods are proposed for preliminary estimation of the pullout capacity of suction caissons and the lateral load-carrying capacity of monopiles.

## **1.4 Organization of Thesis**

This thesis consists of five chapters and is written in “manuscript” format.

- Chapter 1 is the starting chapter presenting the objectives and backgrounds of this study.
- Chapter 2 presents a comprehensive literature review related to suction caisson and large-diameter monopile foundations in sand.
- Chapter 3 is on the pullout capacity of suction caissons under inclined loading in dense sand. This chapter has been published as a technical paper in the “International Journal of Offshore and Polar Engineering.” A part of this work has been also published in the “Proceedings of 24<sup>th</sup> International Ocean and Polar Engineering Conference,” Busan, Korea, 2014 (Appendix A).

- Chapter 4 presents the work on laterally loaded large-diameter monopiles for different load eccentricities in dense sand. This chapter has been submitted for publication in an international journal. Also, a part of this work has been published in the “Proceedings of the 34<sup>th</sup> International Conference on Ocean, Offshore and Arctic Engineering”-OMAE2015 (Appendix B).
- Chapter 5 summarizes the outcomes of the present study and presents some recommendations for future studies.

## 1.5 Contributions

The following technical publications are the outcome of this research work:

- (i) Ahmed, SS, and Hawlader, BC (2015). Numerical Analysis of Inclined Uplift Capacity of Suction Caisson in Sand. *International Journal of Offshore and Polar Engineering*, Vol. 25, no. 2, pp. 145–155.
- (ii) Ahmed, SS, and Hawlader, BC (2015). Numerical Analysis of Large Diameter Monopiles in Dense Sand Supporting Offshore Wind Turbines. *Submitted for publication in an international journal*, Under review.
- (iii) Ahmed, SS, and Hawlader, BC (2014). Finite Element Modeling of Inclined Load Capacity of Suction Caisson in Sand with Abaqus/Explicit. *Proc. of the 24<sup>th</sup> International Ocean and Polar Engineering Conference*, Busan, Korea, June 15–20, pp. 463–469.

- (iv) Ahmed, SS, Hawlader, BC, and Roy, KS (2014). Finite Element Modeling of Large Diameter Monopiles in Dense Sand for Offshore Wind Turbine Foundations. *Proc. of the ASME 34<sup>th</sup> International Conference on Ocean, Offshore and Arctic Engineering*, St. John's, Newfoundland, Canada, May 31–June 5, OMAE2015–42218.

## **Chapter 2**

### **Literature Review**

#### **2.1 Introduction**

The use of pile foundations has been in practice for many years where shallow foundations are impractical. Pile foundations have been in use under various loading conditions in both onshore and offshore structures. In recent years, the world has seen significant expansion of using large-diameter piles in offshore. Large-diameter piles can be used in different forms such as suction caisson and monopile and can be installed in both sand and clay. The length-to-diameter ratio of such piles are generally small compared to other conventional pile foundations. The general shape of large-diameter offshore piles is circular and they are usually open-ended. These piles are typically made of steel and behave as rigid body. The capacity of a large-diameter pile depends on several factors such as loading conditions, type of soil it is installed and the rigidity of the pile. The soil–pile interaction behavior of large-diameter pile has attained great attention in the last few decades.

Limited number of research works have been devoted to understand the behavior of large-diameter piles under different loading conditions in both sand and clay. The current research work emphasizes on the behavior of suction caissons and large-diameter monopiles in dense sand under oblique pullout loading and lateral loading, respectively. In this chapter,

the research works available on suction caissons and large-diameter monopiles in sand are presented.

## **2.2 Suction Caisson: An Overview**

A suction caisson is a large-diameter hollow cylinder, usually made of steel having top end closed and bottom end open. Suction caissons are also known as suction pile, suction bucket, suction anchor, suction can etc. The length-to-diameter ratio of a suction caisson is much smaller than that of a conventional pile foundation, typically less than 10. Wall thickness-to-diameter ratio is also smaller, generally in the range of 0.3% – 0.6%. In long caissons, stiffeners are often added along the internal perimeter (ring stiffeners) or longitudinally to prevent them from buckling during installation. A schematic of typical suction caissons is shown in Fig. 2.1.

The use of suction caisson is gaining popularity over traditional offshore foundation systems because of its inherent advantages such as: fast installation, elimination of pile driving process, reduction in material costs and reusability. Suction caissons are now widely being used for mooring offshore structures such as Tension Leg Platform (TLP) and Floating Production, Storage and Offloading (FPSO) vessels (Fig. 2.2). According to Sparrevik (2002), there are as many as 300 suction caissons in operation around the world. Later, Andersen et al. (2005) reported that, there have been nearly 500 suction caissons installed in more than 50 locations around the world. Major projects using suction caissons around the world are listed in Table 2.1.

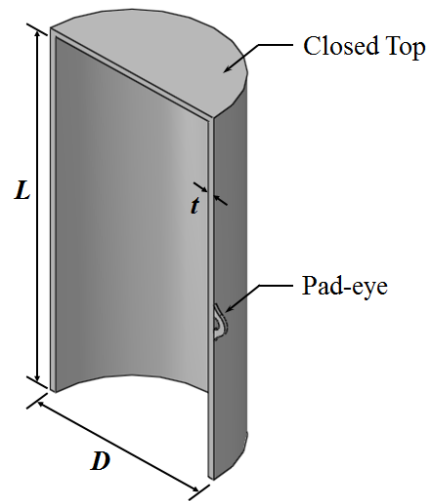


**Figure 2.1:** Schematic of a typical suction caisson

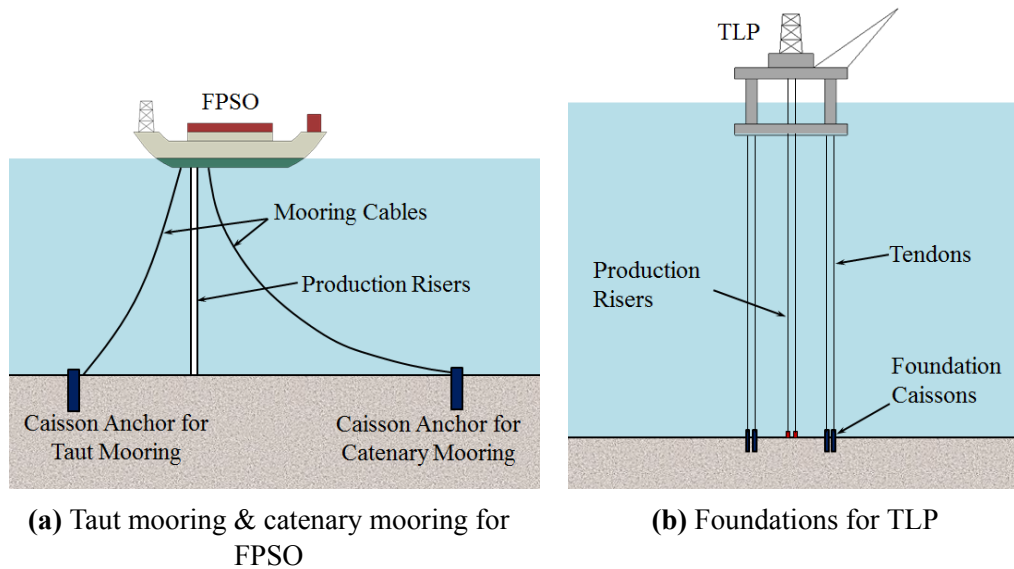


**Figure 2.2:** Use of suction caisson (redrawn after Maniar, 2004)

The pullout capacity is one of the main requirements when a suction caisson is used in mooring systems for deep water oil and gas development projects. The caisson is normally pulled by a chain connected to the pad eye on the side of the pile (Fig. 2.1). The inclined pullout capacity of a suction caisson depends on both horizontal and vertical load capacity.

**Table 2.1:** Major field applications of suction caissons (modified from Tran, 2005)

Year	Name	Size, $D \times L$ (m $\times$ m)	Purpose	Water depth, (m)	Soil type	References
1958	Sampler <sup>1</sup>	0.45 $\times$ 1.2	Anchoring	20 – 80	C	Mackereth (1958)
1972	Sounding tool <sup>2</sup>	3	Anchoring	> 20	S	North Sea Report (1972)
1980	Gorm <sup>2</sup>	3.5 $\times$ 8.5 – 9	Anchoring	40	L	Senpere and Auvergne (1982)
1989	Gullfaks C <sup>2</sup>	28 $\times$ 22	Foundation	218	L	Tjelta et al. (1990)
1991	Snorre	17 $\times$ 12	Anchoring	330	C	Fines et al. (1991); Stove et al. (1992)
1994	Draupner E <sup>2</sup>	12 $\times$ 6	Foundation	70	S	Tjelta (1995)
1995	Nkossa <sup>3</sup>	4.5 – 5 $\times$ 12	Mooring	200	C	Colliat et al. (1995); Colliat et al. (1996)
1995	Harding <sup>2</sup>	5 $\times$ 8 – 10	Mooring	110	L	Sparrevik (1998)
1995	YME <sup>2</sup>	5 $\times$ 7	Mooring	100	S	Sparrevik (1998)
1996	Norne <sup>2</sup>	5 $\times$ 10	Mooring	350	C	Sparrevik (1998)
1996	Sleipner T <sup>2</sup>	14 $\times$ 5	Foundation	–	S	Lacasse (1999)
1997	Njord <sup>2</sup>	5 $\times$ 9 – 10	Mooring	330	C	Solhjell et al. (1998)
1997	Curlew <sup>2</sup>	5 – 7 $\times$ 10 – 13	Mooring	90	L	Alhayari (1998)
1997	Aquila <sup>4</sup>	4.5 – 5 $\times$ 16	Mooring	850	C	Alhayari (1998)
1997	Visund <sup>2</sup>	5 $\times$ 11	Mooring	335	C	Solhjell et al. (1998)
1997	Lufeng <sup>5</sup>	5 $\times$ 10	Mooring	30	C	Sparrevik (1998); Andersen et al. (2005)
1997	Marlim P19-P26 <sup>6</sup>	4.8 $\times$ 13.5	Mooring	720 – 1050	C	Mello et al. (1998)
1998	Laminaria <sup>7</sup>	5.5 $\times$ 13	Mooring	400	C	Erbrich and Hefer (2002)
1998	Marlim P33-P35 <sup>6</sup>	4.7 $\times$ 17	Mooring	780 – 850	C	Barusco (1999)
1998	Aasgard A <sup>2</sup>	5 $\times$ 11	Mooring	350	C	Haland (2002)
1999	Kuito <sup>3</sup>	3.5 $\times$ 11 – 14	Mooring	400	C	Tjelta (2001); Andersen et al. (2005)
1999	Aasgard B & C <sup>2</sup>	5 $\times$ 10 – 12	Mooring	350	C	Haland (2002); Andersen et al. (2005)
1999	North Nemba Flare <sup>3</sup>	5 $\times$ 5.5	Foundation	115	C	Kolk et al. (2001)
2000	Misaki <sup>8</sup>	18 $\times$ 5	Foundation	25	L	Masui et al. (2001)
2001	Hanze <sup>2</sup>	6.5 $\times$ 6.2	Mooring	42	L	Sparrevik (2002)
2001	Girassol <sup>3</sup>	4.5 – 8 $\times$ 10 – 20	Mooring	1400	C	Colliat and Dendani (2002)
2002	Horn Mountain <sup>10</sup>	6 $\times$ 30 – 32	Anchoring	1800	C	Audibert et al. (2003)
2002	Na Kita <sup>10</sup>	4.3 $\times$ 24	Mooring	1920	C	Newlin (2003)
2003	Barracuda & Caratinga <sup>6</sup>	5 $\times$ 16.5	Mooring	825 – 1030	C	Hesar (2003); Andersen et al. (2005)
2003	Bonga <sup>3</sup>	5 $\times$ 16 – 17.5	Mooring	980	C	Andersen et al. (2005)
2004	Thunder Horse <sup>10</sup>	5.5 $\times$ 27.5	Mooring	1830	C	Andersen et al. (2005)
<sup>1</sup> UK lakes		<sup>2</sup> North Sea	<sup>3</sup> West Africa	<sup>4</sup> Adriatic Sea	<sup>5</sup> South China Sea	
<sup>6</sup> Brazil		<sup>7</sup> Timor Sea	<sup>8</sup> Japan	<sup>9</sup> Irish Sea	<sup>10</sup> Gulf of Mexico	
<sup>C</sup> Clay		<sup>S</sup> Sand	<sup>L</sup> Layered			

## **2.2.1 Research on Suction Caisson**

Efficient and economic design of suction caisson for offshore application requires good understanding of various aspects related to installation issues and holding capacity of caisson. Many researchers devoted themselves in acquiring the essential knowledge for the better design of suction caisson in both sand and clay. The following sections will go through the notable research works associated with the development and design of suction caisson.

### **2.2.1.1 Field Trials**

Although, conducting full-scale field tests is expensive and time consuming, extensive field tests have been carried out by several researchers to evaluate the installation characteristics and holding capacity of suction caissons in both sand and clay, as useful geotechnical information relevant to the more efficient design of future caissons can be obtained. During the tests, a number of information related to suction caisson installation and performance under various loading conditions has been documented. Some of the notable field tests are discussed in the following parts of this section.

The first full-scale field test on suction caisson has been reported by Hogervorst (1980), who performed full-scale suction caisson trials after obtaining promising results from initial field trials on smaller suction piles. The suction caissons used in the field trials were 3.8 m in diameter having length ranging from 5 to 10 m. The field tests were conducted

at a number of inshore locations in the Netherlands with sandy soils, with layered soils and with overconsolidated clay. The purposes of the tests were to study the installation characteristics of the caissons and evaluate the holding capacity under axial and lateral loading. The successful completion of the field trials proved the potential applicability of the suction caissons to be used as mooring system for floating production facilities and also demonstrated the viability of installing the caissons by the application of suction.

A series of field trial program was carried out by the joint venture of NGI/Fugro McClelland for the determination of design parameters related to Draupner E (previously Europipe 16/11E) riser platform in North Sea (Tjelta, 1994). The caisson used in the test program had a diameter of 1.5 m and length of 1.7 m. The test program consisted of penetration by weight and suction, rapid loading tests, long-term loading tests, cyclic loading tests and permeability tests. The effective completion of the test program had led to the successful installation of Draupner E (previously Europipe 16/11E) platform (Tjelta, 1995) and later Sleipner T platform (Lacasse, 1999) in dense sand using suction caisson foundation.

Cho et al. (2002) described a number of field tests on steel suction caissons having inside diameters ranging from 0.5 to 2.5 m and length of 5 m, conducted by the Daewoo Engineering & Construction Co. Ltd. The test site soil condition was predominantly silty sand and the tests were performed at water depth of about 10 m. The objectives of the field tests were to provide data for further validation of the mobilized friction angle concept (Bang et al., 2000) and to develop a suitable suction caisson installation technology in field.

**Table 2.2:** Large scale field tests on suction caissons installed in clay

<b>Year</b>	<b>Location</b>	<b>Size, <math>D \times L</math> (m <math>\times</math> m)</b>	<b>Tests undertaken</b>	<b>References</b>
1990	Lysaker, Oslo	$0.7 \times 1.5$ (2 cells)	Effects of attachment of anchor on pullout resistance and mechanism; Impact of load cycling	Keaveny et al. (1994)
1999	Tokyo Bay	$0.8 \times 1$	Effects of loading angle and loading rate on pullout capacities	Maeno et al. (2002)
2003	China	$0.5 \times 0.5$	Horizontal ultimate bearing capacity	Liu et al. (2004)

Bang and Karnoski (2007) described the installation and retrieval of three steel suction caissons in sand having diameter of 1.5 m and length of 2.3 m. All the caissons were installed off the coast of Port Heuneme, California at water depth of 12.5 m as part of the cable burial study program of US Navy, where the caissons were used as cable anchoring devices. The caissons, as well as the cable, were removed after three years of field trials on the cable. The feasibility and cost-effectiveness of successful retrieval of suction caisson by using the same equipment for installation was established. Also, the effect of soil cementation and probable caisson material corrosion by aging on the caisson–soil interface friction behavior was recognized.

Field tests on suction caisson are also available in clay, which are not discussed in detail and are summarized in Table 2.2, as this study focuses on simulating the suction caisson behavior in sand.

### **2.2.1.2 Laboratory Model Tests**

A large number of small-scale laboratory tests on model suction caissons were performed by several researchers to investigate various aspects of suction caisson performance under different loading conditions in both sand and clay. The laboratory tests performed by the researchers can be split into two categories: tests on vacuum anchors, and tests on suction anchors.

#### **Tests on Vacuum Anchors**

The vacuum anchors are shallow surface foundations generally used for providing temporary anchorage and require pumping the water out during their application to generate required capacity (Wang et al., 1975). Some significant tests on vacuum anchors in sand are presented in the following paragraphs.

Goodman et al. (1961) conducted laboratory model tests on vacuum anchors to determine the feasibility of anchoring mobile military field equipment. Different types of soils ranging from sand of medium fineness to highly plastic clay were used for the testing. The dimensions ( $D \times L$ ) of the used anchors in the tests were  $79 \times 99$  mm and  $89 \times 188$  mm. They demonstrated that the use of vacuum anchors in different soils is feasible for anchoring floating equipment; however, their response in clay is better than that in sand.

A series of laboratory tests on vacuum anchors were performed by Brown and Nacci (1971) in both loose sand and dense sand to study their behavior and water flow characteristics.

The test anchor was 254 mm in diameter and 44 mm in embedded length. A total of 29 tests were conducted of which 14 tests were carried out in loose sand and other 15 were done in dense sand. The test results illustrated the effectiveness of vacuum anchors for providing short-term anchorage in sand and revealed their high holding capacity to anchor weight ratio along with reusability and reversibility. A linear relationship between pullout capacity and applied suction was also noted. Based on the test results, in conjunction with observed behavior and failure mechanisms, a theory was proposed to predict the pullout capacity of such anchors.

Wang et al. (1975) conducted laboratory tests on eight model anchors installed in medium fine sand, silt and clay to investigate the feasibility and efficiency of the vacuum anchors. The anchors used in the test program had inside diameters of 114 mm, 140 mm, 200 mm and 337 mm with length to diameter ratios ( $L/D$ ) of 0.1 and 0.5. The performance of anchors were found to be dependent on anchor geometry (skirt length and diameter), soil properties (internal friction angle and cohesion), and suction. Also, a linear increase in pullout capacity with increasing suction was observed for a given dimension, corroborating the earlier findings by Brown and Nacci (1971). Subsequently, Wang et al. (1977) developed equations to estimate the pullout capacity of vacuum anchors based on observed failure mechanisms and adopting the Mohr-Coulomb failure criteria. Also, sample design examples were presented by Wang et al. (1978) to demonstrate the practical applications of the anchors.

A series of 12 laboratory tests on vacuum anchors installed in sand having diameter of 400

mm and length of 250 mm were conducted by Helfrich et al. (1976). The purpose of the test program was to study the laboratory pullout characteristics and the failure mode of the test anchor in sand and the dependence of anchor performance on the flow rate of water through the anchor chamber. As before, a linear relationship between pullout capacity and applied suction was observed and predictions based on the Mohr-Coulomb failure criteria matched well (within 13%) with measured pullout capacities.

### **Tests on Suction Anchors**

Larsen (1989) performed 15 laboratory tests on model suction caissons having diameters of 100, 200 and 300 mm and a length of 450 mm installed in both sand and clay. The purpose of the test program was to study the mechanical behavior of soil and caisson during installation and to evaluate the horizontal pullout capacity under static and cyclic loads. From the test results, it was found that, the penetration resistance primarily depends on the friction outside the caisson during down-suction. Also, the ultimate pullout capacities were identical under static and cyclic loads for the caissons installed in sand. However, for the caissons installed in clay, ultimate pullout capacity under cyclic load was found to be reduced to 1/2 to 2/3 of the measured capacity under static load.

Steensen-Bach (1992) conducted a total of 77 tests on suction caissons with embedment/diameter ratios of 1.67, 2.0 and 3.33 having diameters of 48, 65 and 80 mm installed in both sand and clay. The objective of the tests was to investigate the contribution of suction generated during pullout to the capacity and to attain additional test data to

improve design procedures.

Villalobos et al. (2009) performed a number of laboratory tests on model suction caissons in loose sand having the dimensions ( $D \times L$ ) of  $293 \times 146.5$  mm and  $203.5 \times 203.5$  mm to evaluate the drained capacity under monotonic loading. The test results were successfully interpreted within the framework of work hardening plasticity, and expressions for yield surface and post-yield behavior of caisson were deduced. One of the key observations of the test results was the capability of suction caisson to sustain moments and horizontal loads even under tensile loads.

A series of laboratory tests were performed by Gao et al. (2013) to investigate the effects of aspect ratio, load inclination angle and loading position on inclined loading pullout behavior of model suction caissons in sand. The model caissons used in the study were 101 mm in diameter with lengths of 202, 404 and 606 mm. With smaller load inclination angle, the maximum pullout capacity was located for the loading position between  $2/3$  and  $3/4$  of caisson length from top. However, at large load inclination angle, the effects of loading position on pullout capacity was found insignificant. Also, pullout capacity of caisson for higher aspect ratios was found greater, although, deformation characteristics were observed to be independent of aspect ratio.

A number of Laboratory tests on model suction caissons in clay are also available in literature. Cauble (1996) reported 14 laboratory tests on a model suction caisson installed in  $K_0$ -normally consolidated clay samples to simulate installation of caisson by suction

and pushing, and to investigate the caisson behavior under sustained tensile pullout. Datta and Kumar (1996) carried out 18 laboratory tests on suction caissons installed in soft clayey soils to evaluate suction force generated under the caisson during pullout. El-Gharbawy and Olson (1998) conducted a series of static as well as cyclic loading tests on suction caisson models to study their behavior and pullout capacity in clay. Li and Wang (2013) performed laboratory model tests on suction caissons in soft clay to investigate the effects of frictional factor, aspect ratio and loading directions on the failure mode and ultimate bearing capacity.

### **2.2.1.3 Centrifuge Tests**

Geotechnical centrifuge tests on model suction caissons at different acceleration levels were conducted by a number of researchers to simulate the behavior of suction caisson at field scale. Although, higher cost than small-scale model tests and several limitations are involved in performing centrifuge tests, a lot of valuable information related to the design of suction caisson can be obtained from these tests. A review of selected centrifuge tests on suction caissons in sand are discussed in the following paragraphs.

Allersma et al. (2000) performed a series of centrifuge tests to investigate the effects of aspect ratio ( $L/D$ ), loading position and load inclination angle on the static horizontal bearing capacity of suction caissons installed in sand and clay. All the tests were performed at 150g acceleration. The test results were compared with the API recommendations and 3D finite element (FE) calculations conducted by Plaxis. The bearing capacities calculated by API method were found to be somewhat conservative compared to the test results, whereas,

FE calculations were in good agreement with the test results. The optimum bearing capacity was obtained at loading position of  $2/5$  of the caisson height from bottom and bearing capacity was observed to increase with decreasing load inclination angle. However, a larger resistance during installation for lower loading positions was noted. The bearing capacity was also seen to increase with increasing soil density. Furthermore, a linear relationship between pile length and bearing capacity was noticed. Based on the study, the authors suggested the use of both centrifuge tests and FE analysis as a good basis for the design of suction caissons.

Tran and Randolph (2008) performed a series of centrifuge tests at  $100g$  acceleration to investigate the variation of suction pressure during the installation of suction caisson in dense sand. The tests were conducted for caissons of different size and surcharge. The suction pressure was observed to increase linearly with embedment depth following a distinct pressure slope (critical hydraulic gradient). The total driving force required to install the caisson by suction pressure was found significantly less than the force required during installation by jacking. The use of a larger surcharge during installation decreased the required suction pressure for a given penetration depth. The overall behavior and pressure variation with depth were similar for caissons of different sizes.

A total of 80 centrifuge tests were conducted by Kim et al. (2009) on suction caissons in sand to evaluate the horizontal, vertical and inclined loading capacities and the effects of load inclination angle and loading point on them. The pullout capacity was found to increase

with the loading point moving downward and reached the maximum at loading point between 70 – 75% of height from top with small inclination angle. Also, the maximum and minimum loading capacities were obtained when the applied loading was purely horizontal and vertical, respectively for a given loading point.

Bang et al. (2011) reported a series of centrifuge tests on model suction caissons embedded in sand to evaluate the inclined pullout capacity. An analytical solution method was also proposed. The key variables of the study were load inclination angle and mooring position. For relatively small load inclination angles ( $0^\circ$  and  $22.5^\circ$ ) the pullout capacity was found to increase with the mooring position shifting toward the caisson bottom and the maximum pullout capacity was located at approximately 70 – 75% of the caisson length from the top. On the other hand, for higher load inclination angle ( $45^\circ$  and higher) the pullout capacity was observed to increase with the mooring position moving downward the caisson bottom and the maximum was reached when the mooring position was near the tip of the caisson. Comparisons between the test results and proposed analytical solution proved the competence of the analytical solution method.

Jang and Kim (2013) performed a series of centrifugal tests to estimate the maximum horizontal pullout capacity of suction caisson installed in sand for mooring position located at 75% of caisson depth from top by varying the aspect ratio ( $L/D$ ). The horizontal pullout capacity of suction caisson was found to be directly proportional to the aspect ratio of the caisson for the range between 1 and 3.

**Table 2.3:** Centrifuge tests on suction caissons installed in clay

References	Remarks
Randolph et al. (1998)	Investigation on rapid reduction of capacity for any loss of suction and the extent of loss of suction; The response under monotonic and cyclic loading
Watson et al. (2000)	Installation resistance; Behavior of caisson under combined vertical, horizontal and moment loading
Cao et al. (2001), Cao et al. (2002a)	Investigation on self-weight and suction induced penetration
Lee et al. (2003)	Evaluation of horizontal and inclined loading capacities and the effects of loading point along with loading direction on them

Centrifuge tests have also been carried out by some researchers on anchor piles (having larger  $L/D$  ratio) in sand. For instance, Ramadan et al. (2013a) performed a series of centrifuge tests to study the behavior of offshore anchor piles under mooring forces in saturated dense sand and proposed modified equations to plot  $p - y$  curves.

A large number of centrifuge tests were also performed for the suction caissons installed in clay which are summarized in Table 2.3.

#### **2.2.1.4 Finite Element (FE) Analysis**

With the rapid improvement of computing power in last few decades, the finite element (FE) techniques have enjoyed significant improvement. A large number of FE software has been developed with which numerical simulations can be performed with greater accuracy and reliability. The easiness along with low cost of FE simulations compared to large scale field tests and centrifuge tests have attracted several researchers to perform FE analyses of suction caissons installed in both sand and clay. Different plasticity models have been adopted to simulate the nonlinear stress–strain behavior of soil. A review of numerical

analyses conducted in sand are presented here.

Erbrich (1994) conducted a series of finite element analysis using the Abaqus FE software to estimate the capacity of suction caisson foundations of fixed offshore platforms. The simulation of nonlinear behavior of dense sand was attained by implementing the Drucker-Prager and the Drucker-Prager with cap plasticity models. A good agreement between the FE predictions and the results of model tests performed by Wang et al. (1978) proved the applicability of FE analysis to estimate the capacity of suction caisson foundations.

Bang and Cho (1999) carried out an analytical feasibility study using three-dimensional FE analyses to evaluate the effects of various cross section shapes on the overall performance of suction caissons to be used for providing required mooring capacities for very large Mobile Offshore (military) bases. The 3D analyses were performed by Abaqus FE software to evaluate the vertical, horizontal and inclined load capacities of suction caissons having circular, Y-shaped and triangular cross-sections installed in sand. The Drucker-Prager plasticity model was adopted to model the nonlinear behavior of sand.

Deng and Carter (2000) performed 3D finite element analyses of suction caissons in sand to investigate the effects of aspect ratio, mooring position, load inclination angle, and friction angle, dilatancy and initial stress state of soil. The finite element software package AFENA in conjunction with the Mohr-Coulomb model was used in the analyses. On the basis of the analyses, simplified expressions were developed to estimate the pullout capacity of suction

caisson taking into account the influence of aspect ratio, mooring position, loading angle, and shear strength parameters and dilatancy of soil.

Iftekhharuzzaman and Hawlader (2012) conducted 3D finite element analyses using Abaqus FE software to evaluate the inclined loading pullout capacity of suction caissons in sand. The Mohr-Coulomb model was adopted to simulate the soil behavior. The key variables investigated were mooring position and load inclination angle. The analyses results were found in good agreement with the centrifuge test results reported by Bang et al. (2011).

Ramadan et al. (2013b) performed 3D finite element analyses to study the soil–pile interaction behavior under mooring forces using Abaqus FE software. The Mohr-Coulomb model was used to model the soil, and was calibrated based on the centrifuge tests of Ramadan (2011). Some equations were proposed to estimate the ultimate capacity of pile for different loading angles.

Achmus et al. (2013) carried out 3D numerical analyses to evaluate the loading capacity of suction caisson in sand using Abaqus FE software. The Mohr-Coulomb failure criteria in conjunction with stress dependent modulus of elasticity were used to simulate the nonlinear response of soil accurately. The effects of caisson size and load eccentricity on bearing capacity and initial stiffness were investigated. Normalized equations to calculate the ultimate capacity and initial stiffness were derived from numerical analyses results.

A number of FE analyses on suction caissons installed in clay also have been conducted to investigate the effects of various aspects on the load bearing capacity and deformation

characteristics of soil around the caisson. A summary of selected numerical analyses performed in clay are presented in Table 2.4.

**Table 2.4:** Summary of finite element analyses of suction caissons in clay

References	FE software	Soil constitutive model	Type of model	Remarks
Zdravkovic et al. (1998)	FSAFEM, ICFEP	Modified Cam Clay	3D	The effects of aspect ratio ( $L/D$ ), load inclination angle and soil-structure adhesion on pullout capacity were investigated
Sukumaran and McCarron (1999); Sukumaran et al. (1999)	ABAQUS	Von Mises Yield Criterion	2D; 3D	The effects of load inclination angle, loading point, and aspect ratio on caisson response were investigated
Handayanu et al. (1999); Handayanu et al. (2000)	ABAQUS	Cam Clay	3D	The response of suction caissons subjected to vertical uplift and inclined loads were studied and compared with model test results
Cao et al. (2002b); Cao et al. (2003)	ABAQUS	Modified Cam Clay	2D	Simulation of passive suction and evaluation of axial pullout capacity were performed; Test results were compared with centrifuge test results (Cao et al., 2001); (Cao et al., 2002a)
Supachawarote et al. (2004)	ABAQUS	Von Mises Yield Criterion	3D	The effects of load inclination angle, loading point, aspect ratio, and shaft friction on inclined loading capacity of suction caisson were examined

## 2.3 Large Diameter Monopiles as Offshore Wind Turbine Foundation

### System: An Overview

A monopile is a large diameter hollow steel pile driven in soil having an aspect ratio or slenderness ratio ( $L/D$ ) of less than 8 and diameters ranging between 3 to 6 m and are considered to behave as rigid. Monopiles are generally installed at shallow water depths not exceeding 35 m. These piles are the most popular foundation option for offshore wind turbines. The schematic of a typical monopile foundation supporting offshore wind turbine is shown in Fig. 2.3. According to European Offshore Statistics 2013 (EWEA, 2014), monopiles were most common (75%) along with other substructures.

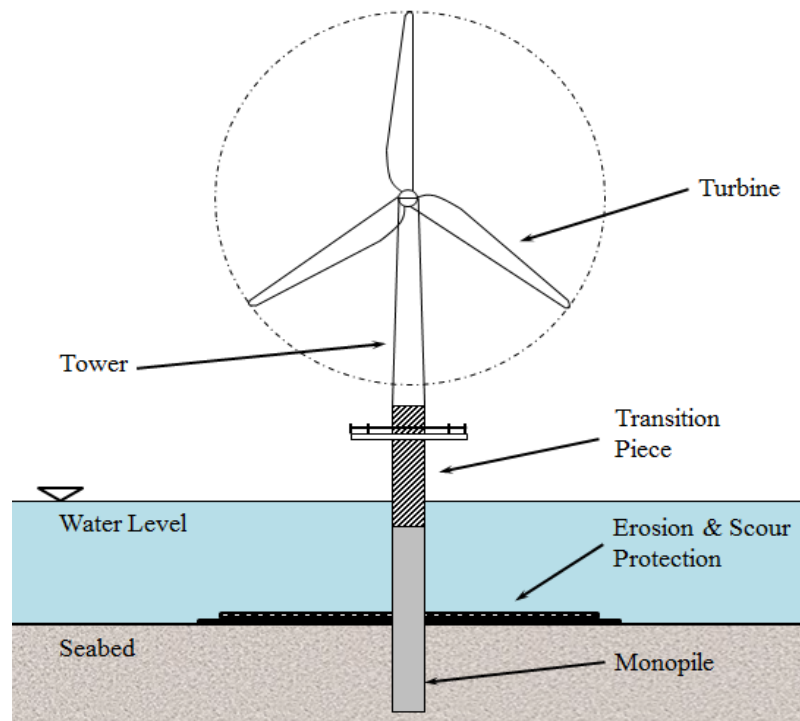


**Figure 2.3:** Schematic of a monopile supporting offshore wind turbine (redrawn after Malhotra, 2011)

### 2.3.1 Capacity of Laterally Loaded Rigid Piles

According to Fan and Long (2005), analysis methods for laterally loaded single piles can be subdivided into four categories:

- Limit State Method and Elasticity Method;
- Finite Element (FE) Method;
- Subgrade Reaction Method; and
- $p - y$  Curve Method.

In the current design practice of monopiles for supporting offshore wind turbines, the API and DNV method are used. These design standards are based on  $p - y$  curve method.

#### 2.3.1.1 $p-y$ Curve Method for Sand

The  $p - y$  curve method is a special subgrade reaction method in which a nonlinear relation is established between lateral resistance of soil ( $p$ ) and the lateral displacement ( $y$ ) of pile. The soil resistance is modelled using nonlinear springs. The applied lateral force ( $F$ ) is related to the lateral displacement of pile ( $y$ ) by  $p - y$  curves. These curves depend on soil type, depth and loading type. At greater depth soil reacts stiffer, and a stiffer soil response leads to a steeper curve. The lateral load ( $F$ ) is based on the spring stiffness of the soil ( $k$ ) at the corresponding depth and the deflection ( $y$ ):

$$F(z) = k(z)y(z) \tag{2.1}$$

The original  $p-y$  curve method for piles in cohesionless soil was derived from field tests on Mustang Island (USA) (Cox et al., 1974; Reese et al., 1974). These field tests consisted of 2 static and 5 cyclic load tests applied to two 0.61 m diameter ( $D$ ) piles with wall thickness ( $t$ ) of 95 mm, length ( $L$ ) of 21 m and an  $L/D$  ratio of 34.4. The wall thickness over diameter  $t/D$  ratio equated to about 64.

The  $p-y$  curves by Reese et al. (1974) are semi-empirical and consist of four segments (Fig. 2.4):

- (i) The initial linear portion of the curve, which is dependent on the initial stiffness ( $E_0$ ) and  $E_0$  increases linearly with depth ( $z$ ) as  $E_0 = kz$ ;
- (ii) Parabolic segment between the initial linear portion and lateral displacement ( $y$ ) of  $D/60$ ;
- (iii) Linear segment between lateral displacements of  $D/60$  and  $3D/80$ ; and
- (iv) Constant soil resistance segment after lateral displacement of  $3D/80$ .

Here,  $D$  is the diameter of the pile.

The original  $p-y$  curves for sand consisting of four sections were replaced with a constant hyperbolic function formulated by Murchison and O'Neill (1984). The following hyperbolic function is accepted and recommended by several design standards (e.g., API, 2007; DNV, 2011):

$$p = Ap_u \tanh \left( \frac{kz}{Ap_u} y \right) \quad (2.2)$$

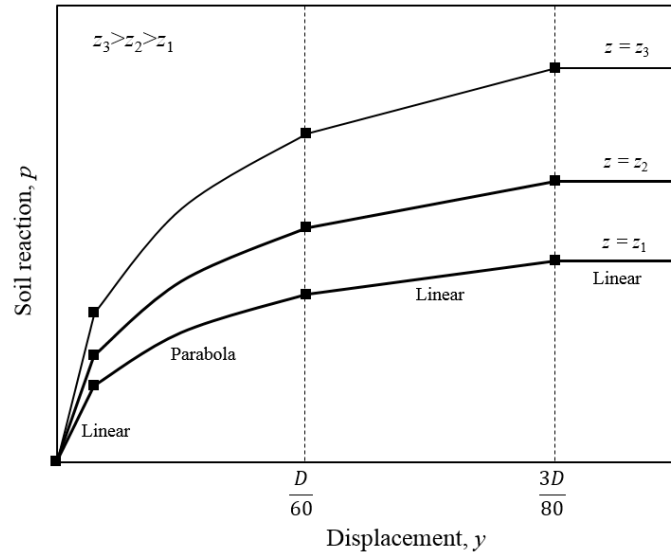


**Figure 2.4:**  $p - y$  curves generated by the Reese et al. (1974) approach

Where,  $A$  is a factor to account for cyclic or static condition. For static loading, the value of  $A$  depends upon depth and diameter of the pile as in Eq. 2.3, while for cyclic loading,  $A = 0.9$  is recommended (API, 2000).

$$A = \left( 3 - 0.8 \frac{z}{D} \right) \leq 0.9 \quad (2.3)$$

The ultimate soil resistance ( $p_u$ ) can be obtained by Eq. 2.4

$$p_u = \min (p_{us}, p_{ud}) \quad (2.4)$$

$$p_{us} = (C_1 z + C_2 D) \gamma' z \quad (2.5)$$

$$p_{ud} = C_3 D \gamma' z \quad (2.6)$$

Where,  $C_1$ ,  $C_2$  and  $C_3$  are empirical coefficients based on internal friction angle ( $\phi'$ ) of soil.

### 2.3.1.2 Limitations of $p - y$ Curve Method for Large-Diameter Pile

The current design standards for large diameter offshore piles (e.g., API, 2007; DNV, 2011) are based on  $p-y$  curve method. The  $p-y$  curve method is known to have several limitations while designing large diameter piles. Doherty and Gavin (2012) highlighted the following points while discussing the limitations of  $p - y$  curve method:

- Mode of failure;
- Effect of diameter;
- Horizontal earth pressure coefficient;
- Impact of pile properties; and
- Cyclic loading considerations

The  $p - y$  curves were developed based on field tests on slender, flexible piles; whereas, the monopile foundation for offshore wind turbines behaves in rigid manner (LeBlanc et al., 2010). In addition to the formation of a soil passive wedge in front of the pile above the point of rotation, the soil will also mobilize a passive wedge below the point of rotation, which is not considered in the current methodology.

The effect of diameter on initial stiffness was investigated by Ashford and Juirnarongrit (2003) and Juirnarongrit and Ashford (2005) by FE analysis, who concluded that, there is no effect from the diameter on the initial stiffness of the pile–soil interaction curves. Fan and Long (2005) also performed FE analysis and confirmed the same observation. However, numerical modeling by Lesny and Wiemann (2006) and Sørensen et al. (2009) suggests an

effect of changing the diameter on the initial stiffness of the pile–soil interaction curves.

The horizontal earth pressure coefficient at rest ( $K_0$ ) is considered to be independent of the soil state. The impact of varying  $K_0$  value was investigated by Fan and Long (2005), who conducted FE analysis on laterally loaded monopile and concluded that, an increase in ( $K_0$ ) resulted in a significant increase in the ultimate soil resistance.

The effects of variations of bending stiffness ( $EI$ ) of the pile was investigated by Ashour and Norris (2000) and Fan and Long (2005). Ashour and Norris (2000) used the strain wedge method and found the stiffness and ultimate resistance increased dramatically as the  $EI$  of the pile increased. In contrast, Fan and Long (2005) reported no significant influence of  $EI$  of the pile on the  $p - y$  curve.

LeBlanc et al. (2010) examined the effects of cyclic loading on  $p - y$  curves by laboratory model tests. The pile stiffness was always found to increase with cyclic loading and the increase was independent of relative density. The finding of LeBlanc et al. (2010) is contradictory with the current methodology of degrading static  $p - y$  curves to account for cyclic loading.

### **2.3.2 Research on Large Diameter Monopiles**

A brief summary of the notable research works on laterally loaded large diameter monopiles installed in sand are presented in the following sections.

### 2.3.2.1 Field Trials on Laterally Loaded Rigid Piles

A large number of field trials were carried out by several researchers to assess various information related to the design of laterally loaded piles in both sand and clay. Most of the available field tests were conducted on long, flexible piles. Only a few number of large-scale field trials on laterally loaded rigid piles are available in literature.

Hald et al. (2009) presented the results of full-scale load measurement of a monopile installed in sand in the Horns Rev Offshore Wind Farm. The instrumented monopile had an outside diameter of 4 m with embedment length of 21.9 m and the water depth was 9.9 m relative to mean sea level. The purpose of the field measurement was to collect and process load response and timely concurring environmental (wind, wave and current) data and to apply those data for verifying and developing design methodologies for offshore wind farms. The load response below the mudline had been evaluated and the measured pile response was found different from the predicted response according to traditional  $p - y$  curves, particularly in the top of the pile. Stiffer soil response from the field test than that predicted by the  $p - y$  curves was observed from the measured moment distribution along the pile. The measured response was reported to be 30 – 50% smaller than the response predicted by the  $p - y$  curves developed from the soil data.

Doherty et al. (2012) reported the results of a field test performed on an instrumented monopile installed at a dense sand research site in Blessington, Ireland. The test monopile was 0.34 m in outer diameter with an embedment length of 2.2 m resulting in an aspect

ratio ( $L/D$ ) of 6.5. The test pile was instrumented with 11 levels of strain gauges to capture the load transfer and bending moments along the shaft. The lateral capacity of the monopile observed from the field test was compared to that obtained by conventional design procedures (e.g., DNV, 2007; API, 2010). The authors concluded that, conventional design procedures grossly underestimate the lateral capacity of the monopile.

Full-scale field trials of laterally loaded rigid piles installed in clay are also available in literature. For example, Baguelin et al. (1972) conducted field tests on a steel pile 950 mm×950 mm and 4.4 m deep, jacked into saturated clay and load was applied at 2 m above ground level. Briaud et al. (1983) performed field tests on a reinforced concrete bored pile in clay having diameter of 920 mm and length of 6 m which was subjected to a lateral load applied at 740 mm above ground level.

### **2.3.2.2 Laboratory Model Tests**

LeBlanc et al. (2010) performed a series of laboratory tests on a laterally loaded model monopile installed in sand having 80 mm diameter and 360 mm penetration depth with a load eccentricity of 430 mm. Both static and cyclic loading tests were performed. The test results showed the increase in pile stiffness with the increase in number of cycles and was found to be independent of relative density. The observation contrasts with the current methodology of degrading static  $p - y$  curves to account for cyclic loading.

Uncuoğlu and Laman (2011) conducted a series of model tests on a laterally loaded short rigid pile in a two-layer sand soil profile. The model pile was 50 mm in diameter and

200 mm in length and the load was applied at a height of 300 mm. Also, the effects of the elasticity modulus, dilatancy and interface behavior of the sand was investigated numerically by performing a series of three-dimensional non-linear finite element analyses. The lateral load capacities in the layered sand conditions was calculated using the methods proposed by Brinch Hansen (1961) and Meyerhof et al. (1981). The results obtained from experimental studies, numerical analyses and a conventional method were compared with each other. The results proved that the parameters investigated had a considerable effect on the behavior of short rigid piles subjected to lateral loads. It was also shown that the value of the ultimate lateral load capacity could vary significantly depending on the methods used.

Roesen et al. (2012) carried out lateral cyclic loading test on an open-ended aluminum pile with a diameter of 100 mm and a length of 600 mm embedded in saturated dense sand. The influence of the number of load cycles on the accumulated rotation, under cyclic loading with constant frequency, load amplitude and mean load level was investigated. One-third of the total accumulated rotation was observed to be obtained within the first ten cycles. Also, after a certain number of load cycles, further accumulation of rotation was not observed.

Nicolai and Ibsen (2014) performed two series of tests on a stiff open-ended aluminum pile in sand with a diameter of 100 mm, an embedded length of 500 mm and a thickness of 5 mm. The first series of tests was carried out to test the validity and applicability of the approach presented by LeBlanc et al. (2010) with sands of different relative densities. The cyclic loading effects on the resistance of the pile was investigated in the second series of tests.

Both the resistance and the stiffness of the pile were found to increase after cyclic loading, in contrast with the current design codes that suggest a degradation of the pile resistance due to cyclic loading.

A number of laboratory model tests on laterally loaded rigid piles in clay are also reported in literature. For example, Meyerhof and Sastry (1985) carried out model tests on a fully instrumented rigid model pile jacked into homogeneous sand and clay, where the pile was subjected to vertical eccentric loads and to central inclined loads. Lombardi et al. (2013) conducted a series of laboratory tests to study the long term behavior a monopile in kaolin clay which was subjected to between 32,000 and 172,000 cycles of horizontal loading.

### **2.3.2.3 Centrifuge Tests**

Klinkvort and Hededal (2011) performed a total number of six static and five cyclic centrifuge tests on a laterally loaded monopile in dry sand. The prototype dimension of the piles was modelled to a diameter of 1 m and penetration depth on 6 m with acceleration levels ranging between  $25g$  and  $62.5g$ . The purpose of the test series was to investigate the scaling laws in the centrifuge both for monotonic and cyclic loading. Higher capacity for the small piles tested at high  $g$  levels was observed; a similar findings by Nunez et al. (1988).

Kirkwood and Haigh (2013) conducted a series of centrifuge tests on a monopile installed in sand to investigate the effects of cyclic lateral loading. The prototype monopile was 4.5 m in diameter and the embedment length was 20 m. The acceleration level used was

100g. The prototype load eccentricity used in the tests was 30 m. The greatest pile head displacements were observed for a cyclic loading ratio of  $-0.37$ .

Klinkvort et al. (2013) performed a series of centrifuge model tests on cylindrical stiff model monopiles that were installed at  $1g$  and in-flight before being loaded laterally in normally consolidated dense dry sand, simulating drained conditions. The tests were carried out on solid steel piles at a stress distribution identical to a prototype diameter ( $D$ ) of 1 m in dry sand. The penetration depth  $L$  and load eccentricity ( $e$ ) were kept constant at  $6D$  and  $15D$ , respectively for all the tests. The test series showed that the ratio of pile diameter to average grain size for centrifuge modeling of monopiles, the non-linear stress distribution and the installation process are key modeling parameters. It is possible to scale centrifuge results of rigid monopiles to prototype scale with due consideration of these effects.

Klinkvort and Hededal (2013) carried out five monotonic and twelve cyclic centrifuge tests on a laterally loaded monopile in dense sand. The prototype diameter ( $D$ ) of the pile was between 1 m and 3 m with acceleration level ranging between  $15.5g$  and  $75g$ . The penetration depth ( $L$ ) and load eccentricity ( $e$ ) were kept constant at  $6D$  and  $15D$ , respectively, for all the tests. The tests were designed so that the cyclic loading of the pile was performed with a magnitude of a maximum of 36% of the ultimate static lateral capacity. The accumulation of displacement was found to increase with increasing magnitude of cyclic loading. Also, higher initial stiffness due to cyclic loading was observed than the monotonic stiffness.

Klinkvort and Hededal (2014) conducted a series of monotonic centrifuge tests on model monopiles subjected to stress distributions equal to prototype monopiles with pile diameters ( $D$ ) ranging from 1 m to 5 m and load eccentricities ranging from  $8.25D$  to  $17.75D$ . The aspect ratio ( $L/D$ ) was kept constant as 6 and the acceleration level ranged between  $15.5g$  and  $75g$ . The normalized ultimate soil resistance was unaffected by acceleration level and load eccentricity, indicating that the failure mechanism was the same for all tests. Based on the centrifuge tests, a reformulation of soil–pile interaction curves was also proposed.

Centrifuge tests in clay were also conducted by a number of researchers. Doyle et al. (2004) conducted four centrifuge model tests to study the lateral response of large diameter piles in clay subjected to large lateral displacements. Zhang et al. (2011) performed centrifuge tests to investigate the behavior of a short fixed-head pile subjected to lateral cyclic load in overconsolidated soft clay.

#### **2.3.2.4 Finite Element (FE) Analyses**

Abdel-Rahman and Achmus (2005) carried out three-dimensional finite element analyses on large diameter laterally loaded monopiles in sand. An elasto-plastic material law with Mohr-Coulomb failure criterion was used where the stress dependency of the elastic modulus was incorporated parabolically. The finite element analyses were performed by Abaqus. The monopiles used in the FE analyses were 7.5 m in diameter and lengths were 20 m and 30 m with a wall thickness of 90 mm. The results of the FE analyses were compared to the results of the  $p - y$  method (API, 2000). The  $p - y$  curve method was found to

underestimate the pile deformations compared to FE results. The authors pointed out to the overestimation of the initial stiffness of soil in large depths by the  $p - y$  method to be the probable cause.

Lesny and Wiemann (2006) conducted finite element analyses on large diameter monopiles in dense sand and compared the monopile behavior to the standard design method, namely  $p - y$  method (API, 2000). The considered monopiles had diameters ranging between 1 m and 6 m. Commercial finite element software Abaqus was used where the elastic-plastic soil behavior was modeled by incorporating the Mohr-Coulomb failure criterion. The elastic modulus of soil was assumed to increase parabolically with depth. The influence of the pile diameter on the pile-soil stiffness was investigated. The authors concluded that, the standard  $p - y$  method overestimates the pile-soil stiffness of large diameter monopiles at great depths which may result in an insufficient pile length. A simple modification on the initial stiffness of the  $p - y$  curve was also suggested.

Achmus et al. (2009) performed finite element analyses on laterally loaded monopiles in medium dense and dense sand. The diameter of the pile was 7.5 m with lengths ranging between 20 m and 40 m and wall thickness of 90 mm. Finite element software Abaqus was used. The purpose of the analyses was to estimate the progressive deformation of a monopile under monotonic and long-term lateral cyclic load with load eccentricities ranging between 0 m and 40 m. A special numerical concept “degradation stiffness model” was introduced and incorporated in the FE analyses. Based on the analyses results, preliminary

design charts were presented.

Hearn and Edgers (2010) conducted finite element analyses on laterally loaded monopiles in dense sand incorporating linearly increasing modulus of elasticity of sand with depth at a rate corresponding to the API (2000) recommended  $k$  value. Plaxis 3D was used in the FE modeling. The monopile had a diameter of 5 m with embedment length of 26 m and wall thickness of 55 mm. A method for back-calculating  $p-y$  curves from FE analyses was suggested. The authors back-calculated the  $p-y$  curves from the FE analyses and observed that the  $p-y$  curves by the API method were found steeper than those from FE analyses.

Wolf et al. (2013) performed finite element analyses as a case study of a monopile foundation for a wind turbine located at Barrow Offshore Wind Farm. The pile properties were estimated according to the foundation design report for the chosen wind turbine. The pile was a hollow steel cylinder with an embedded length of 29.4 m and an outer diameter of 4.75 m with a wall thickness of 0.1 m. The analyses were conducted by means of the finite element program PLAXIS 3D. Two material models were used in the numerical analysis: the Mohr-Coulomb model and the hardening soil model. The conventional  $p-y$  curves formulated in the API (2010) showed a much stiffer response at depth than either of the applied material models.

Although, the major focus of this thesis is concerned with the behavior of laterally loaded monopiles in sand, some recent FE analyses on laterally loaded monopiles in clay are briefly summarized.

Pradhan (2012) performed three-dimensional finite element analyses to develop  $p-y$  curves for laterally loaded monopiles installed in clay using Plaxis 3D where hardening soil model was used. Haiderali et al. (2013) conducted three-dimensional finite element analyses to investigate the lateral and axial response of monopiles in soft and stiff marine clays. Haiderali and Madabhushi (2013) carried out three-dimensional finite element analyses to investigate the lateral load-deformation behavior of monopiles installed in soft clays of varying undrained shear strength and stiffness.

## **2.4 Summary**

A comprehensive literature review is presented on the two focused areas of the present study, namely inclined loading pullout capacity of suction caisson in sand and lateral load capacity of monopile in sand.

Although, a number of research works are available in literature related to the FE modeling of inclined loading pullout capacity of suction caisson in sand, the effects of pre-peak hardening and post-peak softening behavior of dense sand were not take into account in past. The effects of mean effective stress and relative density on stress–strain behavior of dense sand were not considered, which is required for better estimation of the inclined pullout capacity of suction caissons by FE simulation.

The current design practice of monopile foundations for offshore wind turbines is based on the  $p-y$  curve method. The present literature review reveals the weakness of  $p-y$  curve

method in designing the large diameter monopiles. In addition, the FE analyses performed earlier did not consider the mean stress and strain dependent variation of mobilized friction angle and dilation angle of dense sand. Hence, a proper soil constitutive model is required to evaluate the capacity of large diameter monopiles by FE modeling.

## Bibliography

- Abdel-Rahman, K and Achmus, M (2005). Finite element modelling of horizontally loaded monopile foundations for offshore wind energy converters in Germany. *Proc. of International Symposium on Frontiers in Offshore Geotechnics*, Perth, Australia.
- Achmus, M, Kuo, YS and Abdel-Rahman, K (2009). Behavior of monopile foundations under cyclic lateral load. *Computers and Geotechnics*, vol. 36, pp. 725–735.
- Achmus, M, Akdag, CT and Thieken, K (2013). Load-bearing behavior of suction bucket foundations in sand. *Applied Ocean Research*, vol. 43, pp. 157–165.
- Alhayari, S (1998). Innovative developments in suction pile technology. *Offshore Technology Conference*, Houston, Texas, USA, OTC 8836.
- Allersma, HGB, Brinkgreve, RBJ, Simon, T and Kirstein, AA (2000). Centrifuge and Numerical Modelling of Horizontally Loaded Suction Piles. *International Journal of Offshore and Polar Engineering*, vol. 10, no. 3, pp. 222–228.
- Andersen, KH, Murff, JD, Randolph, MF, Clukey, EC, Erbrich, C, Jostad, HP, Hansen, B, Aubeny, C, Sharma, P and Supachawarote, C (2005a). Suction anchors for deepwater applications. *Proc. of International Symposium on Frontiers in Offshore Geotechnics ISFOG*, Perth, Australia.
- API (2000). Recommended Practice for Planning, Designing and Construction Fixed

- Offshore Platforms—Working Stress Design, *API Recommended Practice 2A-WSD (RP2A-WSD)*, 21st edition, American Petroleum Institute.
- API (2007). Recommended Practice for Planning, Design and Constructing Fixed Offshore Platforms-Working Stress Design. *American Petroleum Institute*. Errata and Supplement 3.
- API (2010). Recommended Practice for Planning, Designing and Constructing Offshore Platforms, *American Petroleum Institute*, 18th edition.
- Ashford, SA and Juirnarongrit, T (2003). Evaluation of pile diameter effect on initial modulus of subgrade reaction. *Journal of Geotechnical and Geoenvironmental Engineering*, vol. 129, no. 3, pp. 234–242.
- Ashour, M, and Norris, G (2000). Modelling lateral soil-pile response based on soil-pile interaction. *ASCE Journal of Geotechnical and Geoenvironmental Engineering*, vol. 126, no. 5, pp. 420–428.
- Audibert, JME, Clukey, E and Huang, J (2003). Suction caisson installation at Horn Mountain—A case study. *Proc. 13th International Offshore and Polar Engineering Conference*, Honolulu, USA, vol. 2, pp. 762–769.
- Baguelin, F, Goulet, G and Jezequel, J (1972). Étude expérimentale du comportement d'un pieu sollicité horizontalement. *Proc. of 5th European Conference on Soil Mechanics and Foundation Engineering*, Madrid, Spain, vol. I, pp. 317–324.

- Bang, S and Cho, Y (1999). Analytical Performance Study of Suction Piles in Sand. *Proceedings of the 9th International Offshore and Polar Engineering Conference*, Brest, France, May 30-June 4, pp. 90–93.
- Bang, S and Karnoski, S (2007). Field Retrieval of Suction Piles in Sand. *Proc. of the 16th International Offshore and Polar Engineering Conference*, Lisbon, Portugal, July 1-6, pp. 1473–1477.
- Bang, S, Preber, T, Cho, Y, Thomason, J, Karnoski, SR and Taylor, RJ (2000). Suction Piles for Mooring of Mobile Offshore Bases. *Journal of Marine Structures*, No. 13, pp. 367–382.
- Bang, S, Jones, KD, Kim, KO, Kim, YS and Cho, Y (2011). Inclined loading capacity of suction piles in sand. *Journal of Ocean Engineering*, Vol. 38, pp. 915–924.
- Barusco, P (1999). Mooring and anchoring systems developed in Marlim field. *Offshore Technology Conference*, Houston, Texas, USA, OTC 10720.
- Briaud, JL, Smith, T and Meyer, B (1983). Pressuremeter gives elementary model for laterally loaded piles. *Symposium of International in situ Testing*, Paris, France, vol. 2, pp. 217–221.
- Brinch Hansen, J (1961). The Ultimate resistance of rigid piles against transversal forces. *The Danish Geotechnical Institute*, Bulletin 12.

- Brown, GA and Nacci, VA (1971). Performance of hydrostatic anchors in granular soils. *Offshore Technology Conference*, Houston, Texas, USA, OTC 1472.
- Cao, J, Phillips, R and Popescu, R (2001). Physical and numerical modelling on suction caissons in clay. *Proc. of the 18th Canadian Congress of Applied Mechanics*, St. John's, Newfoundland, Canada, pp. 217–218.
- Cao, J, Phillips, R, Popescu, R, Al-Khafaji, Z, and Audibert, JME (2002a). Penetration resistance of suction caissons in clay. *Proc. of the 12th International Offshore and Polar Engineering Conference*, Kitakyushu, May 26-31, pp. 800–806.
- Cao, J, Phillips, R, Audibert, JME and Al-Khafaji, Z (2002b). Numerical analysis of the behavior of suction caissons in clay. *Proc. of the 12th International Offshore and Polar Engineering Conference*, Kitakyushu, Japan, May 26-31, pp. 795–799.
- Cao, J, Phillips, R, Popescu, R, Audibert, JME and Al-Khafaji, Z (2003). Numerical analysis of the behavior of suction caissons in clay. *International Journal of Offshore and Polar Engineering*, Vol. 13, No. 2, pp. 154–159.
- Cauble, DF (1996). An experimental investigation of the behavior of a model suction caisson in a cohesive soil. *PhD Dissertation*, Massachusetts Institute of Technology.
- Cho, Y, Lee, TH, Park, JB, Kwag, DJ and Chung, ES (2002). Field tests on suction pile installation in sand. *21st International Conference on Offshore Mechanics and Arctic Engineering*, June 23-28, Oslo, Norway. OMAE2002-28179.

- Colliat, J-L and Dendani, H (2002). Girassol: geotechnical design analyses and installation of suction anchors. *Proc. SUT Offshore Site Investigation and Geotechnics*, pp. 107–119.
- Colliat, J-L, Boisard, P, Andersen, K and Schoeder, K (1995). Caisson foundations as alternative anchors for permanent mooring of a process barge offshore Congo. *Offshore Technology Conference*, Houston, Texas, USA, OTC 7797.
- Colliat, J-L, Boisard, P, Gramet, J-C and Sparrevik, P (1996). Design and installation of suction anchor piles at a soft clay site in the Gulf of Guinea. *Offshore Technology Conference*, Houston, Texas, USA, OTC 8150.
- Cox, WR, Reese, LC and Grubbs, BR (1974). Field testing of laterally loaded piles in sand. *Offshore Technology Conference*, Houston, Texas, USA, OTC 2079.
- Datta, M and Kumar, P (1996). Suction beneath cylindrical anchors in soft clay. *Proc. of the 6th International Offshore and Polar Engineering Conference*, Los Angeles, California, USA, pp. 544–548.
- Deng, W and Carter, JP (2000). Inclined uplift capacity of suction caissons in sand. *Offshore Technology Conference*, Houston, Texas, OTC 12196, pp. 809–820.
- DNV (2007). Design of Offshore Wind Turbine Structures. *Offshore Standard*, DNV-OS-J101, Det Norske Veritas.
- DNV (2011). Design of Offshore Wind Turbine Structures. *Offshore Standard*, DNV-OS-J101, Det Norske Veritas.

- Doherty, P and Gavin, K (2012). Laterally loaded monopile design for offshore wind farms. *Proc. of the ICE-Energy*, vol. 165, pp. 7–17.
- Doherty, P, Li, W, Gavin, K and Casey, B (2012). Field Lateral Load Test On Monopile In Dense Sand. *Offshore Site Investigation and Geotechnics: Integrated Technologies—Present and Future*, 12-14 September, London, UK.
- Doyle, EH, Sharma, JS and Bolton, MD (2004). Centrifuge model tests on anchor piles for tension leg platforms. *Offshore Technology Conference*, Houston, Texas, USA, OTC 16845.
- El-Gharbawy, S and Olson, R (1998). Laboratory Modeling of Suction Caisson Foundations. *Proc. of the 8th International Offshore and Polar Engineering Conference*, Montreal, Canada, May 24-29, pp. 537–542.
- Erbrich, C and Hefer, P (2002). Installation of the Laminaria suction piles—A case history. *Offshore Technology Conference*, Houston, Texas, USA, OTC 14240.
- Erbrich, CT (1994). Modeling of a novel foundation for offshore structures. *Proc. of the 9th UK ABAQUS User's Conference*, Oxford, England, pp. 235–251.
- EWEA (2014). *The European offshore wind industry—key trends and statistics 2013*, European Wind Energy Association.
- Fan, CC and Long, JH (2005). Assessment of existing methods for predicting soil response of laterally loaded piles in sand. *Computers and Geotechnics*, vol. 32, no.4, pp. 274–289.

- Fines, S, Stove, OJ and Guldborg, F (1991). Snorre TLP tethers and foundation. *Offshore Technology Conference*, Houston, Texas, USA, OTC 6623.
- Gao, Y, Qiu, Y, Li, B, Li, D, Sha, C and Zheng, X (2013). Experimental studies on the anti-uplift behavior of the suction caissons in sand. *Applied Ocean Research*, vol. 43, pp. 37–45.
- Goodman, LJ, Lee, CN and Walker, FJ (1961). The feasibility of vacuum anchorage in soil. *Géotechnique*, vol. 1, no. 3, pp. 356–359.
- Haiderali, A and Madabhushi, GSP (2013). Evaluation of the  $p - y$  method in the design of monopiles for offshore wind turbines. *Offshore Technology Conference*, Houston, Texas, USA, OTC 24088.
- Haiderali, A, Cilingir, U and Madabhushi, GSP (2013). Lateral and Axial Capacity of Monopiles for Offshore Wind Turbines. *Indian Geotechnical Journal*, vol. 43, no. 3, pp. 181–194.
- Haland, G (2002). Pro's and con's of foundations used for the Aasgard field development. *Proc. SUT Offshore Site Investigation and Geotechnics*, pp. 93–105.
- Hald, T, Mørch, C, Jensen, L, Bakmar, CL and Ahle, K (2009). Revisiting monopile design using  $py$  curves: results from full scale measurements on Horns Rev. *Proc. of European Offshore Wind Conference*.
- Handayanu, Swamidasa, ASJ and Booton, M (1999). Behavior of tension foundation for

- offshore structures under extreme pull-out loads. *Proc. of 18th International Conference on Offshore Mechanics and Arctic Engineering*, St. John's, Newfoundland, Canada, OMAE99/OFT-4204, pp. 635–641.
- Handayanu, Swamidass ASJ, Booton M (2000). Ultimate strength of offshore tension foundations under vertical and inclined loads. *Proc. of the International Conference on Offshore Mechanics and Arctic Engineering*, New Orleans, Louisiana, vol. 2, pp. 95–100.
- Hearn, EN and Edgers, L (2010). Finite Element Analysis of an Offshore Wind Turbine Monopile. *GeoFlorida 2010: Advances in Analysis, Modeling & Design*, pp. 1857–1865.
- Helfrich, SC, Brazill, RL and Richards, AF (1976). Pullout characteristics of a suction anchor in sand. *Offshore Technology Conference*, Houston, Texas, USA, OTC 2469, pp. 501–506.
- Hesar, M (2003). Geotechnical design of the Barracuda and Caratinga suction anchors. *Offshore Technology Conference*, Houston, Texas, USA, OTC 15137.
- Hogervorst, JR (1980). Field trials with large diameter suction piles. *Offshore Technology Conference*, Houston, Texas, USA, OTC 3817.
- Iftekharuzzaman, Md and Hawlader, B (2012). Numerical modeling of pullout capacity of a suction pile in sand under oblique load. *Second International Conference on*

- Geotechnique, Construction Materials and Environment*, Kuala Lumpur, Malaysia, Nov. pp. 14–16.
- Jang, YS and Kim, YS (2013). Centrifugal Model Behavior of Laterally Loaded Suction Pile in Sand. *KSCE Journal of Civil Engineering*, Vol. 17, No. 5, pp. 980–988.
- Juirmarongrit, T and Ashford, SA (2005). Effect of Pile Diameter on the Modulus of Sub-Grade Reaction. *Report no. SSRP-2001/22*, Department of Structural Engineering, University of California, San Diego.
- Keaveny , JM, Hansen, SB, Madshus, C, and Dyvik, R (1994). Horizontal capacity of large-scale model anchors. *Proc. of the 13th International Conference on Soil Mechanics and Foundation Engineering*, New Delhi, India, pp. 677–680.
- Kim, KO, Kim, YS, Cho, Y, Bang, S and Jones, K (2009). Centrifuge Model Tests on Suction Piles in Sand under Inclined Loading. *Proceedings of the 19th International Offshore and Polar Engineering Conference*, Osaka, Japan, June 21-26, pp. 191–196.
- Kirkwood, P and Haigh, S (2013). Centrifuge Testing of Monopiles for Offshore Wind Turbines. *Proc. of the 23rd International Offshore and Polar Engineering Conference*, Anchorage, Alaska, USA, June 30-July 5, pp. 126–130.
- Klinkvort, RT and Hededal, O (2011). Centrifuge modelling of offshore monopile foundation. *Frontiers in Offshore Geotechnics II—Gourvenec and White (eds)*, Taylor and Francis, pp. 581–586.

- Klinkvort, RT and Hededal, O (2013). Lateral response of monopile supporting an offshore wind turbine. *Proceedings of the ICE-Geotechnical Engineering*, vol. 166, no. 2, pp. 147–158.
- Klinkvort, RT and Hededal, O (2014). Effect of load eccentricity and stress level on monopile support for offshore wind turbines. *Canadian Geotechnical Journal*, vol. 51, no. 9, pp. 966–974.
- Klinkvort, RT, Hededal, O and Springman, SM (2013). Scaling issues in centrifuge modelling of monopiles. *International Journal of Physical Modelling in Geotechnics*, vol. 13, no. 2, pp. 38–49.
- Kolk, HJ, Kay, S, Kirstein, A and Troestler, H (2001). North Nemba Flare Bucket Foundations. *Offshore Technology Conference*, Houston, Texas, USA, OTC 13057.
- Lacasse, S (1999). 9th OTRC Honors Lecture: Geotechnical contributions to offshore development. *Offshore Technology Conference*, Houston, Texas, USA, OTC 10822.
- Larsen, P (1989). Suction anchors as an anchoring system for floating offshore constructions. *Proc. of the 21st annual Offshore Technology Conference*, Houston, Texas, USA, OTC 6029, pp. 535–540.
- LeBlanc, C, Houlsby, GT and Byrne, BW (2010). Response of stiff piles in sand to long-term cyclic lateral loading. *Géotechnique*. vol. 60, no. 2, pp. 79–90.
- Lee, SH, Cho, Y, Kim, KO, Kim, YS, Lee, TH, and Kwag, DJ (2003). Centrifuge model

- tests on embedded suction anchor loading capacities. *Proc. of The 13th International Offshore and Polar Engineering Conference*, Honolulu, Hawaii, USA, May 25–30, vol. II, pp. 789–793.
- Lesny, K and Wiemann, J (2006). Finite element modelling of large diameter monopiles for offshore wind energy converters. *Proceedings of GeoCongress 2006: Geotechnical Engineering in the Information Technology Age*, pp. 1–6.
- Li, S and Wang, J (2013). Analysis of Suction Anchors Bearing Capacity in Soft Clay. *Proc. of the 23rd International Offshore and Polar Engineering*, Anchorage, Alaska, USA, June 30–July 5, pp. 495–500.
- Liu, Z, Wang, J, Qin, C and Li, S (2004). Study on the Horizontal Bearing Capacity of Bucket Foundations. *Proc. of the 14th International Offshore and Polar Engineering Conference*, Toulon, France, May 23-28, pp. 654–658.
- Lombardi, D, Bhattacharya, S and Wood, DM (2013). Dynamic soil-structure interaction of monopile supported wind turbines in cohesive soil. *Soil Dynamics and Earthquake Engineering*, vol. 49, pp. 165–180.
- Mackereth, FJH (1958). A portable core sampler for lake deposits. *Limnology and oceanography*, vol. 3, no. 2, pp. 181–191.
- Maeno, Y, Ishikawa, M, Tobita, Y and Kumagai, Y (2002). Field Measurements of the Pullout Capacity of Mooring Anchors. *Proc. of the 12th International Offshore and Polar Engineering Conference*, Kitakyushu, Japan, May 26-31, pp. 723–730.

- Malhotra, S (2011). Selection, Design and Construction of Offshore Wind Turbine Foundations. *Wind Turbines, Dr. Ibrahim Al-Bahadly (Ed.)*, ISBN: 978-953-307-221-0, InTech, 652 p.
- Maniar, DR (2004). A Computational Procedure for Simulation of Suction Caisson Behavior Under Axial and Inclined Loads. *PhD Thesis*, The University of Texas at Austin, United States.
- Masui, N, Yoneda, H, Zenda, Y, Ito, M, Iida, Y and Hermstad, J (2001). Installation of offshore concrete structure with skirt foundation. *Proc. 11th International Offshore and Polar Engineering Conference*, Stavanger, Norway, vol. 2, pp. 626–630.
- Mello, JRC, Moretti, MJ, Sparrevik, P, Schoder, K and Hansen, SB (1998). P19 and P26 moorings at the Marlim field. The first permanent taut leg mooring with fibre rope and suction anchors. *Proc. Conference on Floating and Production Systems*, pp. 1–11.
- Meyerhof, GG and Sastry, VVRN (1985). Bearing capacity of rigid piles under eccentric and inclined loads. *Canadian Geotechnical Journal*, vol. 22, pp. 267–276.
- Meyerhof, GG, Mathur, SK and Valsangkar, AJ (1981). Lateral resistance and deflection of rigid walls and piles in layered soils. *Canadian Geotechnical Journal*, vol. 18, pp. 159–170.
- Murchison, J and O'Neill, M (1984). Evaluation of  $p - y$  relationships in cohesionless soil: analysis and design of pile foundations. *Proc. of Symposium in Conjunction with the ASCE National Convention*. ASCE, San Fransisco, California, USA, pp. 174–191.

- Newlin, JA (2003). Suction anchor piles for the Na Kita FDS mooring system. Part 2: Installation performance. *Proc. International Symposium on Deep Mooring Systems*, Houston, Texas, USA, pp. 55–75.
- Nicolai, G and Ibsen, LB (2014). Small-Scale Testing of Cyclic Laterally Loaded Monopiles in Dense Saturated Sand. *Proc. of the 24th International Ocean and Polar Engineering Conference*, Busan, Korea, June 15-20, pp. 731–736.
- North Sea Report (1972). Submersible sounding tools to test North Sea floor. *The Oil and Gas Journal*, pp. 74–77.
- Nunez, IL, Hoadley, PJ, Randolph, MF and Hulett, JM (1988). Driving and tension loading of piles in sand on a centrifuge. *Proc. International Conference Centrifuge*, vol. 88, pp. 353–362.
- Pradhan, DL (2012). Development of  $p - y$  Curves for Monopiles in Clay using Finite Element Model Plaxis 3D Foundation. *MSc Thesis*, Department of Civil and Transport Engineering, Norwegian University of Science and Technology.
- Ramadan, MI (2011). Physical and numerical modeling of offshore anchor piles under mooring forces. PhD thesis, Memorial University of Newfoundland, St. John's, NL.
- Ramadan, MI, Butt, SD and Popescu, R (2013a). Offshore anchor piles under mooring forces: centrifuge modeling. *Canadian Geotechnical Journal*, Vol. 50, pp. 373–381.

- Ramadan, MI, Butt, SD and Popescu, R (2013b). Offshore anchor piles under mooring forces: numerical modeling. *Canadian Geotechnical Journal*, Vol. 50, pp. 189–199.
- Randolph, MF, O'Neill, MP, Stewart, DP and Erbrich, C (1998). Performance of Suction Anchors in Fine-Grained Calcareous Soils. *Offshore Technology Conference*, Houston, Texas, USA, OTC 8831.
- Reese, LC, Cox, WR and Koop, FD (1974). Analysis of laterally loaded piles in sand. *Offshore Technology Conference*, Houston, Texas, USA, OTC 2080.
- Roesen, HR, Andersen, LV, Ibsen, LB and Foglia, A (2012). Experimental Setup for Cyclic Lateral Loading of Monopiles in Sand. *Proc. of the 22nd International Offshore and Polar Engineering Conference*, Rhodes, Greece, June 17-22, pp. 857–864.
- Sørensen SPH, Brødbæk KT, Møller M, Augustesen AH and Ibsen LB (2009). Evaluation of the load–displacement relationships for large-diameter piles in sand. *Proc. of the 12th International Conference on Civil, Structural and Environmental Engineering Computing* (Topping BHV, Costa Neves LF and Barros RC (eds)), Civil-Comp Press, Sterling, UK, Paper 244.
- Senpere, D, and Auvergne, GA (1982). Suction anchor piles - A proven alternative to driving or drilling. *Offshore Technology Conference*, Houston, Texas, USA, OTC 4206.
- Solhjell, E, Sparrevik, P, Haldorsen, K and Karlsen, V (1998). Comparison and back calculation of penetration resistance from suction anchor installation in soft to stiff clay

- at the Njord and Visund fields in the North Sea. *Proc. SUT Conference on Offshore Site Investigation and Foundation Behaviour*, pp. 325–349.
- Sparrevik, P (1998). Suction anchors—A versatile foundation concept finding its place in the offshore market. *Proc. 17th International Conference on Offshore Mechanics and Artic Engineering*, Lisbon, Portugal, OMAE98-3096.
- Sparrevik, P (2002). Suction pile technology and installation in deep water. *Offshore Technology Conference*, Houston, Texas, USA, OTC 14241.
- Steensen-Bach, J.O. (1992). Recent model tests with suction piles in clay and sand. *Proc. of the 24th annual Offshore Technology Conference*, Houston, Texas, USA, OTC 6844, pp. II 323–330.
- Stove, OJ, Bysveen, S and Christophersen, HP (1992). New Foundation Systems for the Snorre development. *Offshore Technology Conference*, Houston, Texas, USA, OTC 6882.
- Sukumaran, B and McCarron, WO (1999b). Total and effective stress analysis of suction caissons for Gulf of Mexico conditions. *In Analysis, Design, Construction and Testing of Deep Foundations*, Edited by J.M. Roesset, Proc. of the OTRC'99 Conference, Geotechnical special publication No. 88, pp. 247–260.
- Sukumaran, B, McCarron, WO, Jeanjean, P and Abouseeda, H (1999). Efficient finite element techniques for limit analysis of suction caissons under lateral loads. *Computers and Geotechnics*, vol. 24, pp. 89–107.

- Supachawarote, C, Randolph, MF and Gourvenec, S (2004). Inclined Pull-out Capacity of Suction Caissons. *Proc. of the 14th International Offshore and Polar Engineering Conference*, Toulon, France, May 23-28, pp. 500–506.
- Tjelta, TI, Aas, PM, Hermstad, J and Andenaes, E (1990). The skirted piled Gullfaks C platform installation. *Offshore Technology Conference*, Houston, Texas, USA, OTC 6473.
- Tjelta, T.I. (1994). Geotechnical aspects of bucket foundation replacing piles for Europipe 16/11-E jacket. *Offshore Technology Conference*, Houston, Texas, USA, OTC 7379.
- Tjelta, TI (1995). Geotechnical experience from the installation of the Europipe jacket with bucket foundations. *Offshore Technology Conference*, Houston, Texas, USA, OTC 7795.
- Tjelta, TI (2001). Suction piles: Their position and application today. *Proc. of the 11th International Offshore and Polar Engineering Conference*, Stavanger, Norway, pp. 1–6.
- Tran, MN and Randolph, MF (2008). Variation of suction pressure during caisson installation in sand. *Géotechnique*, vol. 58, no. 1, pp. 1–11.
- Tran, MN (2005). Installation of Suction Caissons in Dense Sand and the Influence of Silt and Cemented Layers. *PhD Thesis*, University of Sydney, Australia.
- Uncuoğlu, E and Laman, M (2011). Lateral resistance of a short rigid pile in a two-layer cohesionless soil. *Acta Geotechnica Slovenica*, vol. 2, pp. 19–43.

- Villalobos, FA, Byrne, BW and Houlsby, GT (2009). An experimental study of the drained capacity of suction caisson foundations under monotonic loading for offshore applications. *Soils and Foundations*, vol. 49, no. 3, pp. 477–488.
- Wang, MC, Nacci, VA and Demars, KR (1975). Behavior of underwater suction anchor in soil. *Ocean Engineering*, vol. 3, pp. 47–62.
- Wang, MC, Demars, KR and Nacci, VA (1977). Breakout capacity of model suction anchors in soil. *Canadian Geotechnical Journal*, vol. 14, pp. 246–257.
- Wang, MC, Demars, KR and Nacci, VA (1978). Applications of suction anchors in offshore technology. *Offshore Technology Conference*, Houston, Texas, USA, OTC 3203, pp. 1311–1320.
- Watson, PG, Randolph, MF and Bransby, MF (2000). Combined Lateral and Vertical Loading of Caisson Foundations. *Offshore Technology Conference*, Houston, Texas, USA, OTC 12195.
- Wolf, TK, Rasmussen, KL, Hansen, M, Ibsen, LB and Roesen, HR (2013). Assessment of  $p - y$  curves from numerical methods for a non-slender monopile in cohesionless soil. *Aalborg: Department of Civil Engineering, Aalborg University*, DCE Technical Memorandum, no. 24.
- Zdravkovic, L, Potts, DM and Jardine, RJ (1998). Pull-out capacity of bucket foundations in soft clay. *Proc. of the International Conference on Offshore Site Investigation and Foundation Behaviour-New Frontiers*, London, United Kingdom.

Zhang, C, White, D and Randolph, MF (2010). Centrifuge modeling of the cyclic lateral response of a rigid pile in soft clay. *Journal of Geotechnical and Geoenvironmental Engineering*, vol. 137, no. 7, pp. 717–729.

## **Chapter 3**

# **Numerical Analysis of Inclined Uplift Capacity of Suction Caisson in Sand**

### **Co-Authorship**

Chapter 3 is prepared according to the Guidelines for Manuscript Format Theses in the Faculty of Engineering and Applied Science at Memorial University. This part of the research has been published as:

Ahmed, SS, and Hawlader, BC (2015). Numerical Analysis of Inclined Uplift Capacity of Suction Caisson in Sand. *International Journal of Offshore and Polar Engineering*, Vol. 25, no. 2, pp. 145–155.

Most of the research work presented in this chapter was conducted by the first author. He also prepared the draft manuscript. The second author supervised the research and reviewed the manuscript.

### 3.1 Abstract

Three-dimensional finite element (FE) analyses are conducted to calculate the pullout capacity of suction caisson subjected to oblique loading. Two sets of FE analyses are performed using Abaqus FE software. In the first set, the sand around the caisson is modeled using the built-in Mohr-Coulomb model (MC) available in Abaqus where constant values of the angle of internal friction ( $\phi'$ ) and dilation ( $\psi$ ) are defined. The effects of key variables, such as loading angle, mooring position and aspect ratio, on pullout capacity and rotation of the caisson are examined. A comparison between FE and centrifuge test results is also shown. The second set of analyses are performed using a modified Mohr-Coulomb model (MMC) where the prepeak hardening, postpeak softening and effects of density and confining pressure on stress-strain behavior of dense sand are implemented via a user subroutine by varying  $\phi'$  and  $\psi$  as a function of plastic shear strain and confining pressure. By comparing the failure surface development in the soil with increase in loading for two different models (MC and MMC), it is shown that the mobilized  $\phi'$  and  $\psi$  vary along the failure planes if the MMC model is used, although the capacity of the caisson could be obtained even if appropriate values of constant  $\phi'$  and  $\psi$  are used in the MC model.

**Keywords:** Suction caisson; Abaqus/Explicit; Pullout force; Dense sand; Loading angle; Mooring position.

## 3.2 Introduction

Suction caissons (also known as suction anchors, suction piles or suction buckets) are a unique form of foundation/mooring system that have several advantages over traditional pile foundation and anchors. The main advantages include fast installation, elimination of the pile driving process, reduction in material costs and reusability. A suction caisson is a large diameter hollow cylinder, usually made of steel having top end closed and bottom end opened that is installed in soil by applying suction with pumping water out of caisson interior. Suction caissons are now widely being used in offshore industries for anchoring large offshore floating facilities to the seafloor. The pullout capacity of the caisson is one of the main concerns. The caissons are usually connected to the floating structures by a mooring line which is attached to a padeye on one side of the caisson.

The pullout behavior of suction caissons installed in both sand and clay is of great interest for oil and gas development industry because of their advantages over other conventional foundation systems. Previous studies mainly focused on caissons in clay. For example, Aubeny et al. (2003) presented a theoretical method to estimate the inclined load capacity of suction caissons based on an upper bound plasticity formulation for clay. Cao et al. (2002a, 2002b and 2003) conducted centrifuge tests and FE analyses for caissons in clay. Similarly, FE analyses have been performed using various soil constitutive models, including Cam Clay and MIT-E3 models, to understand the response of caissons in clay (e.g., Sukumaran et al., 1999; Handayanu et al., 2000; Zdravkovic et al., 2001).

Limited research is available in the literature to estimate the pullout capacity of suction caissons in sand. The mechanisms involved in the installation of a caisson in sand are different from that of in clay. In sand, the seepage due to applied suction plays a significant role. The installation issues of suction caisson in sand and sand/silt layers have been described by Houlsby and Byrne (2005a and 2005b) and Tran et al. (2007). Some centrifuge tests have been conducted in the past to increase the understanding of the pullout behavior of caisson in sand (e.g., Allersma et al., 2000; Lee et al., 2003; Kim et al., 2005; Jones et al., 2007; Kim et al., 2009; Kim et al., 2010; Bang et al., 2011; Jang and Kim, 2013). Bang et al. (2011) reported a series of centrifuge tests at  $100g$  on a model suction caisson in medium dense sand to evaluate the pullout capacities. More recently, Gao et al. (2013) conducted model tests to evaluate the pullout capacity of suction caisson in medium dense sand and reported the effects of load inclination angle, mooring position and aspect ratio.

Numerical modeling of suction caisson in sand is very limited. Deng and Carter (2000) conducted FE analyses of suction caisson in sand assuming axisymmetric loading conditions using the AFENA FE software package and Mohr-Coulomb soil model. Iftekharruzaman and Hawlader (2012) conducted three-dimensional FE analysis using Abaqus/Standard FE software, where they encountered some mesh distortion issues at large displacement.

In this study, three-dimensional FE modeling of suction caissons is performed to evaluate the pullout capacities at different load inclination angles and mooring positions in dense

sand. In the first part of the paper, FE analyses are conducted using the built-in Mohr-Coulomb model available in Abaqus where  $\phi'$  and  $\psi$  are constant. A total of 60 cases are analyzed to determine the pullout capacity of the caisson. A parametric study is also conducted to evaluate the effects of length/diameter ratio on pullout capacity. The finite element results are compared with centrifuge test results available in the literature. In the second part, a set of FE analyses are presented using a modified Mohr-Coulomb model in which the stress-strain behavior of dense sand as observed in laboratory tests is incorporated.

### **3.3 Problem Definition**

A suction caisson of length  $L$  and diameter  $D$  installed in dense sand is simulated in this study. During the installation, the soil in the vicinity of the suction caisson can be disturbed. However, the effects of disturbance on capacity are not considered in this study; instead, the simulations are performed for a wished-in-place suction caisson. The caisson is loaded at the five pad eye locations shown in Fig. 3.1a at different angle  $\theta$  with the horizontal (Fig. 3.1b). The sign convention used for displacement and rotation of the caisson is shown in Fig. 3.1c.

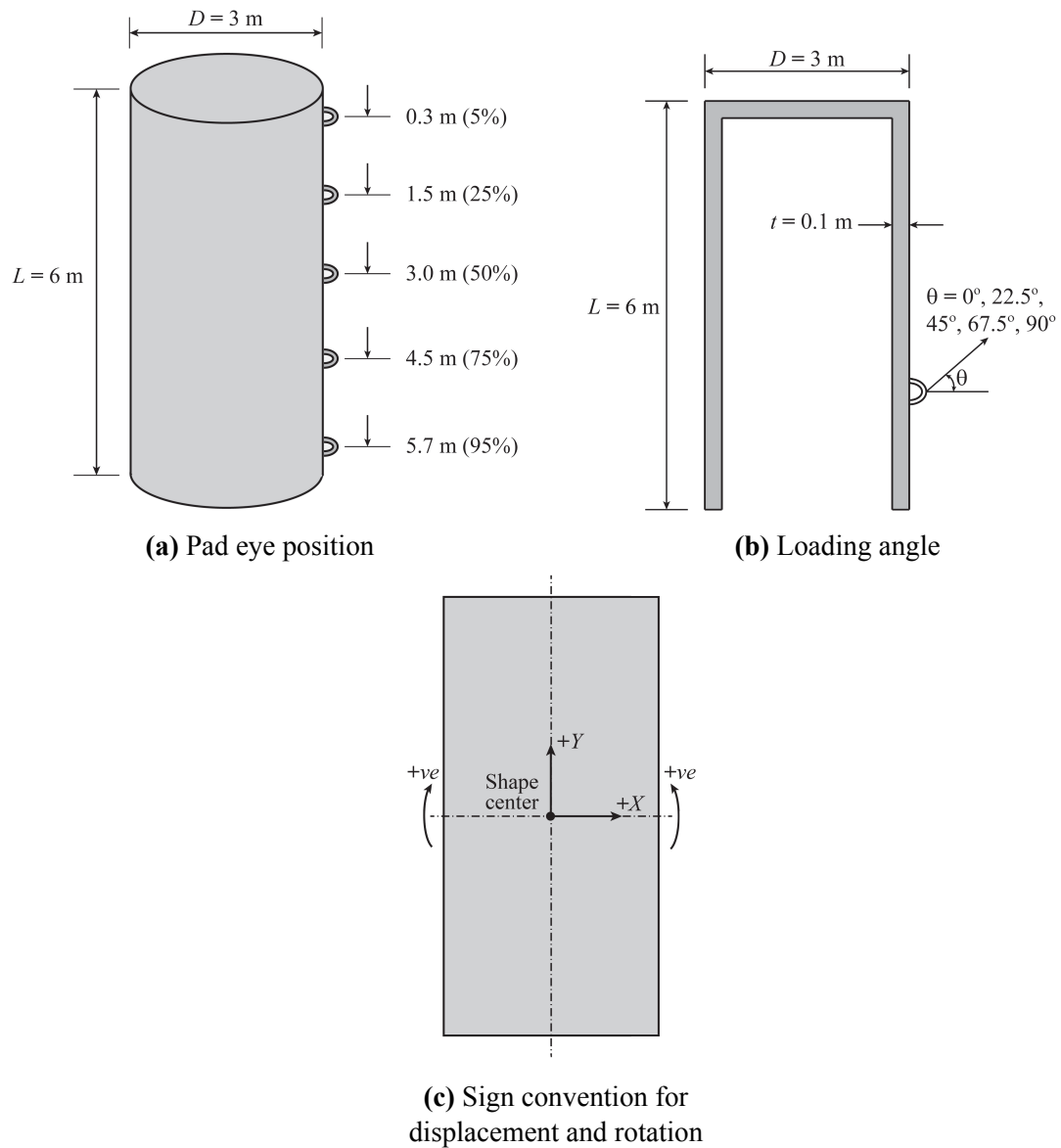


**Figure 3.1:** Problem definition

### 3.4 Finite Element Model

The FE analyses are performed using the FE software Abaqus/Explicit 6.10-EF-1. Taking the advantage of symmetry, only a half-circular soil domain of diameter 42 m ( $= 14D$ ) and depth 20 m ( $= 3.33L$ ) is modeled as shown in Fig. 3.2. The size of the soil domain

is large enough compared to the size of the caisson, and therefore, boundary effects are not found on calculated load, displacement and deformation mechanisms. Achmus et al. (2013) suggested that the diameter of the soil domain greater than  $6.67D$  is sufficient. However, in the present study it is found that it depends upon the direction and location of loading and also on soil strength parameters. Therefore, a larger soil domain is used in this study to avoid any boundary effect. Note that the increase in size of the soil domain does not increase computational cost significantly because the size of the mesh is increased with distance from the caisson (Fig. 3.2).

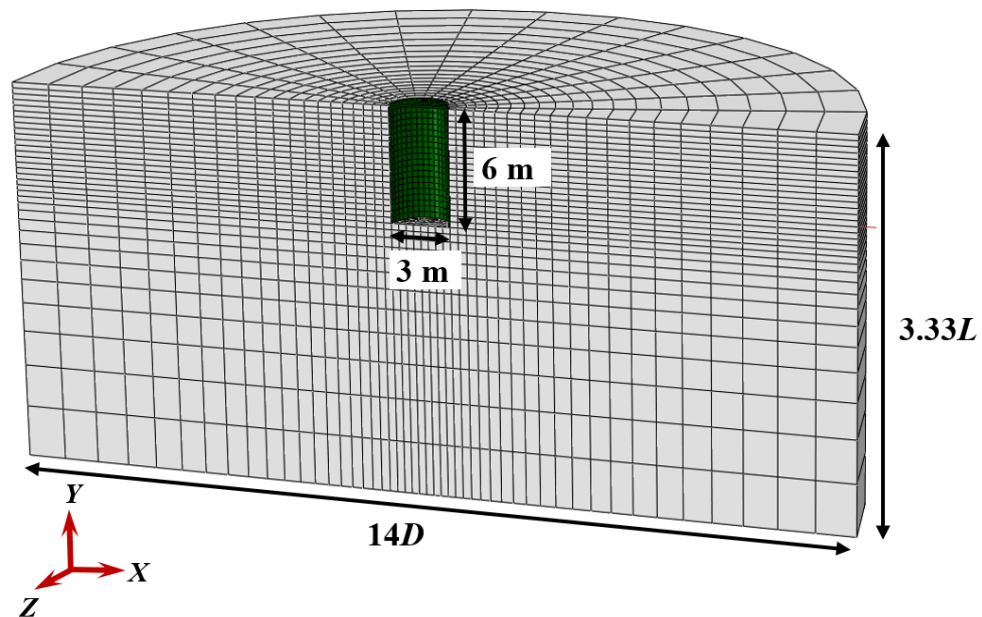


**Figure 3.2:** FE mesh used in the analysis

In the FE model (Fig. 3.2), the vertical plane of symmetry is restrained from any displacement perpendicular to it, while the curved vertical surface of the soil domain is

restrained from any lateral displacement using roller supports at the nodes. The bottom boundary is restrained from any vertical displacement, while the top boundary is free to displace.

The soil and the caisson are modeled using the C3D8R solid homogeneous elements available in Abaqus/Explicit element library, which are 8-noded linear brick elements with reduced integration and hourglass control. The mooring line is modeled as 3D wire using T3D2 element (a 2-node linear 3D truss element) with no interaction with soil domain. Typical FE mesh used in this study is shown in Fig. 3.2.

#### **3.4.1 Modeling of Suction Caisson**

A caisson of 6 m length, 3 m diameter and 100 mm wall thickness is modeled first. This geometry is referred as “base case” in the following sections. Analyses are also performed for different lengths and diameters to show the effects of aspect ratio. In the following sections, the results of base case are presented first. By modeling the caisson as elastic-perfectly plastic material and also as rigid body, it is found that the pullout capacity and rotation do not vary significantly with these modeling techniques. However, the FE model with the caisson as a rigid body is computationally very efficient. Therefore, the caisson is considered as a rigid body in the FE analyses presented in the following sections.

### **3.4.2 Modeling of Mooring Line**

A wire of 50 m length and 100 mm diameter representing the mooring line connected to the suction caisson is modeled using truss elements with material properties of steel. The interface friction between the mooring line and soil is assumed to be zero. The pullout force is applied by a displacement boundary condition at the far end. However, all the results presented in the following sections are in terms of displacement of the padeye location.

### **3.4.3 Modeling of Sand**

The sand is modeled using the built-in Mohr-Coulomb model available in the Abaqus FE software. The submerged unit weight of sand of  $8.2 \text{ kN/m}^3$  is used. The geometry and mechanical properties used in the analysis are shown in Table 3.1. The dimension of the caisson for the base case analysis is similar to Bang et al. (2011). The soil parameters are estimated based on the soil properties mentioned in that study.

### **3.4.4 Interface Behavior**

The soil/caisson interaction is modeled using the Coulomb friction model, which defines the friction coefficient ( $\mu$ ) as  $\mu = \tan(\phi_\mu)$ , where  $\phi_\mu$  is the soil/caisson interface friction angle. The value of  $\phi_\mu/\phi'$  varies between 0 and 1 depending upon surface roughness, mean particle size of sand and method of installation (CFEM, 2006; Tiwari et al., 2010). For smooth steel pipe piles,  $\phi_\mu/\phi'$  is in the range of 0.5 – 0.7 (Potyondy, 1961; Coduto, 2011; Tiwari and Al-Adhath, 2014). For numerical modeling,  $\phi_\mu/\phi'$  within this range has been also used

in the past (e.g. Achmus et al., 2013). In the present study,  $\phi_\mu = 0.6\phi'$  is used. Authors understand that the axial resistance is significantly influenced by the factor. However, the pullout capacity is not significantly influenced by  $\phi_\mu/\phi'$  for typical loading conditions in suction caisson.

**Table 3.1:** Geometry and mechanical properties in FE modeling

<b>Suction caisson</b>	Outer diameter ( $D$ )	3 m
	Length ( $L$ )	6 m
<b>Mooring line</b>	Modulus of elasticity ( $E_p$ )	$2.08 \times 10^8$ kN/m <sup>2</sup>
	Poisson's ratio ( $\nu_p$ )	0.29
<b>Sand</b>	Angle of internal friction ( $\phi'$ )	39°
	Angle of dilation ( $\psi$ )	9°
	Young's modulus ( $E_s$ )	60,000 kN/m <sup>2</sup>
	Poisson's ratio ( $\nu_s$ )	0.3
	Cohesion ( $c'$ ) <sup>1</sup>	0.10 kN/m <sup>2</sup>
	Submerged unit weight ( $\gamma'$ )	8.2 kN/m <sup>3</sup>

<sup>1</sup>Small cohesion is required to be defined in Abaqus FE analysis. For sand, in this study a very small value of  $c' = 0.10$  kN/m<sup>2</sup> is used.

### 3.4.5 Modulus of Elasticity of Sand

The Young's modulus of sand,  $E_s$ , can be expressed as a function of mean effective stress,  $p'$ , as,  $E_s = Kp_{atm}(p'/p_{atm})^n$  (Hardin and Black, 1966; Janbu, 1963); where,  $K$  and  $n$  are two material parameters,  $p_{atm}$  is the atmospheric pressure = (100kPa). However, in this study, no attempt has been taken to vary  $E_s$  with  $p'$ , rather a constant value of  $E_s = 60$  MPa is used.

### **3.4.6 Mooring Positions and Load Inclination Angles**

The effects of mooring position and angle of loading are investigated for the base case parameters listed in Table 3.1. The loads are applied at 5%, 25%, 50%, 75% and 95% mooring positions from the top of the caisson. The inclination angle of the load ( $\theta$ ) is varied as  $0^\circ$ ,  $22.5^\circ$ ,  $45^\circ$ ,  $67.5^\circ$  and  $90^\circ$  for each mooring position. That means, a total of 25 analyses are conducted for the base case to evaluate the effects of mooring position and load inclination angle.

## **3.5 Results**

### **3.5.1 Mesh Sensitivity Analysis**

In general, smaller FE mesh yields more accurate results but computationally expensive. For efficient modeling, small elements are used near the caisson. The size of the elements is increased with increase in radial distance from the caisson as shown in Fig. 3.2. Similarly, the element size is increased with distance from the bottom of the caisson. To select the optimum mesh, several trial analyses are conducted with different mesh sizes. The force-displacement curves for three different sizes of mesh are shown Fig. 3.3 for 50% mooring position and loading angle,  $\theta = 0^\circ$ . As shown in Fig. 3.3, the calculated pullout force is smaller with fine mesh than that of with coarse mesh. In this study, the medium dense mesh is selected to perform the analyses as it is computationally faster, although it is recognized that it gives slightly higher pullout force than that with fine mesh.

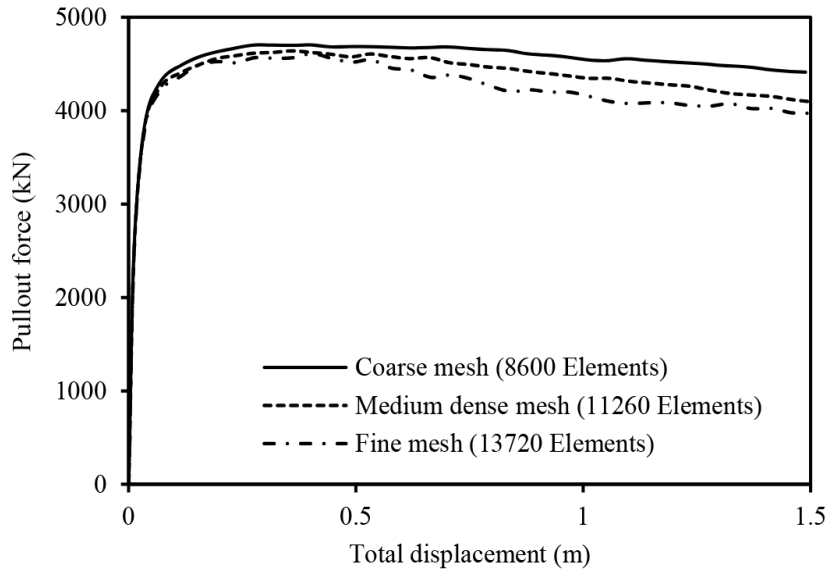


**Figure 3.3:** Mesh sensitivity analysis

### 3.5.2 Force-displacement Curves

The variation of pullout force with total displacement along the direction of pulling is shown in Figs. 3.4 to 3.8 for different mooring positions. The pullout force is obtained from the axial force in the wire (truss element in this case). As Abaqus/Explicit is used, a large displacement could be applied without numerical issues. In this study, a total displacement of 1.5 m is applied.

Several methods are available in the literature to estimate the maximum resistance or capacity of pipelines, anchors or pile foundations from force-displacement curves. As shown in Figs. 3.4 to 3.8, mainly four types of force-displacement curves are obtained from the present FE analyses. Firstly, the force-displacement curve does not show any clear peak as shown for  $\theta = 0^\circ$  in Figs. 3.4 and 3.8. In this cases, the pullout force at 0.3 m

(=  $0.1D$ ) displacement is considered as the pullout capacity as shown by the open triangles in Figs. 3.4 and 3.8. The second type of force-displacement curve shows a clear peak at about  $0.1D$  displacement as shown in Fig. 3.4 for  $\theta = 22.5^\circ$ .

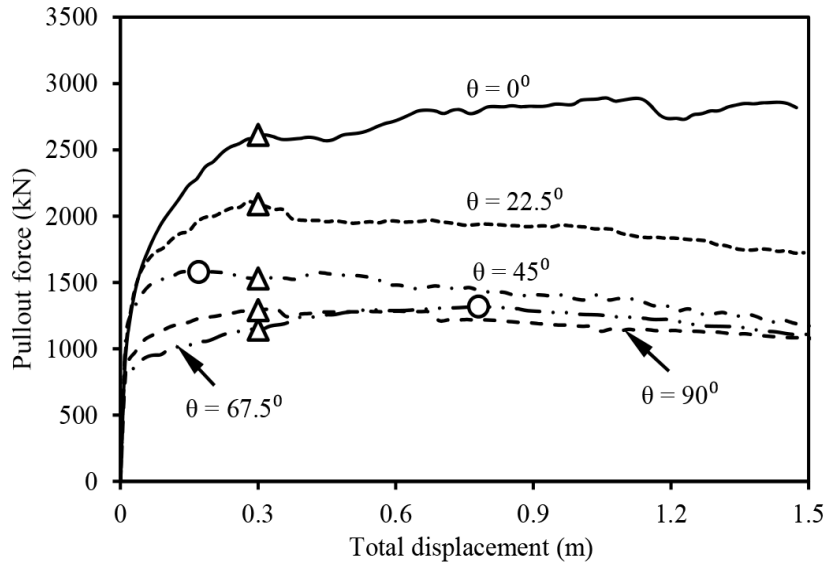


**Figure 3.4:** Force-displacement curve for 5% mooring position

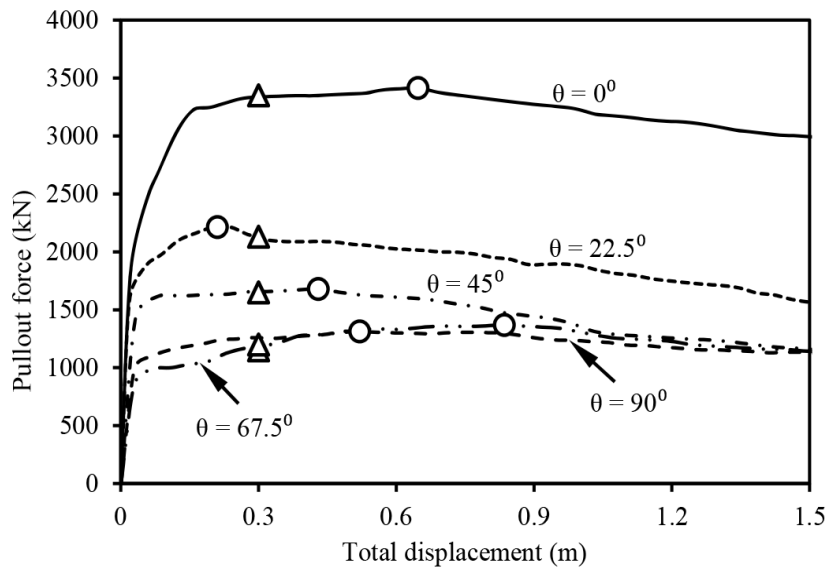


**Figure 3.5:** Force-displacement curve for 25% mooring position

In the third type of force-displacement curves, a clear peak is formed before  $0.1D$  displacement as shown in Fig. 3.4 for  $\theta = 45^\circ$  and in Figs. 3.5 and 3.6 for  $\theta = 22.5^\circ$  with open circles. Finally, in the fourth type the peak force is developed at displacements more than  $0.1D$  as shown in Figs. 3.4 to 3.8 for  $\theta = 67.5^\circ$  with open circles. However, it is found that in all cases the difference between the peak forces (circles) and the force at  $0.1D$  displacement (triangles) is very small. Therefore, in this study the force at  $0.1D$  displacement is considered as the pullout force. The decrease in pullout force at large displacement is mainly because of significant upward movement and rotation of the caisson at large displacement as discussed in the following sections.

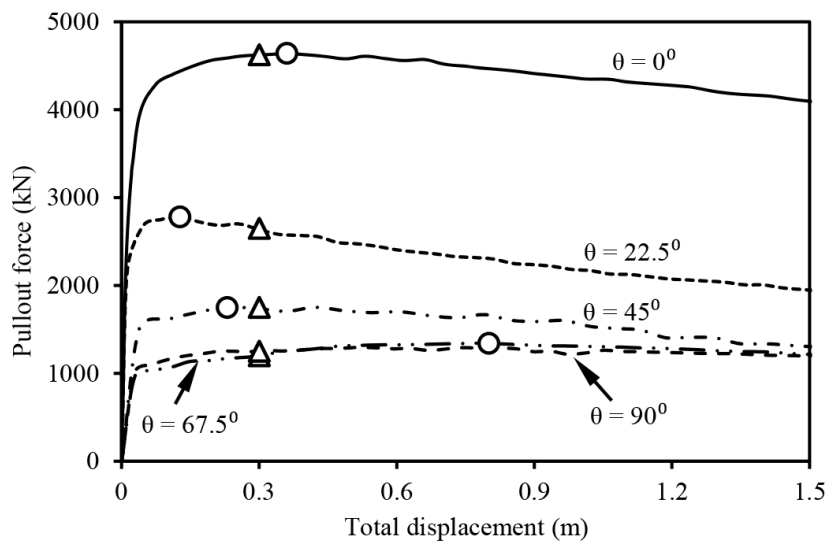


**Figure 3.6:** Force-displacement curve for 50% mooring position

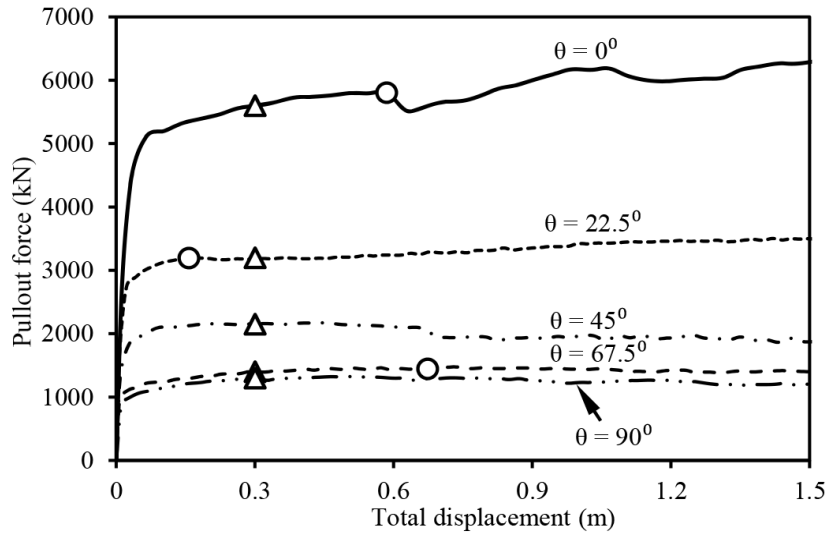


**Figure 3.7:** Force-displacement curve for 75% mooring position

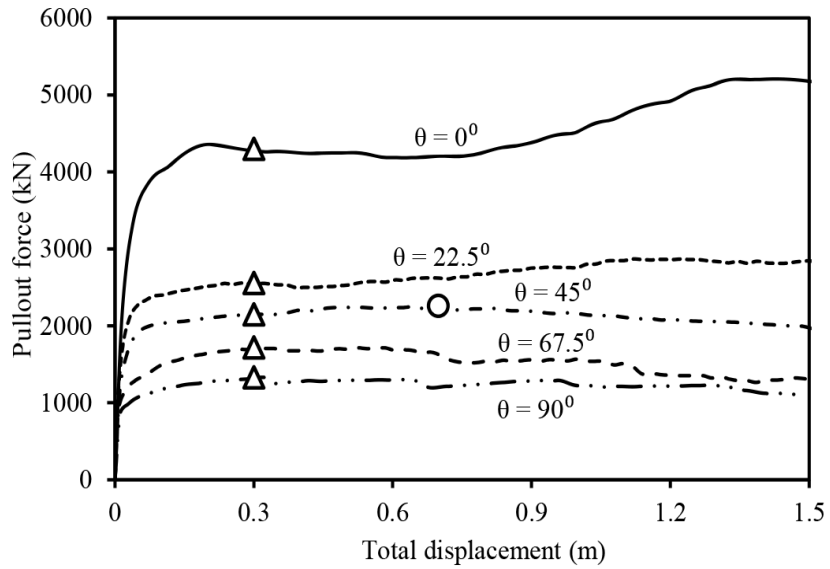


**Figure 3.8:** Force-displacement curve for 95% mooring position

### 3.5.3 Pullout Capacity

The pullout capacities for different loading angles and mooring positions are shown in Fig. 3.9. The lines with open symbols represent the FE results, while the data points of the

corresponding solid symbol show the centrifuge test results (Bang et al., 2011) of similar conditions. The pullout capacities obtained from the present FE analysis follow the similar trend to that obtained in the centrifuge tests (Bang et al., 2011). For a given mooring position, the maximum pullout capacity is obtained for lateral loading ( $\theta = 0^\circ$ ), while the minimum pullout capacity is obtained for  $\theta = 90^\circ$ . The difference between the pullout capacity for  $\theta = 90^\circ$  and  $\theta = 67.5^\circ$  is very small for mooring position up to 75%, because in these cases the caisson moves almost vertically. Note that, even at  $\theta = 90^\circ$  the caisson does not move purely vertically as the pad eye is located on one side of the caisson and therefore some counterclockwise rotation has occurred. The maximum pullout capacity is developed approximately at 75% mooring position for  $\theta \leq 45^\circ$ .

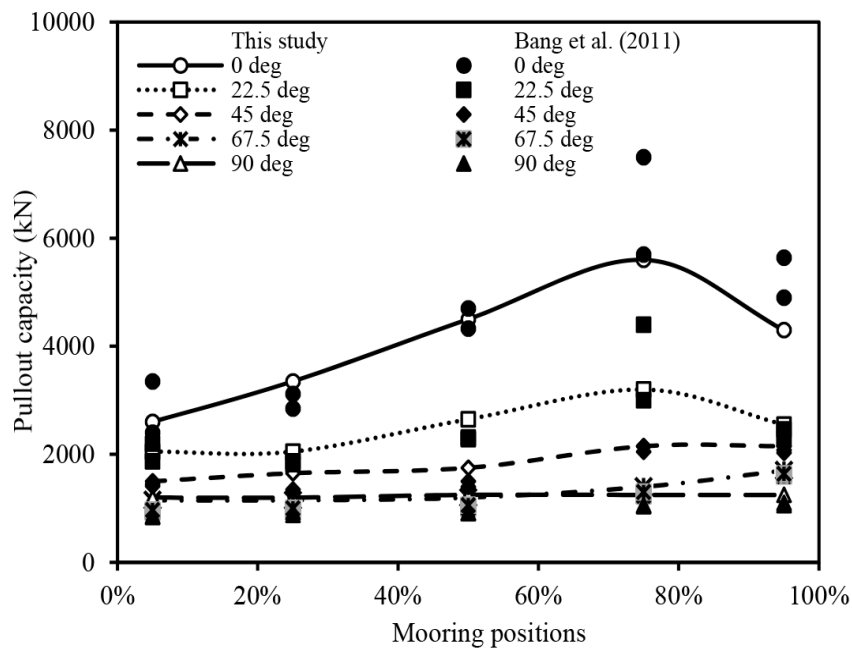


**Figure 3.9:** Comparison of pullout capacity between FE and centrifuge tests

### 3.5.4 Rotation

The rotation of the caisson has a significant effect on force-displacement behavior. The rotation of the caisson about the geometric center with total displacement is plotted in Figs. 3.10 to 3.14 for different mooring positions and different load inclination angles. The sign convention used for rotations is shown in Fig. 3.1c in which positive value represents clockwise rotation. As shown in Fig. 3.10 for the 5% mooring position, the caisson rotates clockwise for  $\theta = 0^\circ$ ,  $22.5^\circ$  and  $45^\circ$ . However, for  $\theta = 90^\circ$ , a counterclockwise rotation is observed. For  $\theta = 67.5^\circ$ , very small rotation of the caisson is observed. A similar trend is found for the 25% and 50% mooring positions (Figs. 3.11 and 3.12). The opposite trend of rotation is noticed for the 75% and 95% mooring positions (Figs. 3.13 and 3.14). In these cases, the caisson rotates in the counterclockwise direction.

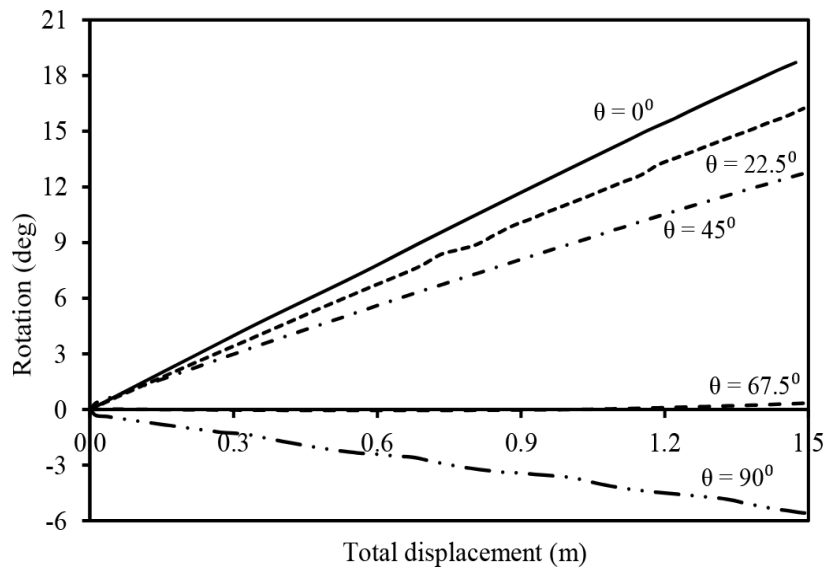


**Figure 3.10:** Rotation-displacement curve for 5% mooring position

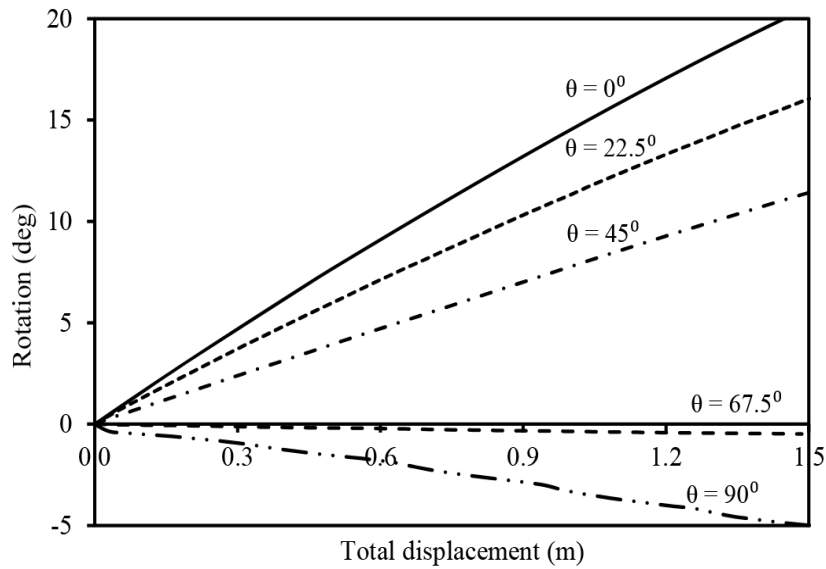


**Figure 3.11:** Rotation-displacement curve for 25% mooring position

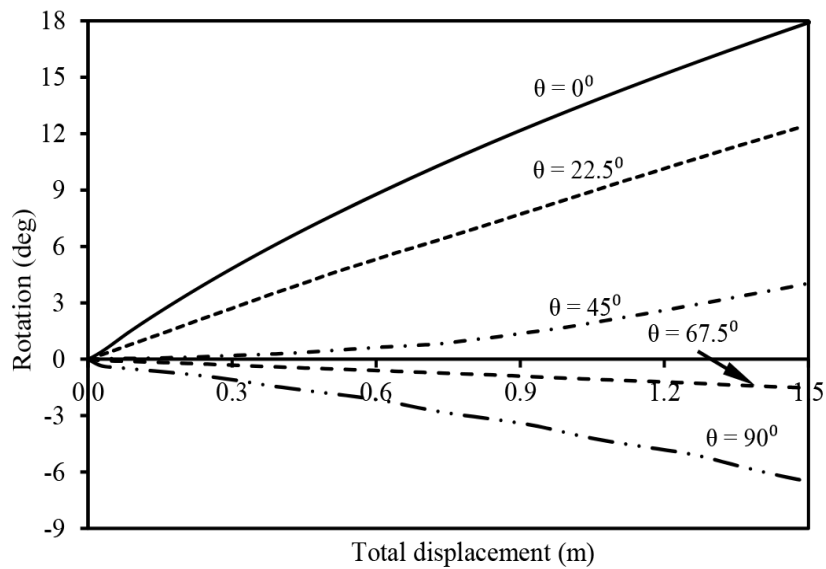


**Figure 3.12:** Rotation-displacement curve for 50% mooring position

The rotation of the caisson with pullout force is plotted in Figs. 3.15 to 3.19. As shown in Figs. 3.15 to 3.17, the maximum clockwise rotation (+ve) has occurred for  $\theta = 0^\circ$  at the 5%, 25% and 50% mooring positions. The rotation is decreased with increase in  $\theta$  and

becomes negative (counterclockwise) for  $\theta = 67.5^\circ$  and  $90^\circ$ . On the other hand, rotation is negative for all  $\theta$  at 75% and 95% mooring positions (Figs. 3.18 and 3.19). The pattern of rotation obtained from the present FE analyses is very similar to model test results of Gao et al. (2013). The open triangles in Figs. 3.15 to 3.19 show the pullout capacity ( $0.1D$  displacement). As shown, the rotation of the caisson is significantly different at the pullout capacity for different values of  $\theta$  and mooring positions.

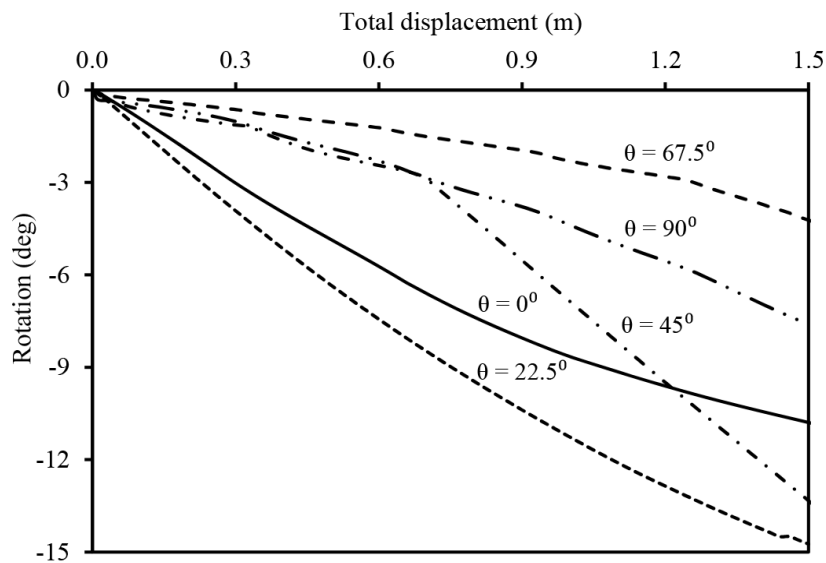


**Figure 3.13:** Rotation-displacement curve for 75% mooring position

The rotation of the caisson at the pullout capacity ( $0.1D$  displacement) is shown in Fig. 3.20 for different mooring positions and load inclination angles. The clockwise positive rotation has occurred for the 5%, 25% and 50% mooring positions for  $\theta = 0^\circ$ ,  $22.5^\circ$  and  $45^\circ$ . The maximum positive rotation has occurred for the 50% mooring position at  $\theta = 0^\circ$ . On the other hand, counterclockwise (negative) rotation has occurred for the 75% and 95% mooring positions. Very small rotation is calculated for large values of  $\theta$  ( $= 67.5^\circ$  and

90°), which is also almost independent of mooring position. This is one of the reasons of calculating similar pullout capacity at these loading angles, as shown in Fig. 3.9.

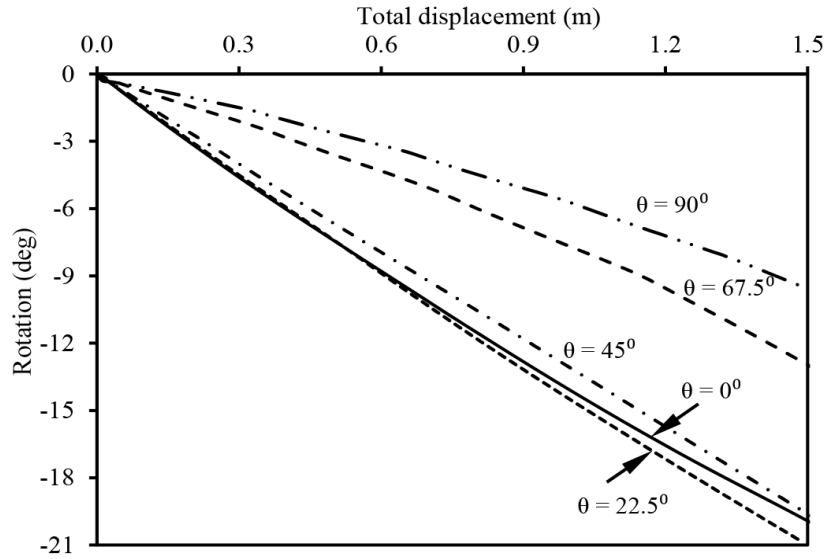


**Figure 3.14:** Rotation-displacement curve for 95% mooring position

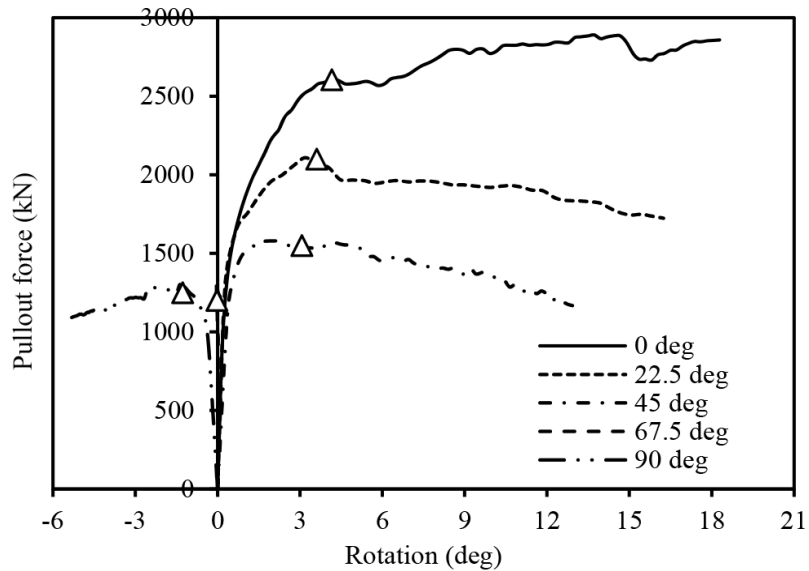


**Figure 3.15:** Force-rotation curve for 5% mooring position

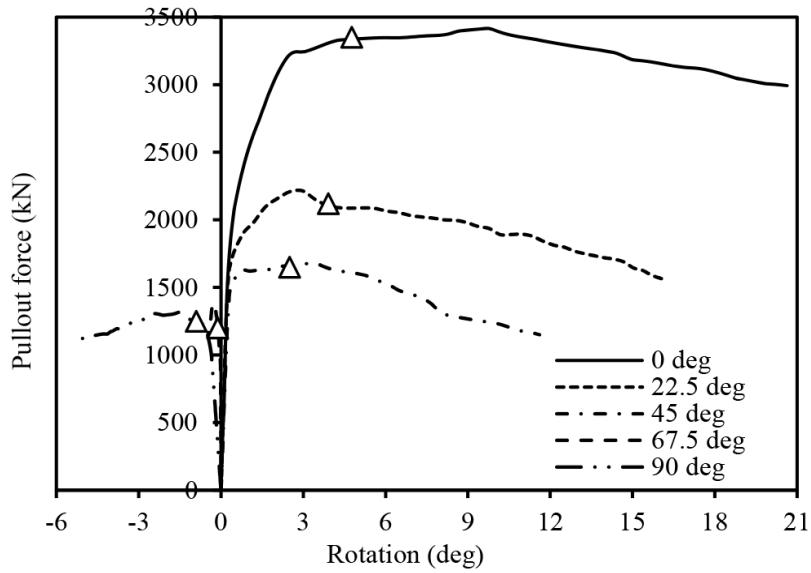


**Figure 3.16:** Force-rotation curve for 25% mooring position

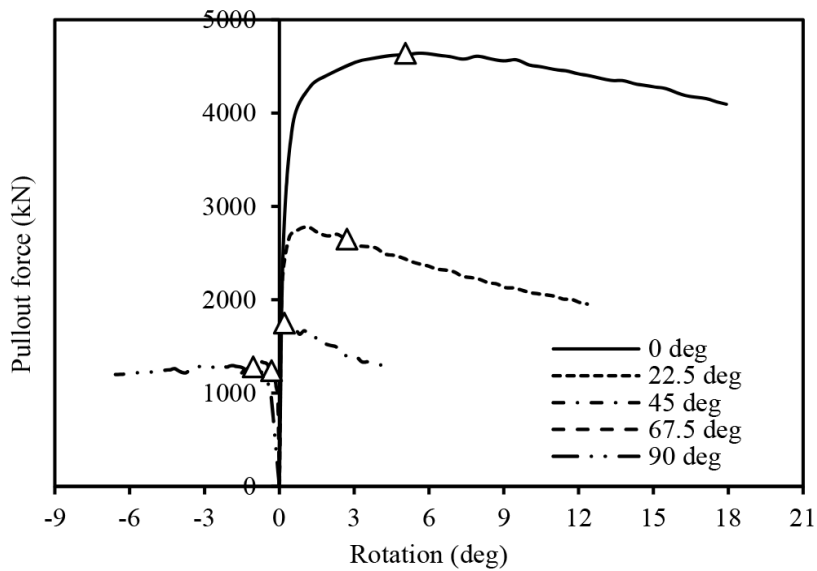


**Figure 3.17:** Force-rotation curve for 50% mooring position

### 3.5.5 Lateral Displacement

Figure 3.21 shows the lateral displacement of the geometric centerline of the caisson with depth for different mooring positions at  $\theta = 0^\circ$  at the pullout capacity ( $0.1D$  displacement).

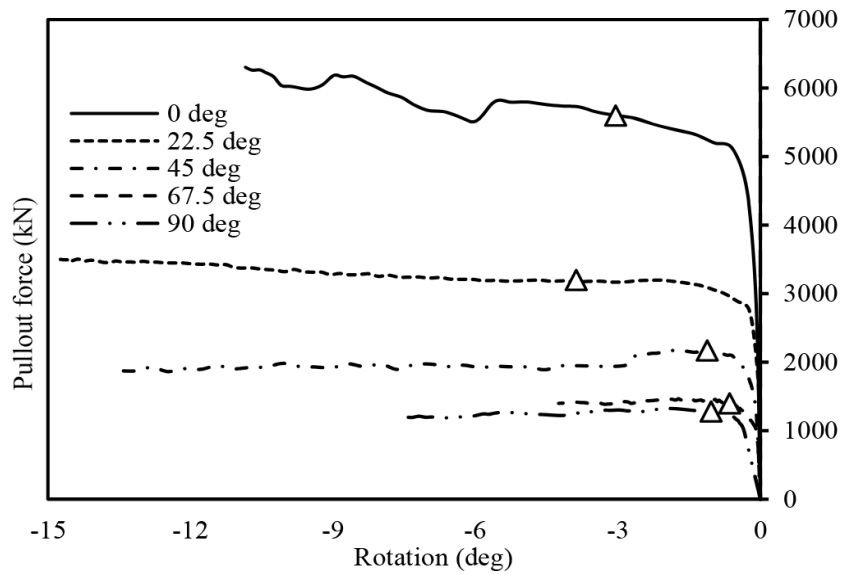


**Figure 3.18:** Force-rotation curve for 75% mooring position

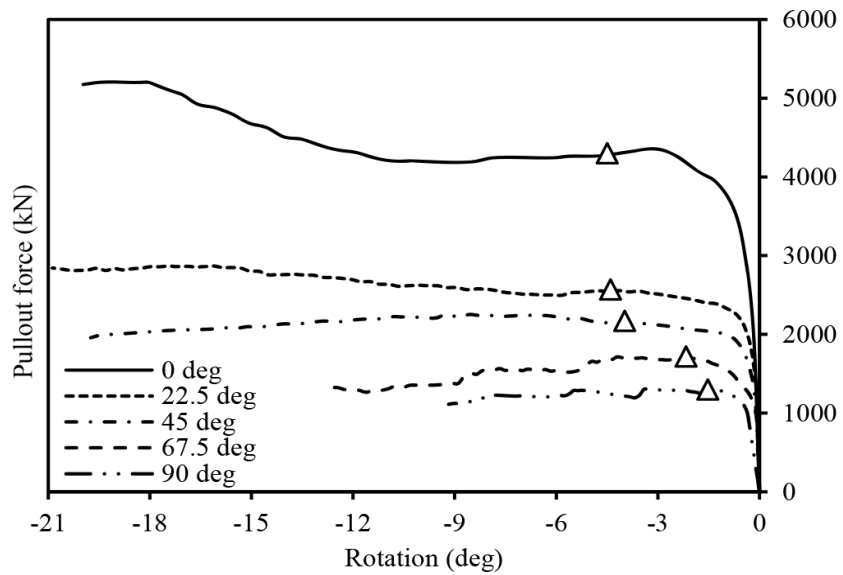


**Figure 3.19:** Force-rotation curve for 95% mooring position

The lateral displacements for loading at the 5%, 25% and 50% mooring positions are opposite to that of the 75% and 95% mooring positions. The minimum lateral displacement and rotation of the caisson have occurred for loading at  $\theta = 0^\circ$  and the 75% mooring

position.

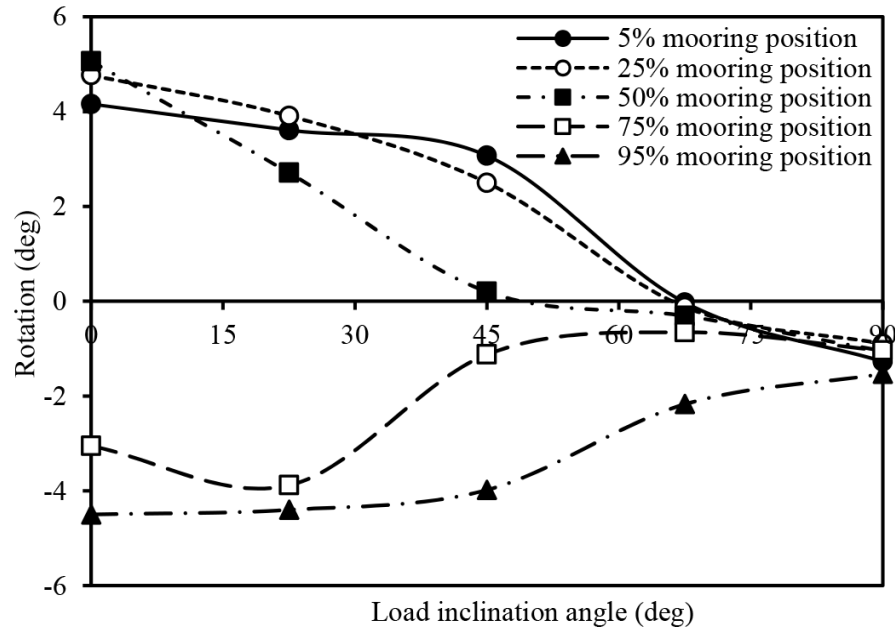


Figure 3.20: Rotation of caisson at pullout capacity

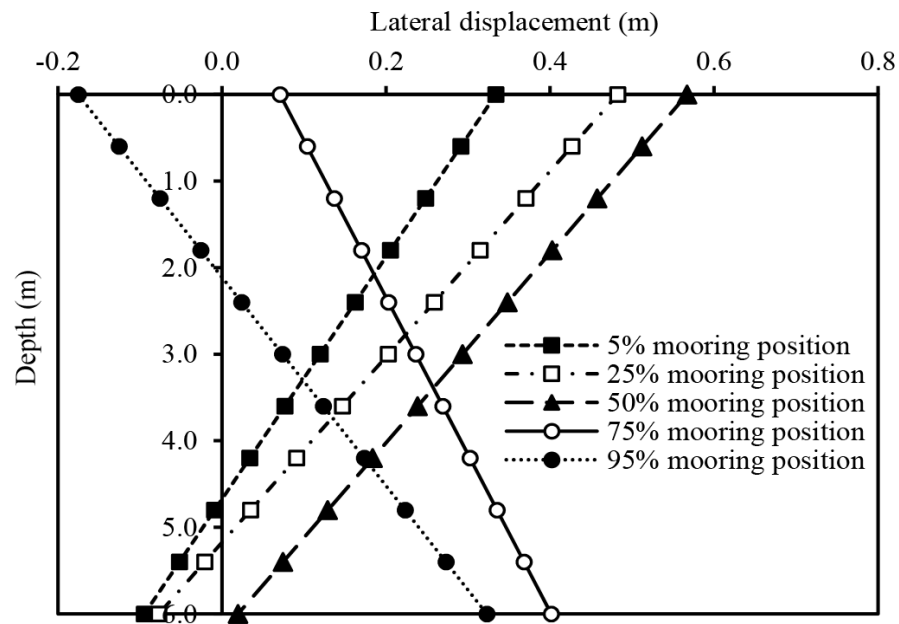


Figure 3.21: Lateral displacement of caisson for  $\theta = 0^\circ$

### 3.5.6 Shape of Soil Failure Wedge

The shape of the failure wedge of soil due to inclined loading applied on the caisson is dependent on mooring position and loading angle. The maximum principal plastic strain and the magnitude of total displacements for loading at the 25% and 75% mooring positions at  $\theta = 0^\circ$  are shown in Figs. 3.22 and 3.23, respectively. As shown in Fig. 3.22a, significant plastic strain develops in a narrow zone in the right side of the caisson, and a wedge of soil is pushed upward forming heave in the right side of the caisson. The plastic strain inside the wedge is not very significant. The movement of this wedge is governed by the passive resistance of the soil. In the left side, a gap is formed near the bottom of the caisson and a wedge of soil moves downward resulting in settlement at the seabed. This gap is possibly due to the very low value of cohesion used in the FE analyses. The failure of this soil wedge is mainly governed by the active failure condition.

When the caisson is loaded at the 25% mooring position, the rotation is in the opposite direction of the rotation for the 75% mooring position. Therefore, the soil failure pattern is different, as shown in Fig. 3.23. The formation of the failure wedge in the  $xy$  plane for different mooring positions and loading angles obtained from the present FE analyses is shown schematically in Figs. 3.24 and 3.25. When the caisson is loaded at  $\theta = 67.5^\circ$  and  $90^\circ$ , the caisson rotates counterclockwise and failure wedges (as shown in Fig. 3.24) are formed irrespective of the mooring positions. On the other hand, when the caisson is loaded at  $\theta = 0^\circ, 22.5^\circ$  and  $45^\circ$ , the failure pattern depends on the mooring position because

the caisson rotates in a different direction (Fig. 3.25). When the caisson is loaded at the 5%, 25% and 50% mooring positions, the failure wedge shown in Fig. 3.25a is formed. However, when it is loaded at the 75% and 95% mooring positions, a larger passive wedge is formed, as shown in Fig. 3.25b. This important phenomenon should be considered in the calculation of the pullout capacity of the caisson.

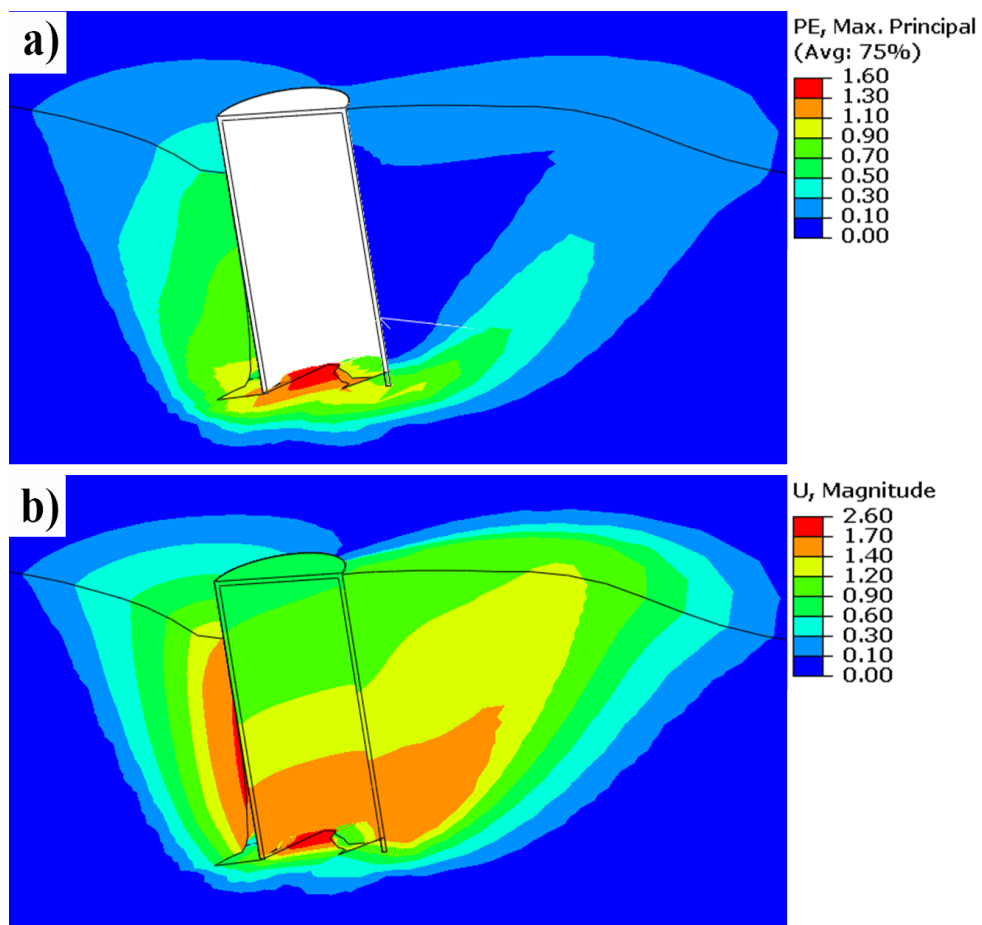


**Figure 3.22:** Maximum principal plastic strain and total displacement profile for 75% mooring position and 1.5 m displacement at  $\theta = 0^\circ$

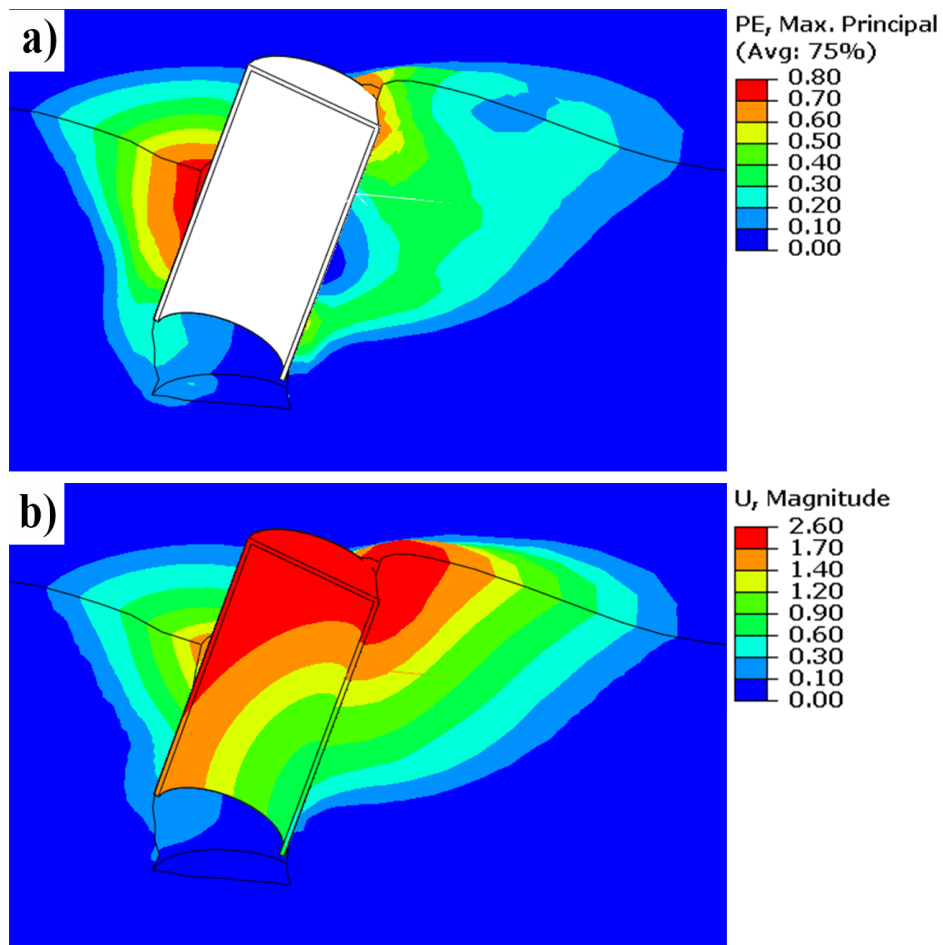


**Figure 3.23:** Maximum principal plastic strain and total displacement profile for 25% mooring position and 1.5 m displacement at  $\theta = 0^\circ$

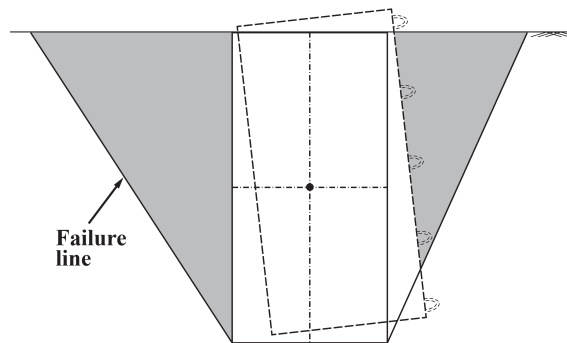


**Figure 3.24:** Failure wedge for  $\theta = 67.5^\circ$  and  $90^\circ$  and all mooring positions

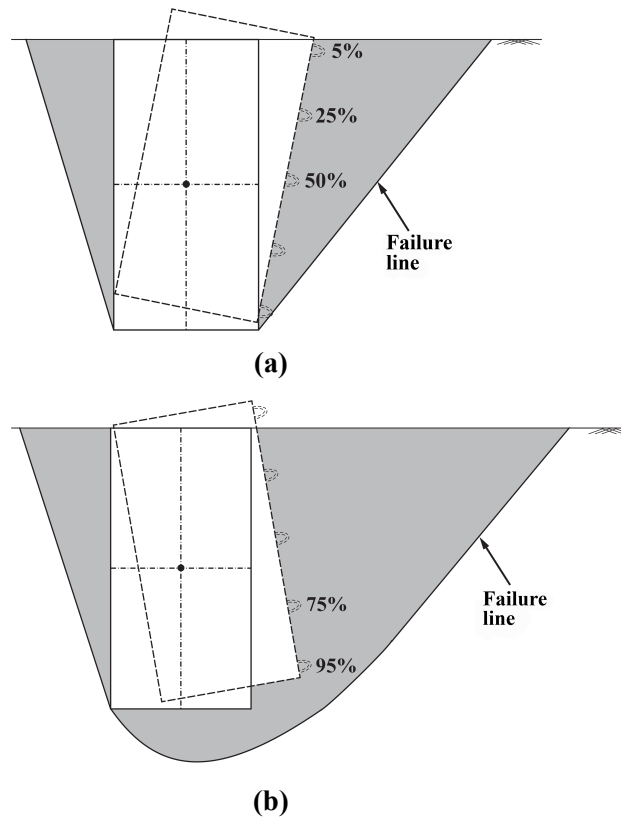


**Figure 3.25:** Failure wedge for  $\theta = 0^\circ, 22.5^\circ$  and  $45^\circ$ : (a) mooring positions 5%, 25% and 50%, (b) mooring positions 75% and 95%

### 3.6 Effect of Aspect Ratio ( $L/D$ )

The results presented in the previous sections are for the base case, where length  $L = 6$  m and diameter  $D = 3$  m are used. In this section, the pullout capacities for different  $L/D$  ratios are presented. A total of 35 additional analyses are performed to investigate the effect of  $L/D$  ratio on pullout capacity. The dimensions of the caisson are listed in Table 3.2. All the analyses are conducted for the 5%, 25%, 50%, 75% and 95% mooring positions. Only one value of  $\theta (= 0^\circ)$  is used and the results are compared with the centrifuge tests results of Jang and Kim (2013) where the applied load was in the lateral direction. The

soil parameters used in the analysis are listed in Table 3.1. The typical force-displacement curves for the 50% mooring position with different  $L/D$  ratios are shown in Fig. 3.26. The pullout force and displacement are normalized as in Deng and Carter (2000), where  $\sigma'_v$  is the initial vertical effective stress at the bottom of the caisson. The normalization with  $\sigma'_v$  is required because the shear strength of sand depends on effective stress, and for a given  $L/D$  ratio,  $\sigma'_v$  is higher for larger-diameter caissons than for smaller-diameter caissons. As shown in Fig. 3.26, the normalized pullout force increases with an increase in the  $L/D$  ratio, and for a given  $L/D$  ratio, the normalized force is slightly higher for  $L = 6$  m than for  $L = 9$  m.

The normalized pullout capacity for different mooring positions is shown in Fig. 3.27. For all four  $L/D$  ratios, the maximum pullout force is obtained for the 75% mooring position. Although limited, the centrifuge test results of Jang and Kim (2013) are also shown in Fig. 3.27. The present FE results compare well the centrifuge test results.

**Table 3.2:** Geometric parameters for different aspect ratios

$L/D$	$L$ (m)	$D$ (m)	$L$ (m)	$D$ (m)
1.5	9	6	6	4
2.0	9	4.5	6	3
2.5	9	3.6	6	2.4
3.0	9	3	6	2

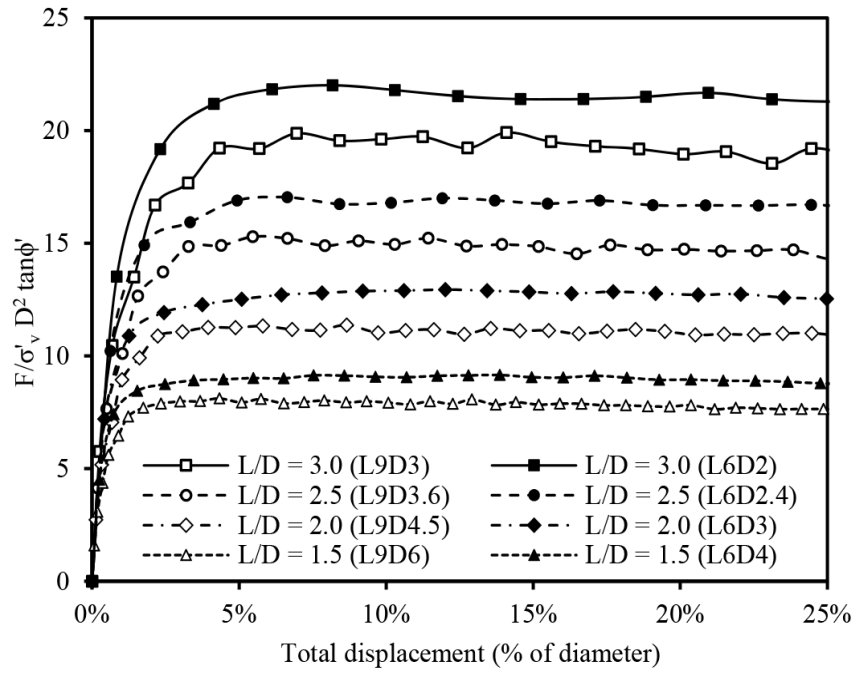


**Figure 3.26:** Normalized Force-displacement curves for 50% mooring position

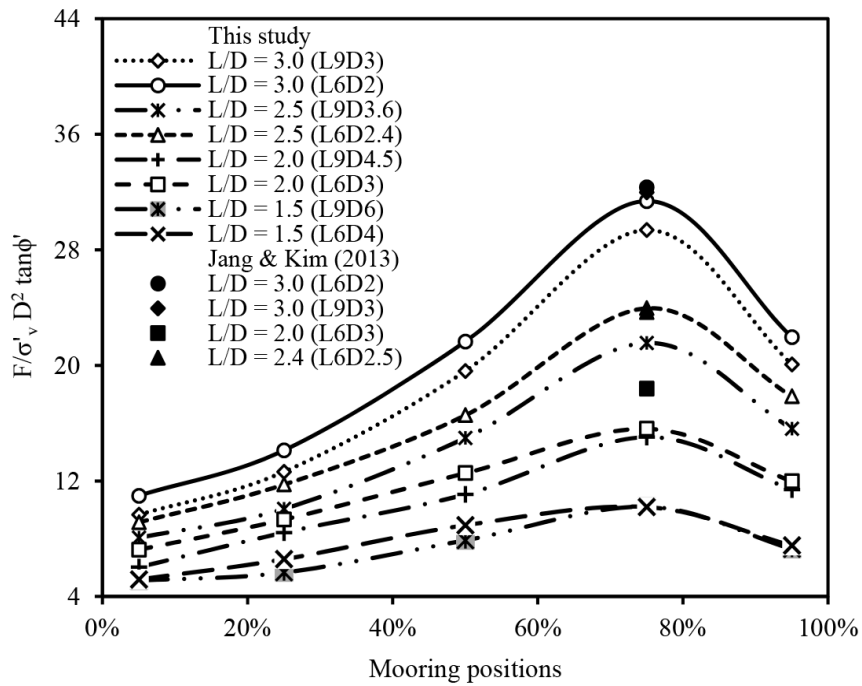


**Figure 3.27:** Normalized pullout capacity for  $\theta = 0^\circ$  for different mooring positions

### 3.7 Analyses Using Modified Mohr-Coulomb Model

In the analyses presented in the previous section, the built-in Mohr-Coulomb model is used where constant values of  $\phi'$  and  $\psi$  are assigned. However, in laboratory tests, dense sand shows postpeak softening behavior and the behavior of sand also depends on the mode of shearing, such as triaxial shear (TX), direct shear (DS) or direct simple shear (DSS) conditions. In this section, FE analyses are performed using a modified Mohr-Coulomb (MMC) model (Roy et al., 2014a), where prepeak hardening, postpeak softening, density and confining pressure-dependent friction and dilation angles are considered. The key features of this model are as follows:

- (i) The difference between the angle of internal friction at the peak ( $\phi'_p$ ) and critical state ( $\phi'_c$ ) increases with increase in relative density ( $D_r$ ) and the reduction of confining pressure.
- (ii) The maximum dilation angle ( $\psi_p$ ) can be calculated as  $\psi_p = (\phi'_p - \phi'_c)/k_\psi$ , where  $k_\psi$  is a soil parameter (Bolton, 1986).
- (iii) The angle of internal friction and the dilation angle are not constant but vary with plastic shear strain  $\gamma^p$ . With an increase in  $\gamma^p$ , the mobilized  $\phi'$  and  $\psi$  increase (i.e., hardening) up to the peak value and then decrease at large  $\gamma^p$  (i.e., softening).

All the above features of dense sand behavior have been modeled using a set of equations listed in Table 3.3. A detailed discussion of this model and its performance are available in Roy et al. (2014a and 2014b). The MMC model has been implemented in Abaqus with

the aid of a user-subroutine written in FORTRAN. The soil parameters used in the present analysis are as follows:  $A_\psi = 3.8$ ,  $k_\psi = 0.6$ ,  $\phi'_{in} = 29^\circ$ ,  $C_1 = 0.22$ ,  $C_2 = 0.11$ ,  $m = 0.25$ ,  $\phi'_c = 31^\circ$  and  $D_r = 80\%$ . The inset in Table 3.3 shows the variation of mobilized  $\phi'$  and  $\psi$  for these soil parameters for  $p' = 50$  kPa.

**Table 3.3:** Equations for Modified Mohr-Coulomb Model (MMC) (after Roy et al., 2014a)

Description	Constitutive Equation	Soil Parameters
Relative density index	$I_R = I_D(Q - \ln p') - R$	$I_D = D_r(\%)/100$ , $Q = 10$ , $R = 1$ (Bolton, 1986)
Peak friction angle	$\phi'_p = \phi'_c + A_\psi I_R$	$\phi'_c$ , $A_\psi$
Peak dilation angle	$\psi_p = \left( \frac{\phi'_p - \phi'_c}{k_\psi} \right)$	$k_\psi$
Strain softening parameter	$\gamma_c^p = C_1 + C_2 I_D$	$C_1$ , $C_2$
Plastic strain at $\phi'_p$	$\gamma_p^p = \gamma_c^p \left( \frac{p'}{p'_a} \right)^m$	$p'_a$ , $m$
Mobilized friction angle at zone-II	$\phi' = \phi'_{in} + \sin^{-1} \left[ \left( \frac{2\sqrt{\gamma^p \gamma_p^p}}{\gamma^p + \gamma_p^p} \right) \sin(\phi'_p - \phi'_{in}) \right]$	
Mobilized dilation angle at Zone-II	$\psi = \sin^{-1} \left[ \left( \frac{2\sqrt{\gamma^p \gamma_p^p}}{\gamma^p + \gamma_p^p} \right) \sin(\psi_p) \right]$	
Mobilized friction angle at zone-III	$\phi' = \phi'_c + \exp \left[ - \left( \frac{\gamma^p - \gamma_p^p}{\gamma_c^p} \right)^2 \right] (\phi'_p - \phi'_c)$	
Mobilized dilation angle at Zone-III	$\psi = \exp \left[ - \left( \frac{\gamma^p - \gamma_p^p}{\gamma_c^p} \right)^2 \right] \psi_p$	

Symbols:  $A_\psi$ : slope of  $(\phi'_p - \phi'_c)$  vs.  $I_R$ ;  $m$ ,  $C_1$ ,  $C_2$ : soil parameters;  $I_R$ : relative density index;  $k_\psi$ : slope of  $(\phi'_p - \phi'_c)$  vs.  $\psi_p$ ;  $\phi'_{in}$ :  $\phi'$  at the start of plastic deformation;  $\phi'_c$ : critical state friction angle;  $\gamma^p$ : engineering plastic shear strain

As mentioned before, constant values of  $\phi'$  and  $\psi$  are commonly used in the design of pile foundations. The American Petroleum Institute (API, 1987) recommended that  $\phi'$  (in degrees) can be estimated as  $\phi' = 16D_r^2 + 0.17D_r + 28.4$ . For  $D_r = 80\%$ ,  $\phi' = 39^\circ$  is calculated. Now using  $\phi' = 39^\circ$  and  $\psi = 9^\circ$  an analysis has been also performed using MC model.

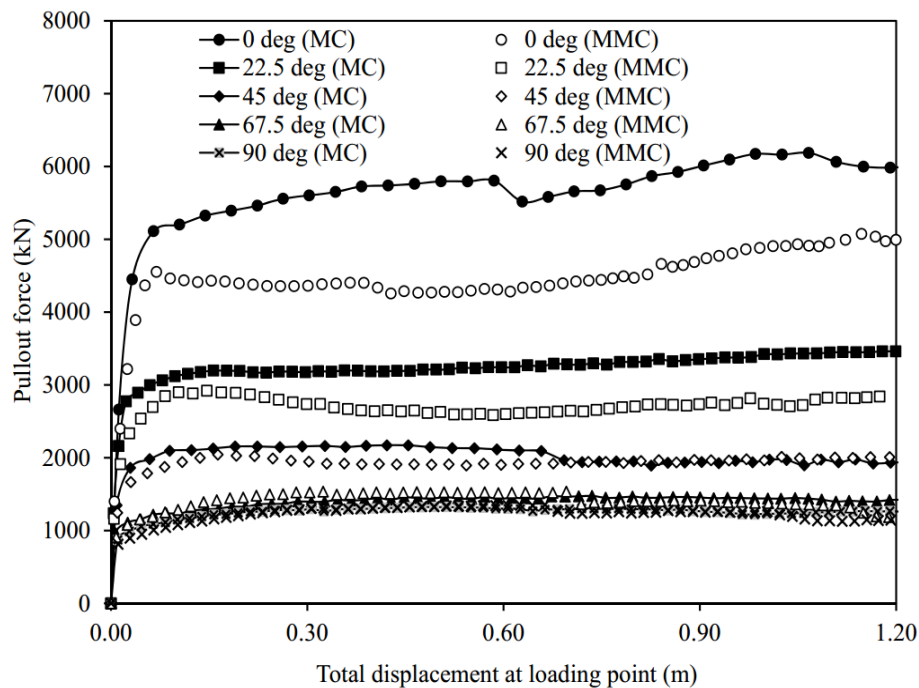


**Figure 3.28:** Force-displacement curve for 75% mooring position with MC and MMC model

Figure 3.28 shows the pullout force for the base case caisson geometry loaded at the 75% mooring position. For lower values of  $\theta$  ( $\leq 45^\circ$ ) the pullout force is higher for the MC model than that for the MMC model. The difference reduces with an increase in  $\theta$ . In order to explain the mechanisms, the plastic shear strains developed at 10% and 30% pad eye

displacement for  $\theta = 0^\circ$  are plotted in Fig. 3.29. Figure 3.29 shows that the size of the passive failure wedge obtained by the MC model is slightly larger than that obtained by the MMC model, which is one of the contributing factors of the higher pullout capacity by the MC model (Fig. 3.26).

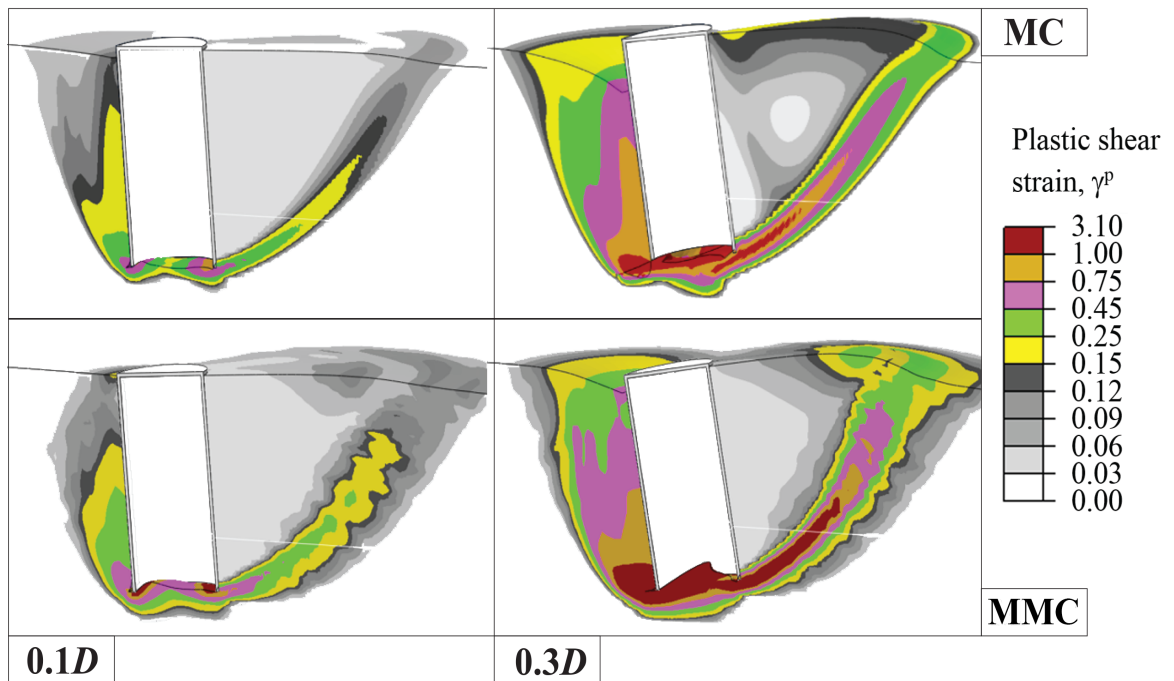


**Figure 3.29:** Development of plastic shear strain at  $0.1D$  and  $0.3D$  pad eye displacement

Figure 3.30 shows the mobilized  $\phi'$  and  $\psi$  at these pad eye displacements for the MMC model. As shown in the inset of Table 3.3, the maximum  $\phi'$  and  $\psi$  are mobilized at  $\gamma_p^p$ , and their values are less than the peak values in the prepeak ( $\gamma^p < \gamma_p^p$ ) or in the postpeak ( $\gamma^p > \gamma_p^p$ ) zones. The left side of Fig. 3.30 shows that, at 10% displacement, the postpeak condition is developed near the caisson (colored zone), while the gray zones represent the prepeak shear zones where some plastic shear strains develop, although less than  $\gamma_p^p$ .

With the increase in displacement, plastic shear strain increases along the failure plane that reduces the mobilized  $\phi'$  and  $\psi$  to the critical state. In other words, the mobilized  $\phi'$  and  $\psi$  are not constant along the failure plane in the simulation with the MMC model. On the other hand, with the MC model, they are constant ( $\phi' = 39^\circ$  and  $\psi = 9^\circ$ ).

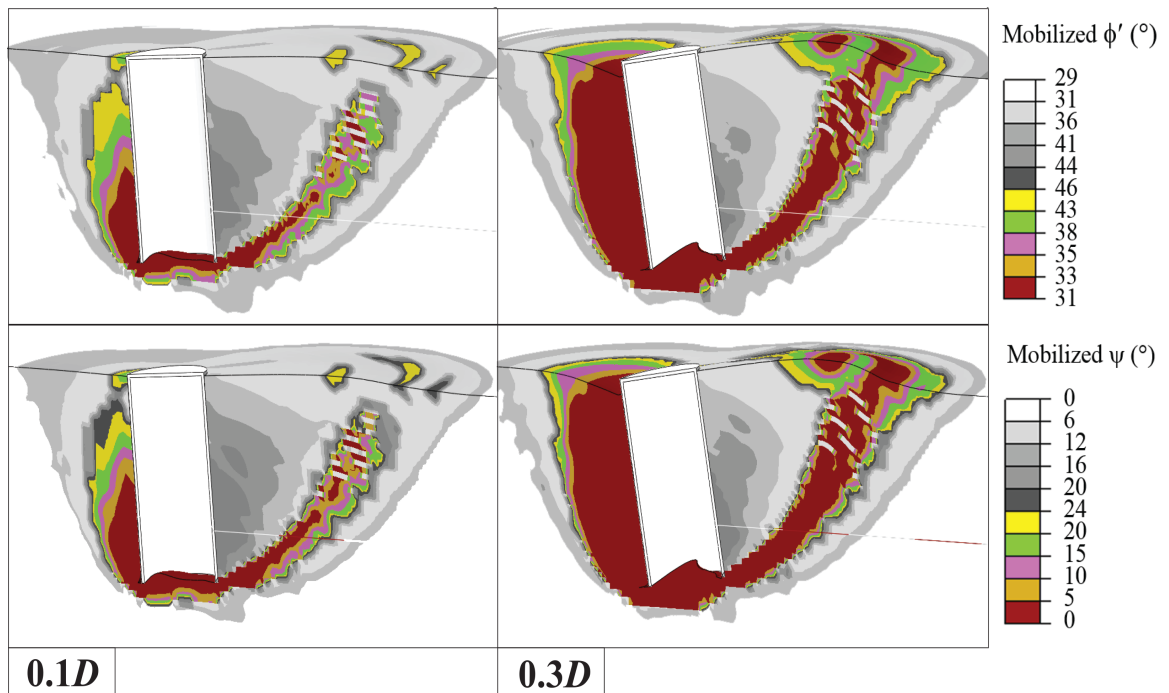


**Figure 3.30:** Mobilized  $\phi'$  and  $\psi$  using MMC for  $0.1D$  and  $0.3D$  pad eye displacement

From the above analyses, it can be concluded that, although the force-displacement curves could be matched, the mobilized shear strength in the soil is different for the MC and MMC models.

### 3.8 Conclusions

Comprehensive three-dimensional FE analyses are performed to investigate the response of suction caissons in dense sand subjected to oblique loading. The analyses are performed using Abaqus/Explicit FE software. The effects of constitutive behavior of sand on pullout capacity are examined using two soil-constitutive models. In the first set of analyses, the built-in elastic perfectly plastic Mohr-Coulomb (MC) model in Abaqus is used. The second set analyses are conducted to capture the prepeak hardening, postpeak softening, and effects of density and confining pressure on stress-strain behavior of dense sand by employing a modified form of Mohr-Coulomb model (MMC) with the aid of a user-subroutine. Large displacements are applied to examine the effects of rotation of the caisson on pullout force. The results obtained from the present FE analyses compare well with available centrifuge test results. The pullout capacity is also examined for three key factors: mooring position, load inclination angle and  $L/D$  ratio.

When the MC model is used, the pullout force at  $0.1D$  can be used as pullout capacity for the cases analyzed. The pullout force decreases at large displacement except for  $\theta = 0^\circ$ . The upward movement and rotation of the caisson are the causes of the reduction of force. The rotation of the caisson at the pullout capacity varies with  $\theta$  and mooring position. The rotation has a significant effect on pullout capacity. The failure wedge formed as a result of displacement of the caisson is a function of  $\theta$  and mooring position. The maximum pullout capacity is obtained for 75% mooring position at  $\theta = 0^\circ$ . Moreover, the increase of  $L/D$

ratio increases the normalized pullout capacity.

For the MMC model, the pullout force is slightly lower than that for the MC model, and the difference between these two is higher for low load inclination angles. Noticeable postpeak degradation is found for  $\theta \leq 45^\circ$ . Although the force-displacement curves could be matched, the mobilized  $\phi'$  and  $\psi$  are different in the MC and MMC models along the failure plane.

### **3.9 Acknowledgements**

The work presented in this paper has been funded by a Discovery grant from the Natural Sciences and Engineering Research Council of Canada (NSERC), Mitacs, and Petroleum Research Newfoundland & Labrador (PRNL). The authors express their thanks to Md. Iftekharruzaman and Kshama Roy for their help with FE model development.

## Bibliography

Achmus, M, Akdag, CT and Thieken, K (2013). Load-bearing behavior of suction bucket foundations in sand. *Applied Ocean Research*, Vol. 43, pp. 157–165.

Allersma, HGB, Brinkgreve, RBJ, Simon, T and Kirstein, AA (2000). Centrifuge and Numerical Modelling of Horizontally Loaded Suction Piles. *International Journal of Offshore and Polar Engineering*, Vol. 10, No. 3, pp. 222–228.

API (1987). Recommended practice for planning, designing and constructing fixed offshore platforms. *API Recommended practice 2A (RP2A)*, 17th ed., American Petroleum Institute.

Aubeny, CP, Han SW and Murff, JD (2003). Inclined load capacity of suction caissons. *International Journal for Numerical and Analytical Methods in Geomechanics*, Vol. 27, pp. 1235–1254.

Bang, S, Jones, KD, Kim, KO, Kim, YS and Cho, Y (2011). Inclined loading capacity of suction piles in sand. *Journal of Ocean Engineering*, Vol. 38, pp. 915–924.

Bolton, MD (1986). The strength and dilatancy of sand. *Géotechnique*, Vol. 36, No. 1, pp. 65–78.

Cao, J, Phillips, R, Audibert, JME and Al-Khafazi, Z (2002b). Numerical analysis of the

- behavior of suction caissons in clay. *Proc. of the 12th International Offshore and Polar Engineering Conference*, Kitakyushu, Japan, May 26-31, pp. 795–799.
- Cao, J, Phillips, R, Popescu, R, Al-Khafaji, Z, and Audibert, JME (2002a). Penetration resistance of suction caissons in clay. *Proc. of the 12th International Offshore and Polar Engineering Conference*, Kitakyushu, May 26-31, pp. 800–806.
- Cao, J, Phillips, R, Popescu, R, Audibert, JME and Al-Khafaji, Z (2003). Numerical analysis of the behavior of suction caissons in clay. *International Journal of Offshore and Polar Engineering*, Vol. 13, No. 2, pp. 154–159.
- CFEM (2006). Canadian Foundation Engineering Manual. 4th ed., *Canadian Geotechnical Society*, Richmond, BC, Canada.
- Coduto, DP (2011). *Foundation design: Principles & practices*, 2nd ed., Prentice Hall, Upper Saddle River, New Jersey, United States.
- Deng, W, and Carter, JP (2000). Inclined uplift capacity of suction caissons in sand. *Offshore Technology Conference*, Houston, Texas, OTC 12196, pp. 809–820.
- Gao, Y, Qiu, Y, Li, B, Li, D, Sha, C and Zheng, X (2013). Experimental studies on the anti-uplift behavior of the suction caissons in sand. *Applied Ocean Research*, Vol. 43, pp. 37–45.
- Handayanu, Swamidass ASJ, Booton M (2000). Ultimate strength of offshore tension foundations under vertical and inclined loads. *Proc. of the International Conference*

- on Offshore Mechanics and Arctic Engineering*, New Orleans, Louisiana, Vol. 2, pp. 95–100.
- Hardin, BO and Black, WL (1966). Sand stiffness under various triaxial stresses. *Journal of the Soil Mechanics and Foundations Division*, Vol. 92, No. 2, pp. 27–42.
- Houlsby, GT and Byrne, BW (2005a). Calculation procedures for installation of suction caissons in sand. *Proc ICE - Geotechnical Engineering*, Vol. 158, No 3, pp. 135–144.
- Houlsby, GT and Byrne, BW (2005b). Calculation procedures for installation of suction caissons in clay and other soils. *Proc ICE - Geotechnical Engineering*, Vol. 158, No 2, pp. 75–82.
- Iftekhharuzzaman, Md and Hawlader, B (2012). Numerical modeling of pullout capacity of a suction pile in sand under oblique load. *Second International Conference on Geotechnique, Construction Materials and Environment*, Kuala Lumpur, Malaysia, Nov. pp. 14–16.
- Janbu, N (1963). Soil Compressibility As Determined By Oedometer And Triaxial Test. *Proc. of 3rd European Conference on Soil Mechanics and Foundation Engineering*, Wiesbaden, Germany, Vol. 1, pp. 19–25.
- Jang, YS and Kim, YS (2013). Centrifugal Model Behavior of Laterally Loaded Suction Pile in Sand. *KSCE Journal of Civil Engineering*, Vol. 17, No. 5, pp. 980–988.

- Jones, KD, Bang, S and Cho, Y (2007). Pullout capacity of embedded suction anchors in sand. *Journal of Ocean Engineering*, Vol. 34, no. 16, pp. 2107–2114.
- Kim, KO, Kim, YS, Cho, Y, Bang, S and Jones, K (2009). Centrifuge Model Tests on Suction Piles in Sand under Inclined Loading. *Proc. of the Nineteenth International Offshore and Polar Engineering Conference*, Osaka, Japan, June 21–26, Vol. II, pp.191–196.
- Kim, Y, Kim, K, Cho, Y and Bang, S (2010). Centrifuge model tests on suction pile pullout loading capacity in sand. *Int. Conf. on Physical Modelling in Geomechanics*, Vol. 2, pp. 787–792.
- Kim, YS, Kim, KO, Cho, Y, Bang, S and Jones, K (2005). Centrifuge Model Tests on Embedded Suction Anchors. *Proc. of the Fifteenth International Offshore and Polar Engineering Conference*, Seoul, Korea, June 19–24, Vol. II, pp.431–435.
- Lee, SH, Cho, Y, Kim, KO, Kim, YS, Lee, TH, and Kwag, DJ (2003). Centrifuge model tests on embedded suction anchor loading capacities. *Proc. of The Thirteenth International Offshore and Polar Engineering Conference*, Honolulu, Hawaii, USA, May 25–30, Vol. II, pp. 789–793.
- Potyonody, JG (1961). Skin friction between various soils and construction materials. *Géotechnique*, Vol. 11, No. 4, pp. 339–353.
- Roy, K, Hawlader, B and Kenny, S (2014a). Influence of Low Confining Pressure in Modeling of Lateral Pipeline/Soil Interaction in Dense Sand. *Proc. of the ASME*

- 2014 33rd International Conference on Ocean, Offshore and Arctic Engineering, San Francisco, California, USA, June 8–13, pp. V06BT04A050.
- Roy, K, Hawlader, B, Kenny, S and Moore, I (2014b). Finite element modeling of uplift pipeline/soil interaction in dense sand. *Geohazards6*, Kingston, Ontario, Canada, June 15–18.
- Sukumaran, B, McCarron, WO, Jeanjean, P and Abouseeda, H (1999). Efficient finite element techniques for limit analysis of suction caissons under lateral loads. *Computers and Geotechnics*, Vol. 24, pp. 89–107.
- Tiwari, B and Al-Adhadh, AR (2014). Influence of Relative Density on Static Soil–Structure Frictional Resistance of Dry and Saturated Sand. *Geotechnical and Geological Engineering*, Vol. 32, pp. 411–427.
- Tiwari, B, Ajmera, B and Kaya, G (2010). Shear strength reduction at soil–structure interaction. *GeoFlorida 2010: Advances in Analysis, Modeling & Design*, Orlando, Florida, United States, February 20–24, pp. 1747–1756.
- Tran, MN, Randolph, MF and Airey, DW (2007). Installation of suction caissons in sand with silt layers. *Journal of Geotechnical and Geoenvironmental Engineering*, Vol. 133, No. 10, pp. 1183–1191.
- Zdravkovic, L, Potts, DM, and Jardine, RJ (2001). A parametric study of the pull-out capacity of bucket foundations in soft clay. *Géotechnique*, Vol. 51, No. 1, pp. 55–67.

## **Chapter 4**

# **Numerical Analysis of Large-Diameter Monopiles in Dense Sand Supporting Offshore Wind Turbines**

### **Co-Authorship**

Chapter 4 is prepared according to the Guidelines for Manuscript Format Theses in the Faculty of Engineering and Applied Science at Memorial University. This part of the research has been submitted for publication as:

Ahmed, SS, and Hawlader, BC (2015). Numerical Analysis of Large Diameter Monopiles in Dense Sand Supporting Offshore Wind Turbines. *Submitted for publication in an international journal*, Under review.

Most of the research work presented in this chapter was conducted by the first author. He also prepared the draft manuscript. The second author supervised the research and reviewed the manuscript.

## 4.1 Abstract

Large-diameter monopiles are widely used foundations for offshore wind turbines. In the present study, three-dimensional finite element (FE) analyses are performed to estimate the static lateral capacity of monopiles in dense sand subjected to eccentric loading. A modified Mohr-Coulomb (MMC) model that considers the pre-peak hardening, post-peak softening and the effects of mean effective stress and relative density on stress-strain behavior of dense sand is adopted in the FE analysis. FE analyses are also performed with the Mohr-Coulomb (MC) model. The load–displacement behavior observed in model tests can be simulated better with the MMC model than the MC model. Based on a parametric study for different length-to-diameter ratio of the pile, a load–moment capacity interaction diagram is developed for different degrees of rotation. A simplified model, based on the concept of lateral pressure distribution on the pile, is also proposed for estimation of its capacity.

**Keywords:** Monopiles; Finite element; Dense sand; Modified Mohr-Coulomb model; Lateral load; Offshore wind turbine.

## 4.2 Introduction

Wind energy is one of the most promising and fastest growing renewable energy sources around the world. Because of steady and strong wind in offshore environments as compared to onshore, along with less visual impact, a large number of offshore wind farms have

been constructed and are under construction. The most widely used foundation system for offshore wind turbines is the monopile, which is a large-diameter (3 – 6 m) hollow steel driven pile having length-to-diameter ratio less than 8 (e.g., LeBlanc et al., 2010; Doherty and Gavin, 2012; Doherty et al., 2012; Kuo et al., 2011). Monopiles have been reported to be an efficient solution for offshore wind turbine foundations in water depth up to 35 m (Doherty and Gavin, 2012). The dominating load on offshore monopile is the lateral load from wind and waves, which acts at a large eccentricity above the pile head.

To estimate the load-carrying capacity of monopiles, the  $p - y$  curve method recommended by the American Petroleum Institute (API, 2011) and Det Norske Veritas (DNV, 2011) are widely used. However, the reliability of the  $p - y$  curve method in monopile design has been questioned by a number of researchers (e.g., Abdel-Rahman and Achmus, 2005; Lesny and Wiemann, 2006; LeBlanc et al., 2010; Doherty and Gavin, 2012; Doherty et al., 2012; Achmus et al., 2009). The API and DNV recommendations are slightly modified form of the  $p - y$  curve method proposed by Reese et al. (1974) mainly based on field tests results of two 610 mm diameter flexible slender piles. However, the large-diameter offshore monopiles behave as a rigid pile under lateral loading. Moreover, in the API recommendations, the initial stiffness of the  $p - y$  curve is independent of the diameter of the pile, which is also questionable. Doherty and Gavin (2012) discussed the limitations of the API and DNV methods to calculate the lateral load-carrying capacity of offshore monopiles.

Monopiles have been successfully installed in varieties of soil conditions; however, the

focus of the present study is to model monopiles in dense sand. Studies have been performed in the past for both static and cyclic loading conditions (e.g., Achmus et al., 2009; Cuéllar, 2011; Ebin, 2012); however, cyclic loading is not discussed further because it is not the focus of the present study. To understand the behavior of large-diameter monopiles in sand, mainly three different approaches have been taken in recent years namely physical modeling, numerical modeling, and modification of the  $p - y$  curves. LeBlanc et al. (2010) reported the response of a small-scale model pile under static and cyclic loading installed in loose and dense sand. Centrifuge tests were also conducted in the past to understand the response of large-diameter monopiles in dense sand subjected to static and cyclic lateral loading at different eccentricities (e.g., Klinkvort et al., 2010; Klinkvort and Hededal, 2011; Klinkvort and Hededal, 2014). Møller and Christiansen (2011) conducted  $1g$  model tests in saturated and dry dense sand. Conducting centrifuge tests using 2.2 m and 4.4 m diameter monopiles, Alderlieste (2011) showed that the stiffness of the load–displacement curves increases with diameter. The comparison of results of centrifuge tests and the API approach shows that the API approach significantly overestimates the initial stiffness of the load–displacement behavior. In order to match test data, Alderlieste (2011) modified the API formulation by introducing a stress dependent stiffness relation. However, the author recognized that the modified API approach still underestimates the load at small displacements and overestimates at large displacements and is therefore recommended for further studies. It is also to be noted here that, small-scale model tests were conducted in the past to estimate the lateral load-carrying capacity of rigid piles and bucket foundations

(e.g., Prasad and Chari, 1999; Lee et al., 2003; Ibsen et al., 2014). However, contradictory evidences of diameter effects warrant further investigations from a more fundamental understanding (Doherty and Gavin, 2012).

Finite element modeling could be used to examine the response of monopiles under eccentric loading. In the literature, FE modeling of large-diameter monopiles is limited as compared to slender piles. Most of the previous FE analyses were conducted mainly using Plaxis 3D and Abaqus FE software. Back-calculated  $p - y$  curves from FE results show that the API recommendations significantly overestimates the initial stiffness (Møller and Christiansen, 2011; Hearn and Edgers, 2010). Overestimation of the ultimate resistance in FE simulation, as compared to model test results, has been also reported in previous study (Møller and Christiansen, 2011). FE modeling also shows that the soil model has a significant influence on load–displacement behavior (Wolf et al., 2013).

Most of the above FE analyses have been conducted using the built-in Mohr-Coulomb (MC) model. In commercial FE software (e.g., Abaqus), the angle of internal friction and dilation angle are defined as input parameters for the MC model. However, laboratory tests on dense sands show post-peak softening behavior with shear strain, which should be considered in numerical modeling for a better understanding of the response of monopiles in dense sand.

The objective of the present study is to conduct FE modeling of monopile foundations for offshore wind turbines under static lateral loading. A realistic model that captures the key features of stress-strain behavior of dense sand is adopted in the FE modeling, which could

explain the load–displacement behavior observed in model tests. A simplified method is also proposed for preliminary estimation of load-carrying capacity of monopile.

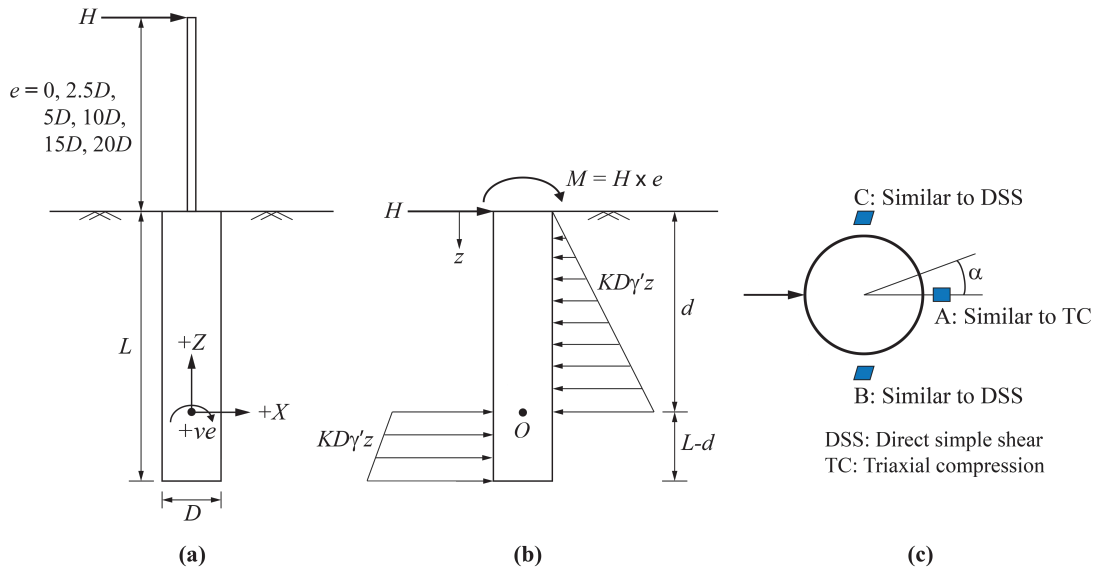


**Figure 4.1:** Problem statement: (a) loading and sign convention, (b) assumed pressure distribution, (c) mode of shearing of soil elements

### 4.3 Finite Element Model

A monopile of length  $L$  and diameter  $D$  installed in dense sand is simulated in this study. During installation, the soil surrounding the monopile can be disturbed. However, the effects of disturbance on capacity are not considered in this study, instead the simulations are performed for a wished-in-place monopile. The monopile is laterally loaded for different load eccentricities as shown in Fig. 4.1 a. Analyses are also performed only for pure moment applied to the pile head. The sign convention used for displacement and rotation of the monopile is also shown in Fig. 4.1a. Figure 4.1b shows an idealized horizontal stress

distribution on the pile. Figure 4.1c shows the loading conditions of the soil elements around the pile. Further discussion on Figs. 4.1b and 4.1c are provided in the following sections.

The FE analyses are performed using Abaqus/Explicit (Abaqus 6.13-1) FE software. Taking the advantage of symmetry, only a half-circular soil domain of diameter  $15D$  and depth  $1.67L$  is modeled (Fig. 4.2). The soil domain shown in Fig. 4.2 is large enough compared to the size of the monopile; and therefore, significant boundary effects are not expected on calculated load, displacement and soil deformation mechanisms; which have been also verified by conducting analyses with larger soil domains. The vertical plane of symmetry is restrained from any displacement perpendicular to it, while the curved vertical sides of the soil domain are restrained from any lateral displacement using roller supports at the nodes. The bottom boundary is restrained from any vertical displacement, while the top boundary is free to displace. The soil and the pile are modeled using the C3D8R solid homogeneous elements available in Abaqus/Explicit element library, which is an 8-noded linear brick element with reduced integration and hourglass control. Typical FE mesh used in this study is shown in Fig. 4.2, which is selected based on a mesh sensitivity analysis. The lateral load ( $H$ ) is applied at a reference point at a distance  $e$  above the pile head along the  $X$  direction. At the pile head, this load generates a lateral load  $H$  and a moment  $M = H \times e$  (Fig. 4.1b). For the pure moment cases, only a moment  $M$  is applied to the pile head without  $H$ .

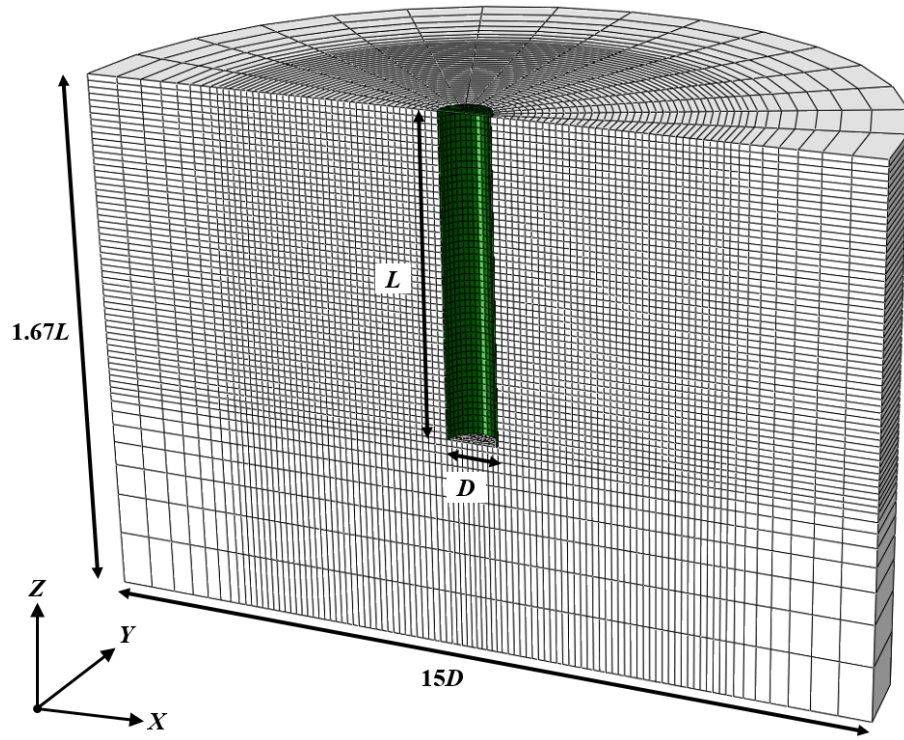


**Figure 4.2:** FE mesh used in this study

### 4.3.1 Modeling of the Monopile

The pile-soil interaction behavior is significantly influenced by the rigidity of pile (e.g., Dobry et al., 1982; Briaud et al., 1983; Budhu and Davies, 1987; Carter and Kulhawy, 1988). To characterize rigid or flexible behavior, Poulos and Hull (1989) used a rigidity parameter,  $R = (E_p I_p / E_s)^{0.25}$ , where  $I_p$  is the moment of inertia of the pile,  $E_p$  and  $E_s$  are the Young's modulus of the pile and soil, respectively. They also suggested that if  $L \leq 1.48R$ , the pile behaves as rigid while it behaves as a flexible pile if  $L \geq 4.44R$ . Monopile used for offshore wind turbine foundations generally behave as a rigid pile (LeBlanc et al., 2010; Doherty and Gavin, 2012). Therefore, all the analysis presented in the following sections, the pile is modeled as a rigid body because it saves the computational

time significantly.

### 4.3.2 Modeling of Sand

The elastic perfectly plastic Mohr-Coulomb (MC) model has been used in the past to evaluate the performance of monopile foundations in sand (e.g., Abdel-Rahman and Achmus, 2006; Sørensen et al., 2009; Achmus et al., 2009; Kuo et al., 2011; Wolf et al., 2013). However, the Mohr-Coulomb model has some inherent limitations. Once a soil element reaches the yield surface, which is defined by the Mohr-Coulomb failure criterion, constant dilation is employed which implies that dense sand will continue to dilate with shearing, whereas laboratory tests on dense sand show that the dilation angle gradually decreases to zero with plastic shearing and the soil element reaches the critical state. In the present study, this limitation is overcome by employing a modified form of Mohr-Coulomb (MMC) model proposed by Roy et al. (2014a,b) which takes into account the effects of pre-peak hardening, post-peak softening, density and confining pressure on mobilized angle of internal friction ( $\phi'$ ) and dilation angle ( $\psi$ ) of dense sand. A summary of the constitutive relationships of the MMC model is shown in Table 4.1. The inset of Table 4.1 shows the typical variation of mobilized  $\phi'$  and  $\psi$  with plastic shear strain ( $\gamma^p$ ). The following are the key features of the MMC model.

The peak friction angle ( $\phi'_p$ ) increases with relative density but decreases with confining pressure, which is a well-recognized phenomena observed in triaxial and direct simple shear (DSS) tests (e.g., Bolton, 1986; Tatsuoka et al., 1986; Hsu and Liao, 1998; Houlsby,

1991; Schanz and Vermeer, 1996; Lings and Dietz, 2004). Mathematical functions for mobilized  $\phi'$  and  $\psi$  with plastic shear strain, relative density and confining pressure have been proposed in the past (Vermeer and deBorst, 1984; Tatsuoka et al., 1993; Hsu and Liao, 1998; Hsu, 2005). Reanalyzing additional laboratory test data, Roy et al. (2014a,b) proposed the improved relationships shown in Table 4.1 (MMC model) and used for successful simulation of pipeline-soil interaction behavior. Further details of the model and parameter selection are discussed in Roy et al. (2014a,b) and are not repeated here.

In Abaqus, the proposed MMC model cannot be used directly using any built-in model; therefore, in this study it is implemented by developing a user subroutine VUSDFLD written in FORTRAN. In the subroutine, the stress and strain components are called in each time increment and from the stress components the mean stress ( $p'$ ) is calculated. The value of  $p'$  at the initial condition represents the confining pressure ( $\sigma'_c$ ), which is stored as a field variable to calculate  $Q$  (see the equation in the first row of Table 4.1). Using the strain increment components, the plastic shear strain increment  $\dot{\gamma}^p$  is calculated as  $\sqrt{3(\dot{\epsilon}_{ij}^p \dot{\epsilon}_{ji}^p)}/2$  for triaxial configuration, where  $\dot{\epsilon}_{ij}^p$  is the plastic strain increment tensor. The value of  $\gamma^p$  is calculated as the sum of  $\dot{\gamma}^p$  over the period of analysis. In the subroutine,  $\gamma^p$  and  $p'$  are defined as two field variables FV1 and FV2, respectively. In the input file, using the equations shown in Table 4.1, the mobilized  $\phi'$  and  $\psi$  are defined in tabular form as a function of  $\gamma^p$  and  $p'$ . During the analysis, the program accesses the subroutine and updates the values of  $\phi'$  and  $\psi$  with field variables.

**Table 4.1:** Equations for Modified Mohr-Coulomb model (MMC) (summarized from Roy et al., 2014a,b)

Description	Constitutive Equation	Soil Parameters
Relative density index	$I_R = I_D(Q - \ln p') - R$	$I_D = D_r(\%)/100$ , $Q = 7.4 + 0.6 \ln(\sigma'_c)$ (Chakraborty and Salgado, 2010), $R = 1$ (Bolton, 1986)
Peak friction angle	$\phi'_p = \phi'_c + A_\psi I_R$	$\phi'_c$ , $A_\psi$
Peak dilation angle	$\psi_p = \left( \frac{\phi'_p - \phi'_c}{k_\psi} \right)$	$k_\psi$
Strain softening parameter	$\gamma_c^p = C_1 + C_2 I_D$	$C_1, C_2$
Plastic strain at $\phi'_p$	$\gamma_p^p = \gamma_c^p \left( \frac{p'}{p'_a} \right)^m$	$p'_a, m$
Mobilized friction angle at zone-II	$\phi' = \phi'_{in} + \sin^{-1} \left[ \left( \frac{2\sqrt{\gamma^p \gamma_p^p}}{\gamma^p + \gamma_p^p} \right) \sin(\phi'_p - \phi'_{in}) \right]$	
Mobilized dilation angle at Zone-II	$\psi = \sin^{-1} \left[ \left( \frac{2\sqrt{\gamma^p \gamma_p^p}}{\gamma^p + \gamma_p^p} \right) \sin(\psi_p) \right]$	
Mobilized friction angle at zone-III	$\phi' = \phi'_c + \exp \left[ - \left( \frac{\gamma^p - \gamma_p^p}{\gamma_c^p} \right)^2 \right] (\phi'_p - \phi'_c)$	
Mobilized dilation angle at Zone-III	$\psi = \exp \left[ - \left( \frac{\gamma^p - \gamma_p^p}{\gamma_c^p} \right)^2 \right] \psi_p$	

Symbols:  $A_\psi$ : slope of  $(\phi'_p - \phi'_c)$  vs.  $I_R$ ;  $m, C_1, C_2$ : soil parameters;  $I_R$ : relative density index;  $k_\psi$ : slope of  $(\phi'_p - \phi'_c)$  vs.  $\psi_p$ ;  $\phi'_{in}$ :  $\phi'$  at the start of plastic deformation;  $\phi'_c$ : critical state friction angle;  $\gamma^p$ : engineering plastic shear strain

### 4.3.3 Model Parameters

The soil parameters used in the FE analyses are listed in Table 4.2. As shown in Fig. 4.1c, the mode of shearing of a soil element around the monopile depends on its location. For example, in Fig. 4.1c, the loading on soil element A is similar to triaxial compression, while the elements B and C are loaded similar to DSS condition. Experimental results

show that the parameters  $A_\psi$  and  $k_\psi$  that define peak friction ( $\phi'_p$ ) and dilation angle ( $\psi_p$ ) (i.e. 2nd and 3rd Eqs. in Table 1) depend on the mode of shearing (e.g., Bolton, 1986; Houlsby, 1991; Schanz and Vermeer, 1996). For example, Bolton (1986) recommended  $A_\psi = 5$  and  $k_\psi = 0.8$  for plane strain condition and  $A_\psi = 3$  and  $k_\psi = 0.5$  for triaxial condition. In a recent study, Chakraborty and Salgado (2010) showed that  $A_\psi = 3.8$  and  $k_\psi = 0.6$  is valid for both triaxial and plane strain condition for Toyoura sand. The soil around the pile under eccentric loading is not only in triaxial or plane strain condition but varies in a wide range of stress conditions depending upon depth ( $z$ ) and  $\alpha$  (Figs. 4.1b, c). Therefore, in this study  $A_\psi = 3.8$  and  $k_\psi = 0.6$  is used for simplicity. In addition, based on Chakraborty and Salgado (2010), the parameter  $Q$  is varied as  $Q = 7.4 + 0.6 \ln(\sigma'_c)$  with  $7.4 \leq Q \leq 10$ .

The soil-pile interaction is modeled using the Coulomb friction model, which defines the friction coefficient ( $\mu$ ) as  $\mu = \tan(\phi_\mu)$ , where  $\phi_\mu$  is the soil-pile interface friction angle. The value of  $\phi_\mu/\phi'$  varies between 0 and 1 depending upon the surface roughness, mean particle size of sand and the method of installation (CFEM, 2006; Tiwari et al., 2010). For smooth steel pipe piles,  $\phi_\mu/\phi'$  is in the range of 0.5 – 0.7 (Potyondy, 1961; Coduto, 2001; Tiwari and Al-Adhadh, 2014). For numerical modeling,  $\phi_\mu/\phi'$  within this range has been also used in the past (e.g., Achmus et al., 2013). In the present study,  $\phi_\mu = 0.65\phi'$  is used, where  $\phi'$  (in degree) =  $16D_r^2 + 0.17D_r + 28.4$  (API, 1987).

The Young's modulus of elasticity of sand ( $E_s$ ) can be expressed as a function of mean effective stress ( $p'$ ) as,  $E_s = Kp_a(p'/p_a)^n$  (Janbu, 1963); where,  $K$  and  $n$  are soil parameters and  $p_a$  is the atmospheric pressure. However, in this study, a constant value of  $E_s = 90$  MPa is used which is a reasonable value for a dense sand having  $D_r = 90\%$ .

The numerical analysis is conducted in two steps. In the first step, geostatic stress is applied. In the second step, the pile is displaced in the  $X$  direction specifying a displacement boundary condition at the reference point at a vertical distance  $e$  above the pile head.

Two sets of FE analyses are performed. In the first set, analyses are performed to show the performance of the model comparing the results of FE analysis and centrifuge tests reported by Klinkvort and Hededal (2014), which is denoted as “model test simulation.” In the second set, a parametric study is conducted for a wide range of aspect ratio ( $\eta = L/D$ ) of the pile and load eccentricity.

## **4.4 Model Test Simulation Results**

### **4.4.1 Simulation of Klinkvort and Hededal (2014) Centrifuge Test Results**

Four centrifuge tests (T6, T7, T8 and T9) conducted by Klinkvort and Hededal (2014) are simulated. These tests were conducted using 18 m long and 3 m diameter (prototype) monopiles installed in saturated dense sand of  $D_r \approx 90\%$ . The lateral load was applied at an eccentricity ( $e$ ) of 27.45, 31.5, 38.25 and 45.0 m in tests T6, T7, T8 and T9, respectively.

**Table 4.2:** Soil parameters used in FE analyses

Parameters	Value
$\nu_{soil}$	0.3
$A_\psi$	3.8
$k_\psi$	0.6
$\phi'_{in}$	29°
$C_1$	0.22
$C_2$	0.11
$m$	0.25
Critical state friction angle, $\phi'_c$	31°
Young's modulus of elasticity, $E_s$ (MN/m <sup>2</sup> )	90
Relative density of sand, $D_r$ (%)	90
Submerged unit weight, $\gamma'$ (kN/m <sup>3</sup> )	10.2
Interface friction co-efficient, $\mu$	$\tan(0.65\phi')$
<sup>1</sup> Cohesion, $c'$ (kN/m <sup>3</sup> )	0.10

<sup>1</sup>Cohesion is required to be defined in Abaqus FE analysis. For sand in this study a very small value of  $c' = 0.10$  kN/m<sup>2</sup> is used.

The soil parameters used in FE simulation with the MMC model are listed in Table 4.2. Figure 4.3 shows the variation of normalized force ( $H/K_p\gamma'D^3$ ) with normalized displacement ( $u/D$ ) obtained from FE analyses along with centrifuge test results. Here  $H$  is the lateral force,  $\gamma'$  is the submerged unit weight of sand,  $D$  is the diameter of the pile,  $K_p$  is the Rankine passive earth pressure coefficient calculated using API (1987) recommended  $\phi'$  mentioned above, and  $u$  is the lateral displacement of the pile head. Note that different parameters have been used in the past to normalize  $H$  (e.g., LeBlanc et al., 2010; Achmus et al., 2013; Klinkvort and Hededal, 2014); however, in order to be consistent, the vertical axis of Fig. 4.3 shows the normalized  $H$  as Klinkvort and Hededal (2014).

The normalized load–displacement behavior obtained from FE analyses match well with

the centrifuge test results except for T7 in which FE analyses show higher initial stiffness than that reported from centrifuge test. Klinkvort and Hededal (2014) recognized this low initial stiffness in T7, although did not report the potential causes. The load–displacement curves do not become horizontal even at  $u/D = 0.5$  although the gradient of the curves at large  $u$  is small as compared to the gradient at low  $u$ . As the load–displacement curve does not reach a clear peak, a rotation criterion is used to define the ultimate capacity ( $H_u$  and  $M_u$ ). Klinkvort (2012) defined the ultimate condition (failure) at  $\theta = 4^\circ$  while LeBlanc et al. (2010) defined it at  $\tilde{\theta} = \theta\sqrt{(p_a/L\gamma')} = 4^\circ$ . In this study, defining the ultimate condition at  $\theta = 5^\circ$  (i.e.,  $\tilde{\theta} = 3.7^\circ$  in this case),  $H_u$  and  $M_u (= H_u \times e)$  are obtained.

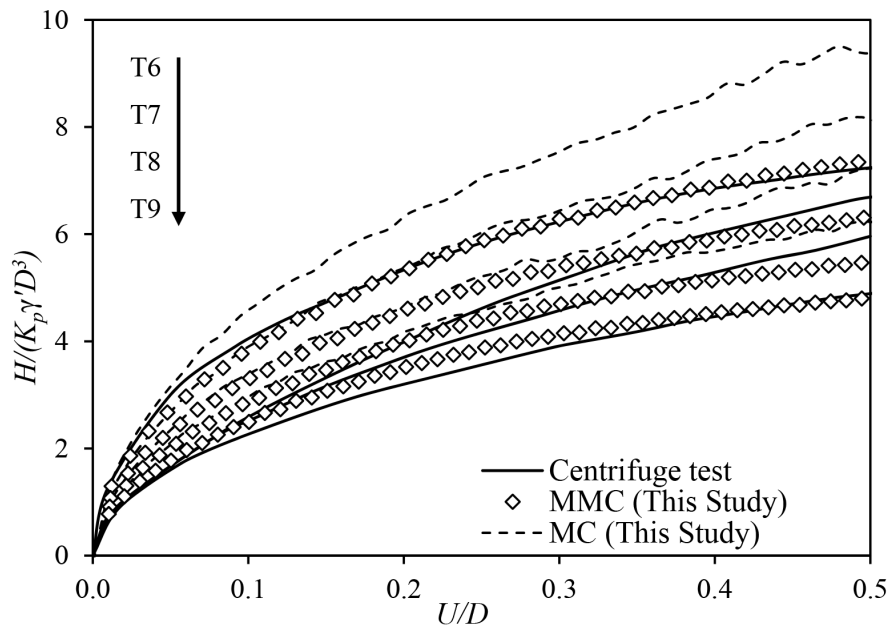


**Figure 4.3:** Comparison between FE simulation and centrifuge test results by Klinkvort and Hededal (2014)

#### 4.4.2 Effects of Vertical Load

The monopiles supporting offshore wind turbines also experience a vertical load due to the weight of superstructure containing the turbine and transition pieces. Typical vertical load on a 2 – 5 MW offshore wind turbine foundation is 2.4 – 10 MN (Malhotra, 2011; LeBlanc et al., 2010; Achmus et al., 2013). The effects of vertical load on the lateral load-carrying capacity of monopile are examined from 21 simulations of a monopile having  $L = 18$  m and  $D = 3$  m under vertical loading  $V$  of 0, 5 and 10 MN for lateral loading at 6 different eccentricities and pure moment. The soil parameters used in the analysis are same as before (Table 4.2). In these simulations, after geostatic step, the vertical load is applied gradually and then the lateral eccentric load is applied as shown in Fig. 4.1a.

The  $H_u - M_u$  interaction curves obtained from these 21 FE simulations for different vertical loading conditions are shown in Fig. 4.4a. As shown, the load-carrying capacity of a monopile increases with vertical load. In this case,  $H_u$  and  $M_u$  increase approximately by 11% for a change of  $V$  from 0 to 10 MN.

The initial stiffness ( $k_{in}$ ) of the load–rotation curve is one of the main concerns in monopile design. As the  $H - \theta$  curve is nonlinear,  $k_{in}$  is defined as the slope of the line drawn from origin to the point at  $\theta = 0.5^\circ$  (inset of Fig. 4.4b). Figure 4.4b shows that  $k_{in}$  decreases with eccentricity; however, the effect of  $V$  on  $k_{in}$  is minimal. For a given eccentricity, the minimum load-carrying capacity (Fig. 4.4a) and stiffness (Fig. 4.4b) are obtained for  $V = 0$ . Achmus et al. (2013) also found similar effect of  $V$  from FE simulation using the

MC model. From centrifuge modeling, Alderlieste (2011) also reported decrease in stiffness with eccentricity. As the effect of  $V$  is not very significant, in the following sections, all the analyses are performed for  $V = 0$ .

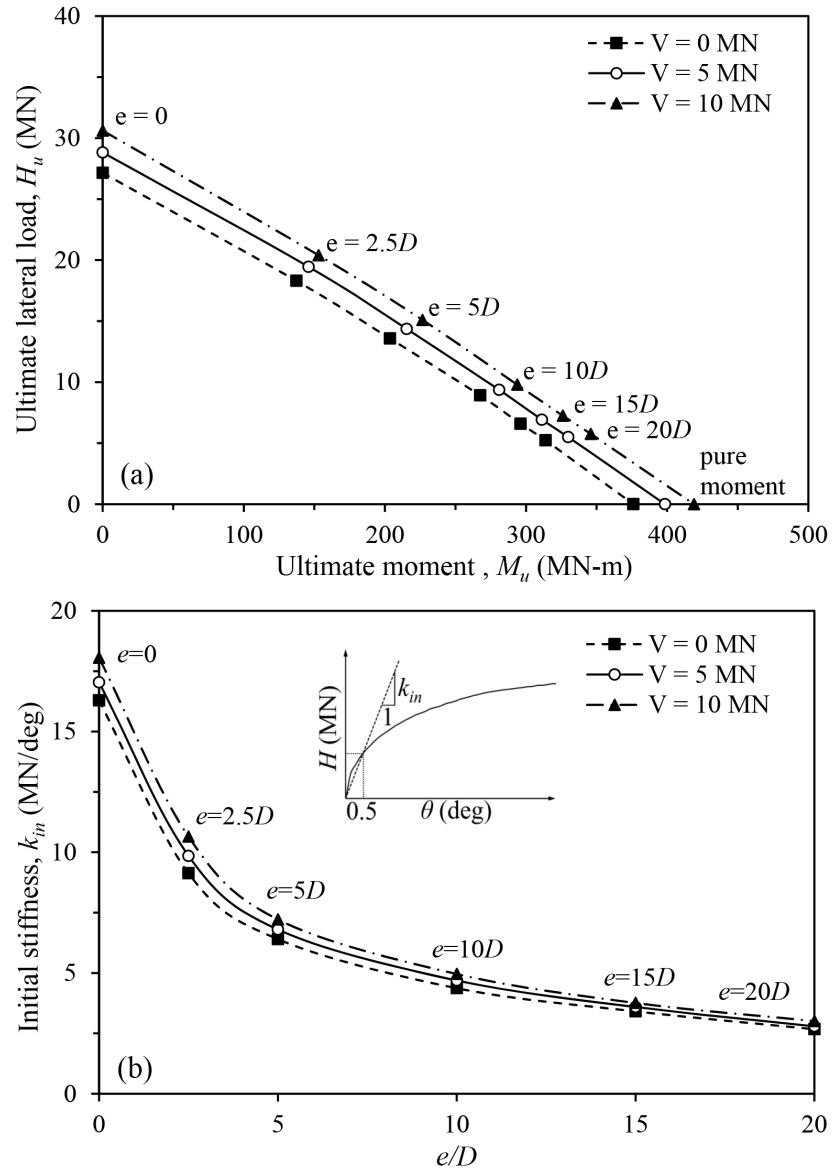


**Figure 4.4:** Effects of vertical load and eccentricity on: (a) ultimate capacity and (b) initial stiffness

#### 4.4.3 FE Simulation with Mohr-Coulomb Model

The built-in Mohr-Coulomb (MC) model in Abaqus FE software has been used in previous studies to simulate the response of monopiles in sand. With the MC model, the soil behavior is elastic until the stress state reaches the yield surface which is defined by the Mohr-Coulomb failure criterion. Constant values of  $\phi'$  and  $\psi$  are needed to be given as input parameters in the MC model. As post-peak softening occurs during shearing of dense sand, estimation of appropriate values of  $\phi'$  and  $\psi$  is a challenging task. Based on the API (1987) recommendations mentioned above  $\phi' = 41.5^\circ$  is calculated for  $D_r = 90\%$ . The value of  $\psi (= 13^\circ)$  is then calculated using the relationship proposed by Bolton (1986) as  $\psi = (\phi'_p - \phi'_c)/0.8$ . Now using  $\phi' = 41.5^\circ$  and  $\psi = 13^\circ$ , FE analysis is also performed using the built-in MC model. The dashed lines in Fig. 4.3 show the simulation results with the MC model. The MC model over-predicts the lateral load-carrying capacity together with overall high stiffness of the load–displacement curve compared to centrifuge tests and FE simulations with the MMC model.

Overestimation of the initial stiffness by the API formulation for large-diameter pile has been reported by a number of researchers (e.g., Achmus et al., 2009; Lesny et al., 2007). Alderlieste (2011) introduced a correction term to define stress-dependent soil stiffness to match the experimental load–displacement curves. Although this modification improves the prediction, it under-predicts  $H$  at low  $u$  but over-predicts at large  $u$ .

One of the main advantages of the MMC model is that the mobilized  $\phi'$  and  $\psi$  decrease

with plastic shear strain (i.e., displacement  $u$ ) which reduces the shear resistance of soil and therefore the gradient of the load–displacement curves reduces with  $u$  (Fig. 4.3).

#### 4.4.4 Soil Failure Mechanism

The mechanisms involved in force–displacement behavior can be explained further using the formation of shear bands (plastic shear strain concentrated zones). The accumulated plastic shear strain ( $\gamma^p$ ) in the simulation of test T9 is shown in left column of Fig. 4.5 for  $\theta = 0.5^\circ, 1^\circ$  and  $5^\circ$ . The plastic shear strains start to develop near the pile head at a small rotation (e.g.,  $\theta = 0.5^\circ$ ) and an inclined downward shear band  $f_1$  forms in front of the pile (right side) because of eccentric lateral loading (Fig. 4.5a). With the increase in  $\theta$ , another inclined upward shear band  $f_2$  forms that reaches the ground surface and creating a failure wedge as shown in Fig. 4.5(b). With further increase in rotation (e.g.,  $\theta = 5^\circ$ ), the third shear band  $f_3$  forms (Fig. 4.5c). During the formation of shear bands, small or negligible  $\gamma^p$  develops in the soil elements outside the shear bands. With increase in rotation,  $\gamma^p$  increases in and around the shear bands. The right column of Fig. 4.5 shows the simulation using the MC model. In this case no distinct shear band is observed; instead, the zone of plastic shear strain accumulation in the right side of the pile enlarges with rotation of the pile because the post-peak softening is not considered.

The difference between the force–displacement curves obtained with the MC and MMC model could be explained further examining mobilized  $\phi'$  and  $\psi$  along the shear bands. In the MC model the plastic shear deformation occurs under constant  $\phi'$  and  $\psi$ . However,

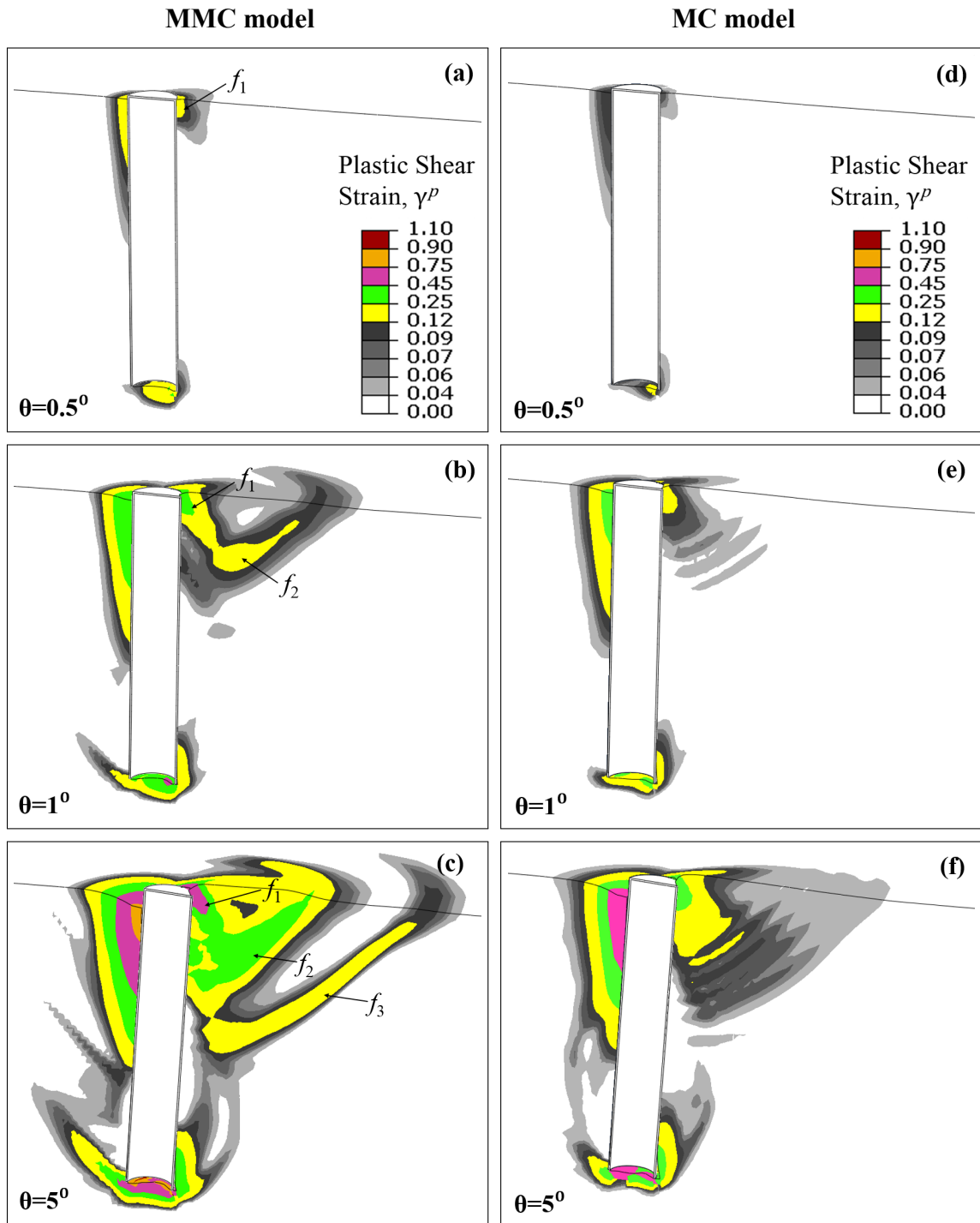


**Figure 4.5:** Development of plastic shear zone around the monopile

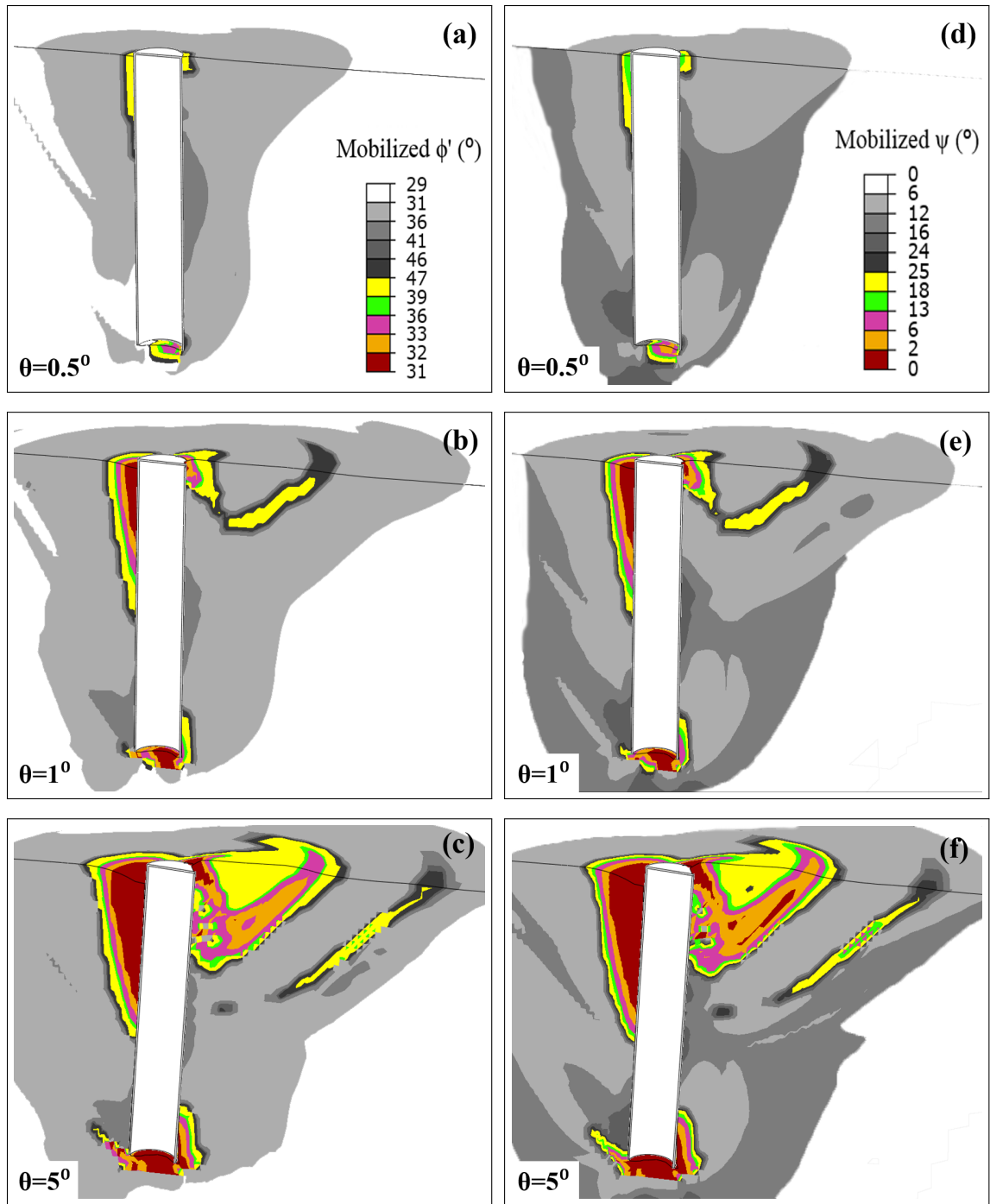


Figure 4.6: Mobilized  $\phi'$  and  $\psi$  around the monopile

in the MMC model  $\phi'$  and  $\psi$  varies with accumulated plastic shear strains. As shown in Fig. 4.5(a-c), significant accumulation of  $\gamma^p$  occurs in the shear bands. The mobilized  $\phi'$  and  $\psi$  for these three values of  $\theta$  ( $0.5^\circ$ ,  $1^\circ$  and  $5^\circ$ ) are shown in Fig. 4.6. As shown in the inset in Table 4.1, the maximum values of  $\phi'$  and  $\psi$  mobilize at  $\gamma_p^p$ , and therefore  $\phi' < \phi'_p$  and  $\psi < \psi_p$  in the pre-yield ( $\gamma^p < \gamma_p^p$ ) and also in the post-yield ( $\gamma^p > \gamma_p^p$ ) conditions. The colored zones in Figs. 4.5(a-c) roughly represent the post-peak condition ( $\gamma^p > \gamma_p^p$ ) developed in soil, while in the gray zone some plastic shear strains develop ( $\gamma^p < \gamma_p^p$ ) but the soil elements in this zone are still in the pre-peak shear zone (see inset of Table 4.1). The colored zones in Fig. 4.6 roughly represent the mobilized  $\phi'$  (Fig. 4.6a-c) and  $\psi$  (Fig. 4.6d-f) in the post-peak while the gray areas represent the pre-peak zone. These figures show that  $\phi'$  and  $\psi$  are not constant along the shear band, rather it depends on accumulated plastic shear strain  $\gamma^p$ . In some segments they could be at the peak, while in the segments where large plastic shear strains accumulate,  $\phi'$  and  $\psi$  are at the critical state. As  $\phi'$  and  $\psi$  reduce with  $\gamma^p$  at large strains, lower normalized lateral force is calculated with the MMC model than the MC model (Fig. 4.3).

The FE results presented in the following sections are conducted with the MMC model.

## 4.5 FE Simulations for Different Aspect Ratios

The aspect ratio  $\eta$  ( $= L/D$ ) is often used to examine the effects of pile geometry on load-carrying capacity. The value of  $\eta$  could be varied by changing the values of  $L$  or  $D$  or both. Analyses are performed for three values of  $\eta$  ( $= 4, 5, 6$ ) by varying  $D$  between 3

and 4.5 m and  $L$  between 12 and 21 m, as shown in Table 4.3. The lateral load is applied at 6 different eccentricities ranging between 0 and  $20D$ . In addition, analyses are performed for pure moment condition. In other words, a total of 42 analyses for six monopiles (7 for each geometry) are conducted. The soil properties listed in Table 4.2 are used in the analysis.

**Table 4.3:** Dimensions used for varying aspect ratio

Aspect ratio, $\eta = L/D$			Load eccentricities, $e$
$\eta = 4$	$\eta = 5$	$\eta = 6$	
$L = 12 \text{ m}, D = 3 \text{ m}$	$L = 15 \text{ m}, D = 3 \text{ m}$	$L = 18 \text{ m}, D = 3 \text{ m}$	0, $2.5D$ , $5D$ , $10D$ , $15D$ , $20D$ and pure moment
$L = 18 \text{ m}, D = 4.5 \text{ m}$	$L = 18 \text{ m}, D = 3.6 \text{ m}$	$L = 21 \text{ m}, D = 3.5 \text{ m}$	

#### 4.5.1 Force–displacement and Moment–rotation Curves

The capacity of a monopile need to be estimated at different states such as the ultimate limit state (ULS) and serviceability limit state (SLS). The SLS occurs at much lower rotation of the pile than ULS. In the design, both ULS and SLS criteria need to be satisfied.

Typical force–displacement and moment–rotation curves are shown in Fig. 4.7a and 4.7b, respectively, for a monopile having  $L = 12 \text{ m}$  and  $D = 3 \text{ m}$  loaded at different eccentricities. Similar to Fig. 4.3, the load–displacement curve does not reach a clear peak and therefore the rotation criterion  $\theta = 5^\circ$  is used to define the ultimate capacity. For serviceability limit state (SLS), the allowable rotation is generally less than  $1^\circ$  (Doherty and Gavin, 2012; DNV, 2011).

Figure 4.7a shows that the lateral load-carrying capacity decreases with increase in

eccentricity. In this figure, the open symbols show the lateral loads for  $0.5^\circ$ ,  $1^\circ$  and  $5^\circ$  rotations. All the points for a given rotation (e.g., open squares) are not on a vertical line in Fig. 4.7a because the depth of rotation slightly decreases with increase in eccentricity (explained later). As expected,  $H$  increases with increase in rotation (e.g.,  $H_u$  for  $\theta = 5^\circ$  is greater than  $H_u$  for  $\theta = 1^\circ$ ).

In the design of long slender piles, the lateral load at pile head displacement of 10% of its diameter is often considered as the ultimate load. The solid triangles show the lateral load-carrying capacity of the pile for  $0.1D$  pile head displacement. In these analyses, it is higher than the lateral load at  $\theta = 1^\circ$  but lower than  $\theta = 5^\circ$ .

Similar to Fig. 4.7a, the open symbols in Fig. 4.7b show the moments at  $\theta = 0.5^\circ$ ,  $1^\circ$  and  $5^\circ$ , while the solid triangles show the moment for  $0.1D$  pile head displacement. Notice that the top most curve in Fig. 4.7b is for pure moment (not for pure lateral load as in Fig. 4.7a because in that case  $M = 0$  as  $e = 0$ ). Although lateral load-carrying capacity decreases with increase in eccentricity (Fig. 4.7a), the corresponding moment increases (Fig. 4.7b).

In summary, both load- and moment-carrying capacity of a large-diameter monopile in dense sand depend on its rotation. As the rotation criterion is commonly used in the current practice (DNV, 2011), the values of  $H$  and  $M$  at  $\theta = 0.5^\circ$ ,  $1^\circ$  and  $5^\circ$  will be critically examined further in the following sections, which is denoted as  $H_{0.5}$ ,  $H_1$ ,  $H_5$  and  $M_{0.5}$ ,  $M_1$ ,  $M_5$ , respectively. Note that,  $H_5$  and  $M_5$  are considered as the ultimate capacity ( $H_u$  and  $M_u$ ) in this study.

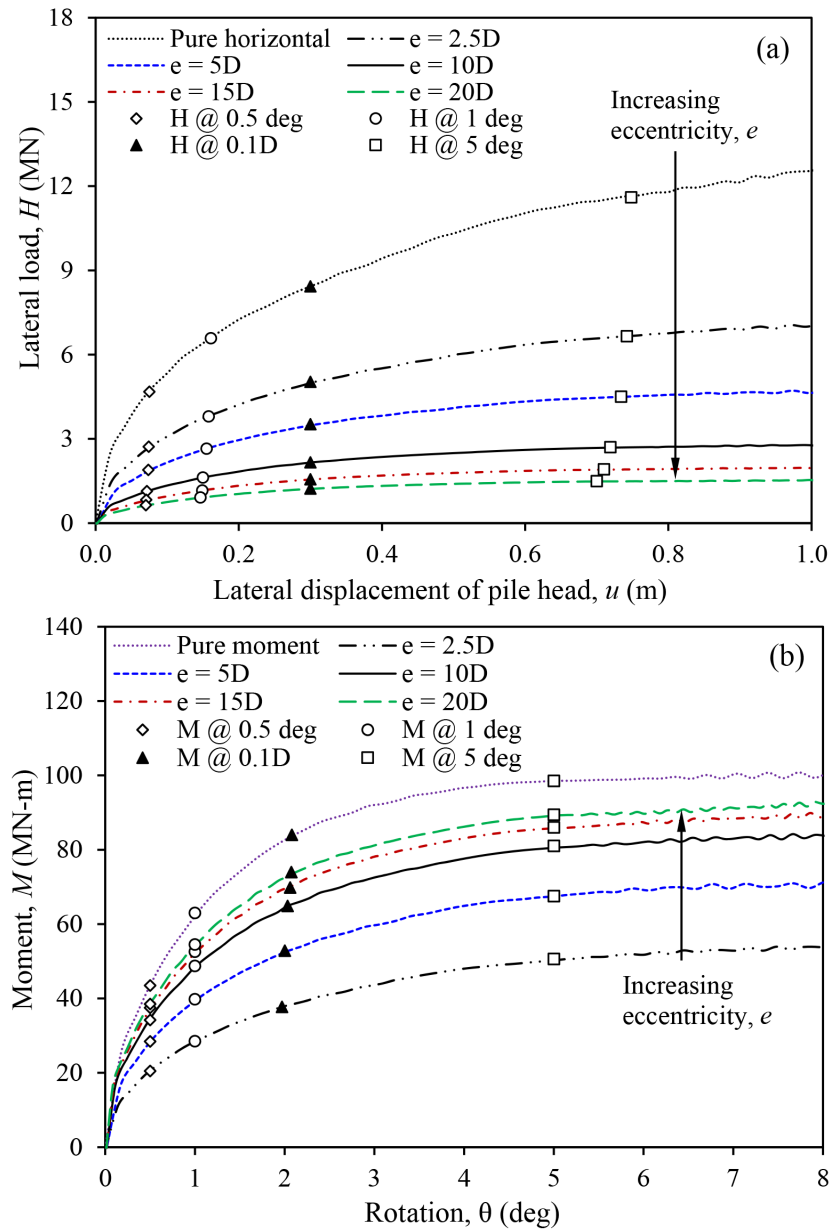


**Figure 4.7:** Analysis for  $L = 12$  m and  $D = 3$  m: (a) lateral force–displacement, (b) moment–rotation

#### 4.5.2 Point of Rotation

One of the limitations of the current  $p - y$  curve based design method is that it has been developed from test results of slender piles where only the top part of the pile deflects

under lateral loading. However, a large-diameter monopile behaves similar to a rigid pile and therefore the monopile tends to rotate around a rotation point and thereby generates pressure along the whole length of the pile.

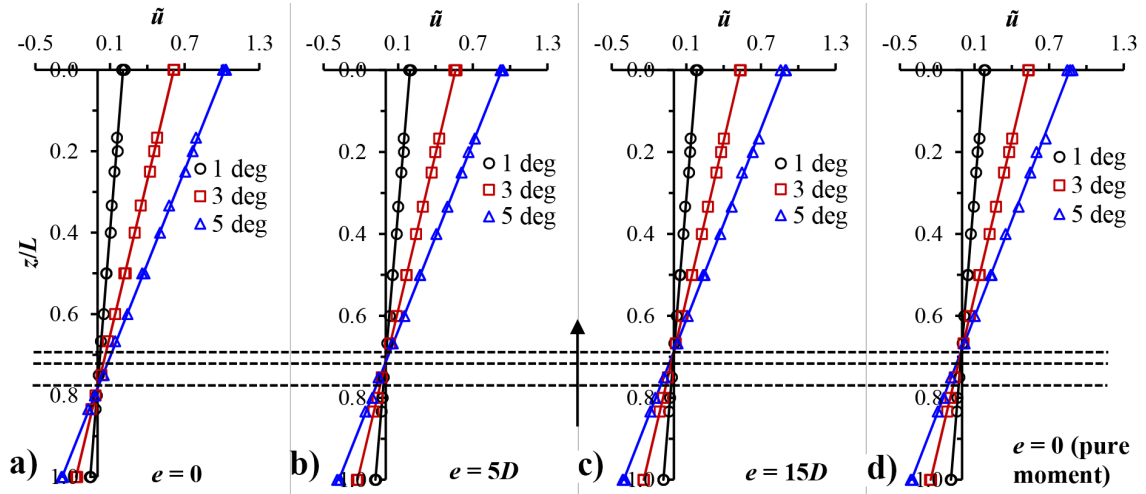


**Figure 4.8:** Lateral displacement for different length-to diameter ratios and eccentricities

In order to identify the point of rotation of the pile in terms of length (i.e.,  $d/L$  in Fig. 4.1b), the lateral displacements of 3 m diameter piles of different length are plotted in Fig. 4.8. As the pile length is different (Table 4.3), the depth  $z$  in the vertical axis is normalized by  $L$ . In order to maintain clarity, the lateral displacements are plotted in a normalized form as  $\tilde{u} = uL_{ref}/L$ , where  $L_{ref}$  is taken as 15 m. Figure 4.8a shows that the point of rotation is located approximately at  $d = 0.78L$  for  $e = 0$  for all three degree of rotations. With increase in  $e$ ,  $d/L$  slightly decreases (Figs. 4.8b and 4.8c). For the pure moment case,  $d \approx 0.7L$  is calculated. Similar responses have been observed for other pile diameters. In summary,  $d/L$  is approximately constant irrespective of the length of the pile for a given  $e$

for these level of rotations. Moreover,  $d/L \approx 0.7L - 0.78L$  for the cases analyzed in this study. Note that Klinkvort and Hededal (2014) also reported  $d \approx 0.7L$  from a number of centrifuge model tests.

### 4.5.3 Force–moment Interaction Diagram

The capacity of a monopile can be better described using force–moment interaction diagrams (Fig. 4.9). In order to plot this diagram, the values of  $H$  and  $M$  are obtained for each of the 42 analyses listed in Table 4.3 for  $\theta = 0.5^\circ, 1^\circ$  and  $5^\circ$  as shown in Figs. 4.7a and 4.7b. Figure 4.9 shows that  $H - M$  interaction lines are almost linear. The capacity (both  $H$  and  $M$ ) increases with increase in length and diameter of the monopile. Comparison of Figs. 4.9a-c show that the capacity of the monopile increases with increase in rotation; however, the shape of the  $H - M$  curves remain almost linear for all three rotations. Similar shape of  $H - M$  diagrams have been reported by Achmus et al. (2013), where FE analyses of suction bucket foundations have been conducted using the built-in Mohr-Coulomb model with constant  $\phi'$  and  $\psi$ .

### 4.5.4 Horizontal Stress Around The Pile

The soil resistance to the lateral movement of the pile depends on two factors: (i) frontal normal stress and (ii) side friction (Briaud et al., 1983; Smith, 1987). The contour plots of the horizontal compressive stresses for three different load eccentricities at  $\theta = 5^\circ$  are shown in Fig. 4.10 for the analysis of the monopile having  $L = 18$  m and  $D = 3$  m. Compressive stress develops in the right side of the pile up to approximately  $0.70 - 0.78L$

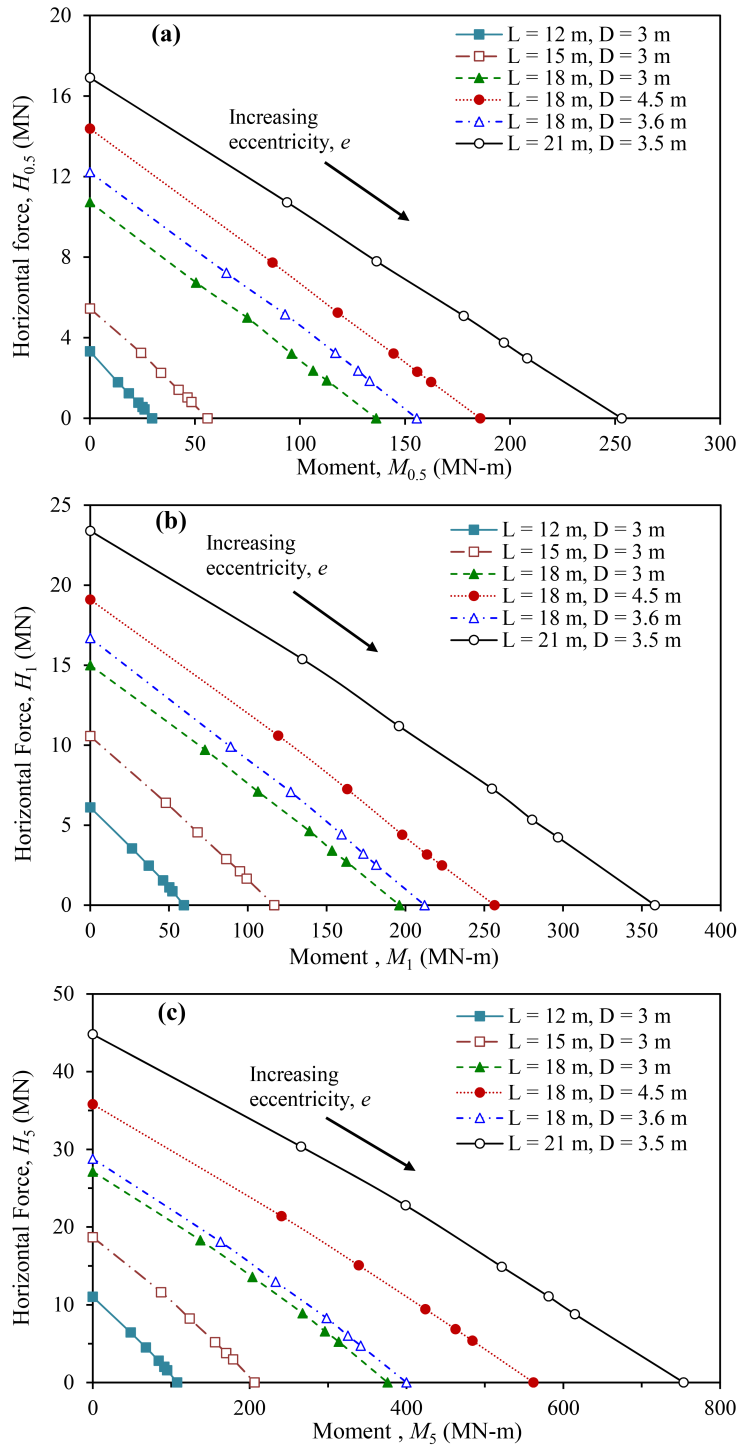


**Figure 4.9:** Lateral load–moment interaction diagrams: (a) for  $\theta = 0.5^\circ$ , (b) for  $\theta = 1^\circ$ , (c) for  $\theta = 5^\circ$

and in the left side near the bottom of the pile. An uneven shape of the stress contour around the shear band  $f_3$  in Fig. 4.5c is calculated (e.g., see the stress contour around the line AB in Fig. 4.10a). The pattern is similar in all three eccentricities. The solid circles show the approximate location of the point of rotation.

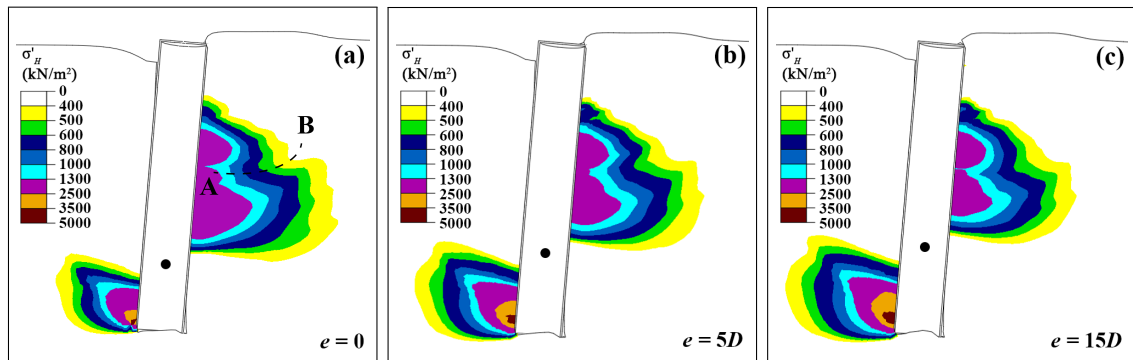


**Figure 4.10:** Development of soil horizontal stress at ultimate state ( $\theta = 5^\circ$ ) in the plane of symmetry

#### 4.5.5 Effects of $\eta$ and $e$ on initial stiffness

Similar to Fig. 4.4b, the initial stiffness ( $k_{in}$ ) is calculated for all 42 analyses listed in Table 4.3 and plotted in Fig. 4.11. The initial stiffness increases with increase in size of the pile and the increase is very significant at low eccentricities; however, at large  $e/D$ , the difference in  $k_{in}$  is relatively small. For a given pile length (e.g.,  $L = 18$  m),  $k_{in}$  is higher for larger diameter pile up to  $e = 5D$ ; however,  $k_{in}$  is almost independent of  $D$  at large eccentricities (e.g.,  $e = 15D$ ). This is consistent with centrifuge tests (Alderlieste, 2011) where it was shown that the decrease in stiffness with eccentricity is more pronounced in larger diameter piles. Similar findings have been reported by Achmus et al. (2013) for

suction bucket foundations.

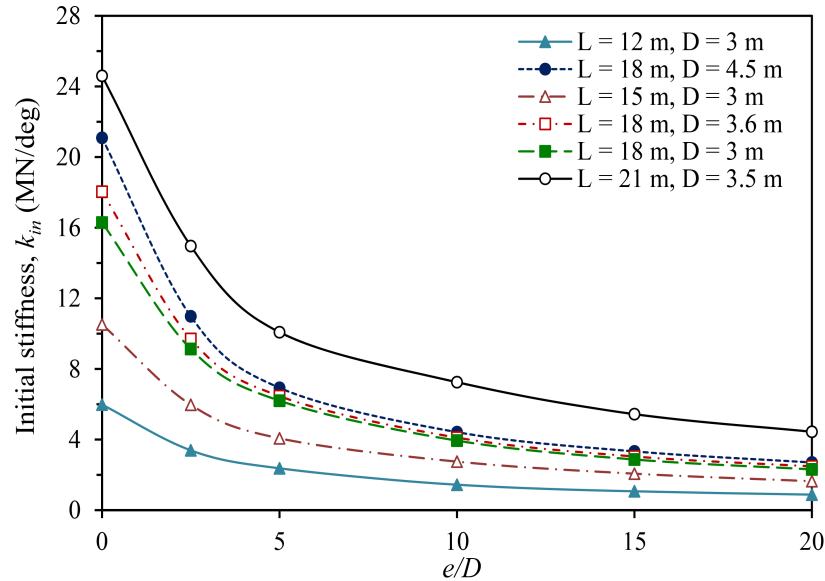


**Figure 4.11:** Effects of length-to-diameter ratio and eccentricity on initial stiffness

## 4.6 Proposed Equation for Lateral Load-carrying Capacity and Moment

Various theoretical methods have been proposed in the past to calculate the ultimate lateral resistance ( $H_u$ ) of free-headed laterally loaded rigid pile based on simplified soil pressure distribution along the length of the pile (Brinch Hansen, 1961; Broms, 1964; Petrasovits and Award, 1972; Meyerhof et al., 1981; Prasad and Chari, 1999). Following LeBlanc et al. (2010), an idealized horizontal pressure distribution ( $p$ ) shown in Fig. 4.1b is used to estimate the lateral load-carrying capacity. Note that the assumed shape of  $p$  in Fig. 4.1b is similar to the horizontal pressure distribution obtained from FE analysis (Fig. 4.10). From

Fig. 4.1b, the force and moment equilibrium equations at the pile head can be written as:

$$H = \frac{1}{2}KD\gamma'(2d^2 - L^2) \quad (4.1)$$

$$M = \frac{1}{3}KD\gamma'(L^3 - 2d^3) \quad (4.2)$$

Combining Eqs. (4.1) and (4.2), and replacing  $M = He$ , the following relationship is obtained:

$$4R^3 + 6R^2\frac{e}{L} - (2 + 3\frac{e}{L}) = 0 \quad (4.3)$$

where,  $R = d/L$ .

For a given  $e/L$ , Eq. (4.3) is solved for  $R$  which is then used to find  $d$ . Now inserting  $d$  in Eq. (4.1) and (4.2),  $H$  and  $M$  are calculated.

In addition to the shape of the pressure distribution profile (Fig. 4.1b), estimation of parameter  $K$  is equally important. Broms (1964) assumed  $K = 3K_p$  (i.e.,  $p = 3K_p D\gamma'z$ ) for the entire length in front of the pile to calculate  $H_u$ . Comparison of field test results show that Brom's method underestimates  $H_u$  (Poulos and Davis, 1980), especially for piles in dense sand (Barton, 1982). Therefore, Barton (1982) suggested  $K = K_p^2$ .

A close examination of all the FE results presented above show that the  $H_u$  calculated using Eqs. 4.1–4.3 reasonably match the FE results at  $\theta = 5^\circ$  if  $K = 4.3K_p$  is used. The open squares in Fig. 4.12 show that the calculated  $H_u$  using the empirical Eqs. 4.1–4.3 match well with the FE results. In this figure,  $H$  is plotted in normalized form as  $\bar{H} = H/K_p\gamma'DL^2$ . As shown before, the lateral load-carrying capacity increases with

decreasing eccentricity (Fig. 4.7a). Therefore, for a given rotation, the points with higher  $\bar{H}_u$  represent the results for lower eccentricities. The rightmost points, where the maximum discrepancy is found, are for the purely lateral load applied to the pile head ( $e = 0$ ). The discrepancy is not very significant for high eccentricities. As in offshore monopile foundations the lateral load acts at relatively high eccentricity, Eqs. 4.1–4.3 and FE results show better match for these loading conditions.

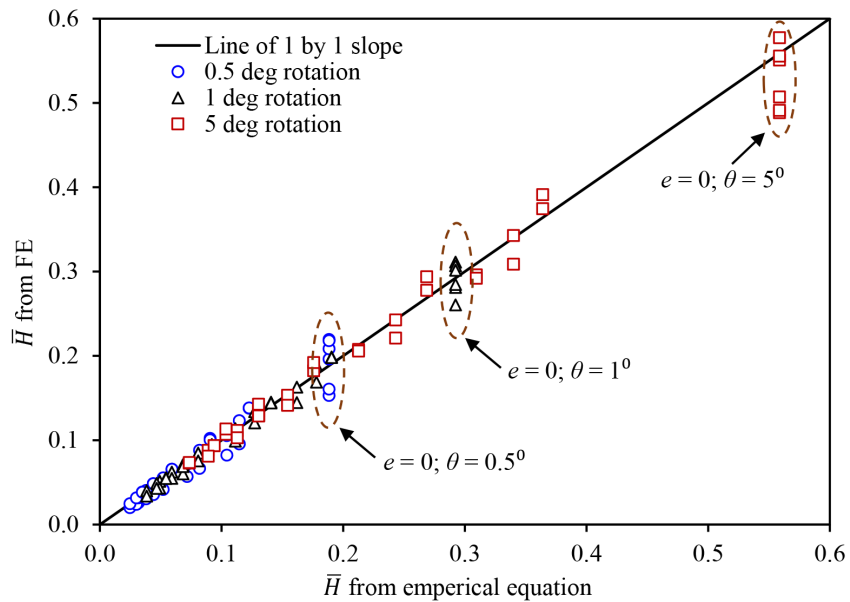


**Figure 4.12:** Comparison between lateral loads calculated from proposed simplified equation and FE analyses

In order to provide a simplified guideline for SLS design, capacities of the monopile at two more rotations ( $\theta = 0.5^\circ$  and  $1^\circ$ ) are also investigated. Reanalyzing  $H$  at these rotations, it is found that if  $K = 1.45K_p$  and  $2.25K_p$  are used for  $\theta = 0.5^\circ$  and  $1^\circ$ , respectively, the calculated  $H$  using Eqs. 4.1–4.3 reasonably match the FE results (Fig. 4.12). Similar to

the mobilization of passive resistance behind a retaining wall with its rotation, this can be viewed as at  $\theta$  equals  $0.5^\circ$  and  $1^\circ$ , while the mobilized  $K$  is 34% and 52% of the  $K$  at the ultimate condition ( $\theta = 5^\circ$ ).

#### 4.7 Lateral Force-Moment Interaction

Figure 4.13 shows the lateral force–moment interaction diagram in which  $H$  and  $M$  are normalized as  $\bar{H} = H/K_p\gamma'DL^2$  and  $\bar{M} = M/K_p\gamma'DL^3$ . The solid lines are drawn using Eqs. 4.1–4.3 for  $\theta = 0.5^\circ, 1^\circ$  and  $5^\circ$  using  $K = 1.45K_p, 2.25K_p$  and  $4.3K_p$ , respectively, as described before. The scattered points (open triangles, squares and circles) show the values obtained from FE analysis for these three levels of rotation. Purely a lateral load at the pile head as shown in the vertical axis or purely a moment without any  $H$  as shown in the horizontal axis are not expected in offshore monopile foundations for wind turbine because  $H$  acts at an eccentricity. However, these analyses are conducted for the completeness of the interaction diagram. As shown in this figure, with increase in eccentricity (i.e.,  $\bar{M}$ ) the lateral load-carrying capacity  $\bar{H}$  decreases. The calculations using the simplified equations with the recommended values of  $K$  reasonably match the FE results for these three levels of rotation. The shape of the  $\bar{M} - \bar{H}$  interaction diagram is similar to experimental observation (LeBlanc et al., 2010) and numerical modeling of large-diameter suction bucket foundation (Achmus et al., 2013).

Reanalyzing available model test results, Zhang et al. (2005) proposed an empirical method to calculate the ultimate lateral load-carrying capacity of rigid pile considering both soil

pressure and pile-soil interface resistance. They calculated the depth of rotation using the empirical equation proposed by Prasad and Chari (1999). Calculated  $H_u$  and  $M_u (= H_u e)$  by the empirical method of Zhang et al. (2005) for the eccentricities considered in the present FE analysis are also shown in Fig. 4.13. The ultimate capacity of the large-diameter monopiles (at  $\theta = 5^\circ$ ) is approximately 35% higher than the Zhang et al. (2005) empirical model.

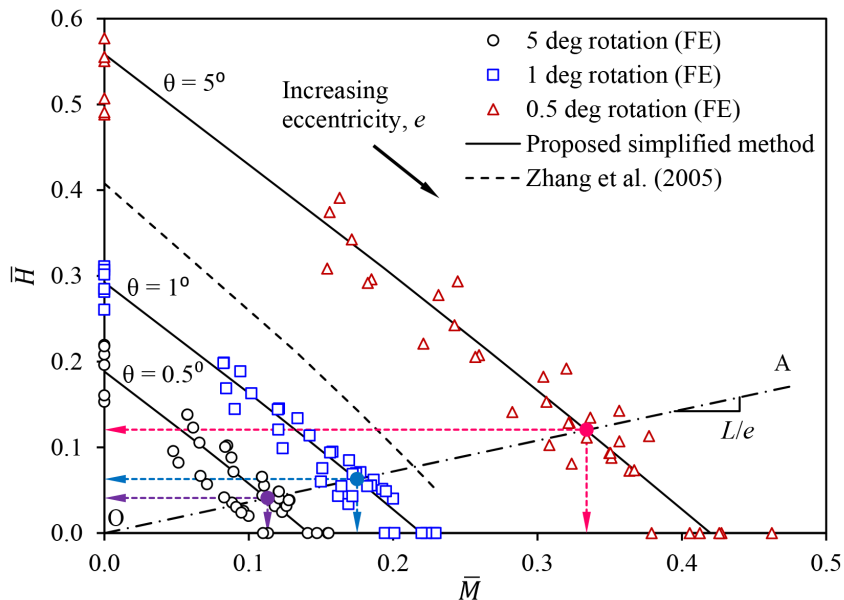


**Figure 4.13:** Normalized force–moment interaction diagram for  $\theta = 0.5^\circ, 1^\circ$  and  $5^\circ$

As  $M = He$ , the slope of a line drawn from the origin in the  $\bar{M} - \bar{H}$  plot (Fig. 4.13) is  $L/e$ . In order to explain this diagram and to provide a worked example, consider a monopile of  $D = 4$  m and  $L = 18$  m installed in dense sand of  $D_r = 80\%$  and  $\gamma' = 10$  kN/m<sup>3</sup> and is subjected to an eccentric lateral load acting at  $e = 50$  m above the pile head. For this geometry, draw the line OA at a slope of  $L/e = 0.36$  (Fig. 4.13). From the intersections

of this line with  $\bar{M} - \bar{H}$  interaction diagram (solid lines), the normalized capacity of the pile  $\bar{H}$  can be calculated as 0.04, 0.06 and 0.12 for  $\theta = 0.5^\circ, 1^\circ$  and  $5^\circ$ , respectively. Now calculating  $\phi' = 38.8^\circ$  based on API (1987),  $K_p = 4.36$  can be obtained, which gives lateral load-carrying capacities of 2.26, 3.39 and 6.78 MN, and corresponding moments of 113, 170 and 339 MN-m for  $\theta = 0.5^\circ, 1^\circ$  and  $5^\circ$ , respectively.

## 4.8 Conclusions

Three-dimensional FE analyses are performed to estimate the lateral load-carrying capacity of monopiles in dense sand for different load eccentricities. Analyses are mainly conducted by employing a modified form of Mohr-Coulomb model (MMC) that captures the typical stress-strain behavior of dense sand. The following conclusions can be drawn from this study:

1. FE analysis with the MMC model simulates the load–displacement behavior for a wide range of lateral displacement of the pile head, including the reduction of stiffness at large displacements, as observed in centrifuge model tests.
2. With the MMC model the mobilization of  $\phi'$  and  $\psi$  with rotation of the pile creates distinct shear bands due to post-peak softening, which could not be simulated using the Mohr-Coulomb model.
3. The load-carrying capacity of the pile depends on its rotation. For  $0.5^\circ$  and  $1^\circ$  rotation of the pile, the mobilized capacity is approximately 34% and 52%, respectively, of the ultimate capacity calculated at  $5^\circ$  rotation.

4. At the ultimate loading condition the depth of the point of rotation of the pile is approximately  $0.7L$  for monopiles used in offshore wind turbine foundation loaded at large eccentricity.
5. The simplified model based on a linear pressure distribution, with a pressure reversal at the point of rotation, can be used for preliminary estimation of load-carrying capacity. The capacity of large-diameter monopiles is higher than the estimated capacity of small-diameter piles based on the empirical equations developed from small-scale model test results.

Finally, it is to be noted that the effects of long-term cyclic loading on monopiles is another important issue which has not been investigated in the present study.

#### **4.9 Acknowledgements**

The work presented in this paper has been funded by NSERC Discovery grant, MITACS and Petroleum Research Newfoundland and Labrador (PRNL).

## Bibliography

- ABAQUS. (2013). *Abaqus User's Manual*. Version 6.13-1, Dassault Systèmes.
- Abdel-Rahman, K, and Achmus, M (2005). Finite element modelling of horizontally loaded monopile foundations for offshore wind energy converters in Germany. *Proc. of International Symposium on Frontiers in Offshore Geotechnics*, Perth, Australia, 6 p.
- Abdel-Rahman, K, and Achmus, M (2006). Behaviour of monopile and suction bucket foundation systems for offshore wind energy plants. *Proc. of 5th International Engineering Conference*, Sharm El-Sheikh, Egypt, 9 p.
- Achmus, M, and Thieken, K (2010). On the behavior of piles in non-cohesive soil under combined horizontal and vertical loading. *Acta Geotechnica*, Vol. 5, no. 3, pp.199–210.
- Achmus, M, Kuo, YS, and Rahman, KA (2009). Behavior of monopile foundations under cyclic lateral load. *Computers and Geotechnics*, Vol. 36, pp. 725–735.
- Achmus, M, Akdag, CT, and Thieken, K (2013). Load-bearing behavior of suction bucket foundations in sand. *Applied Ocean Research*, Vol. 43, pp. 157–165.
- Alderlieste, EA (2011). Experimental modelling of lateral loads on large diameter mono-pile foundations in sand. M.Sc. Thesis, Delft University of Technology, 120 p.
- API. (1987). Recommended practice for planning, designing and constructing fixed

- offshore platforms. API Recommended practice 2A (RP 2A). 17th ed., American Petroleum Institute.
- API. (2011). ANSI/API recommended practice, 2GEO 1st ed., Part 4, American Petroleum Institute.
- Barton, YO (1982). Laterally Loaded Model Piles in Sand: Centrifuge Tests and Finite Element Analyses. PhD Thesis, University of Cambridge.
- Bolton, MD (1986). The strength and dilatancy of sand. *Géotechnique*, Vol. 36, No. 1, pp. 65–78.
- Briaud, J-L, Smith, TD, and Meyer, BJ (1983). Using the pressuremeter curve to design laterally loaded piles. *Proc., 15th Offshore Technology Conf.*, Houston, Paper 4501, 495–502.
- Brinch Hansen, J (1961). The ultimate resistance of rigid piles against transversal forces. Bulletin No. 12, Danish Geotechnical Institute, Copenhagen, Denmark, pp. 5–9.
- Broms, BB (1964). Lateral resistance of piles in cohesive soils. *J. Soil Mech. Found. Div.*, Vol. 90, no. 2, pp. 27–64.
- Budhu, M, and Davies, T (1987). Nonlinear analysis of laterally loaded piles in cohesionless soils. *Can. Geotech. J.*, Vol. 24, no. 2, pp. 289–296.
- Carter, J, and Kulhawy, F (1988). Analysis and design of drilled shaft foundation socketed into rock. Res. Rep. 1493–4, Geotech. Engrg. Group, Ithaca, NY: Cornell University.

- CFEM. (2006). Canadian Foundation Engineering Manual. 4th ed., Canadian Geotechnical Society, Richmond, BC, Canada, 506 p.
- Chakraborty, T, and Salgado, R (2010). Dilatancy and shear strength of sand at low confining pressures. *Journal of Geotechnical and Geoenvironmental Engineering*, Vol. 136, no. 3, pp. 527–532.
- Coduto, DP (2001). Foundation design: Principles & practices, 2nd ed., Prentice Hall, Upper Saddle River, New Jersey, United States, 883 p.
- Cuéllar, VP (2011). Pile Foundations for Offshore Wind Turbines: Numerical and Experimental Investigations on the Behaviour under Short-Term and Long-Term Cyclic Loading. Dr.-Ing. Thesis, Technical University of Berlin, 273 p.
- DNV. (2011). Design of Offshore Wind Turbine Structures, Offshore Standard, DNV-OS-J101, Det Norske Veritas, 213 p.
- Dobry, R, Vincente, E, O'Rourke, M, and Roesset, J (1982). Stiffness and damping of single piles. *J. Geotech. Engrg. Div.*, ASCE, Vol. 108, no. 3, pp. 439–459.
- Doherty, P, and Gavin, K (2012). Laterally loaded monopile design for offshore wind farms. *Proc., ICE-Energy*, Vol. 165, no. 1, pp. 7–17.
- Doherty, P, Li, W, Gavin, K, and Casey, B (2012). Field Lateral Load Test On Monopile In Dense Sand. *Offshore Site Investigation and Geotechnics: Integrated Technologies-Present and Future*.

- Ebin, DMA (2012). The response of monopile wind turbine foundations in sand to cyclic loading. M.Sc. Thesis, Tufts University, 112 p.
- Hearn, EN and Edgers, L (2010). Finite Element Analysis of an Offshore Wind Turbine Monopile. *GeoFlorida 2010: Advances in Analysis, Modeling & Design*, pp. 1857–1865.
- Houlsby, GT. (1991). How the dilatancy of soils affects their behaviour. *Proc. of 10th Eur. Conf. in Soil Mech. and Found. Engrg.*, pp. 1189–1202.
- Hsu, ST, and Liao, HJ (1998). Uplift behaviour of cylindrical anchors in sand. *Canadian Geotechnical Journal*, Vol. 34, pp. 70–80.
- Hsu, ST (2005). A constitutive model for the uplift behavior of anchors in cohesionless soils. *Journal of the Chinese Institute of Engineers*, Vol. 28, no. 2, pp. 305–317.
- Ibsen, L, Larsen, K, and Barari, A (2014). Calibration of Failure Criteria for Bucket Foundations on Drained Sand under General Loading. *Journal of Geotechnical and Geoenvironmental Engineering*, Vol. 140, no. 7: 04014033, 16 p.
- Janbu, N (1963). Soil Compressibility As Determined By Oedometer And Triaxial Test. *Proc. of 3rd European Conference on Soil Mechanics and Foundation Engineering*, Wiesbaden, Germany, Vol. 1, pp. 19–25.
- Klinkvort, RT, and Hededal, O (2011). Centrifuge modelling of offshore monopile foundation. *Frontiers in Offshore Geotechnics II*, ed. 1, Taylor & Francis, pp. 581–586.

- Klinkvort, RT, and Hededal, O (2014). Effect of load eccentricity and stress level on monopile support for offshore wind turbines. *Canadian Geotechnical Journal*, Vol. 51, no. 9, pp. 966–974.
- Klinkvort, RT, Leth CT, and Hededal, O (2010). Centrifuge modelling of a laterally cyclic loaded pile. *Physical Modelling in Geotechnics (Springman, S, Laue, J and Seward, L (eds.))*, CRC Press, London, UK, pp. 959–964.
- Klinkvort, RT (2012). Centrifuge modelling of drained lateral pile - soil response: Application for offshore wind turbine support structures. PhD Thesis, Department of Civil Engineering, Technical University of Denmark, 232 p.
- Kuo, YS, Achmus, M, and Abdel-Rahman, K (2011). Minimum embedded length of cyclic horizontally loaded monopiles. *Journal of Geotechnical and Geoenvironmental Engineering*, Vol. 138, no. 3, pp. 357–363.
- LeBlanc, C, Houlsby, GT, and Byrne, BW (2010). Response of stiff piles in sand to long-term cyclic lateral loading. *Géotechnique*, Vol. 60, no. 2, pp. 79–90.
- Lee, JH, Salgado, R, and Paik, KH (2003). Estimation of load capacity of pipe piles in sand based on cone penetration test results. *Journal of Geotechnical and Geoenvironmental Engineering*, Vol. 129, no. 6, pp. 391–403.
- Lesny, K, and Wiemann, J (2006). Finite-element-modelling of large diameter monopiles for offshore wind energy converters. *Proc., GeoCongress 2006: Geotechnical Engineering in the Information Technology Age*, pp. 1–6.

- Lesny, K, Paikowsky, SG, and Gurbuz, A (2007). Scale Effects in Lateral Load Response of Large Diameter Monopiles. *Proc., Sessions of Geo-Denver*, Denver, Colorado, USA, Geotechnical Special Publication no. 158, 10 p.
- Lings, ML, and Dietz, MS (2004). An Improved Direct Shear Apparatus for Sand. *Géotechnique*, Vol. 54, no. 4, pp. 245–256.
- Møller, IF, and Christiansen, TH (2011). Laterally Loaded Monopile in Dry and Saturated Sand-Static and Cyclic Loading: Experimental and Numerical Studies. Masters Project, Aalborg University Esbjerg, 93 p.
- Malhotra, S (2011). Selection, Design and Construction of Offshore Wind Turbine Foundations. *Wind Turbines, Dr. Ibrahim Al-Bahadly (Ed.)*, ISBN: 978-953-307-221-0, InTech, 652 p.
- Meyerhof, GG, Mathur, SK, and Valsangkar, AJ (1981). Lateral resistance and deflection of rigid wall and piles in layered soils. *Can. Geotech. J.*, Vol. 18, pp. 159–170.
- Petrasovits, G, and Award, A (1972). Ultimate lateral resistance of a rigid pile in cohesionless soil. *Proc., 5th European Conf. on SMFE*, Madrid, Vol. 3, pp. 407–412.
- Potyondy, JG (1961). Skin friction between various soils and construction materials. *Géotechnique*, Vol. 11, No. 4, pp. 339–353.
- Poulos, HG, and Davis, EH (1980). *Pile Foundation Analysis and Design*. John Wiley & Sons, New York, NY, 397 p.

- Poulos, HG, and Hull, T (1989). The role of analytical geomechanics in foundation engineering. *In Foundation engineering: Current principles and practices*, Vol. 2, pp. 1578–1606. Reston, VA: ASCE.
- Prasad, VSNY, and Chari, TR (1999). Lateral capacity of model rigid piles in cohesionless soils. *Soils and Foundations*, Vol. 39, no. 2, pp. 21–29.
- Reese, LC, Cox, WR, and Koop, FD (1974). Analysis of laterally loaded piles in sand. *Offshore Technology Conference*, Houston, Texas, USA, OTC 2080, 11 p.
- Roy, K, Hawlader, B and Kenny, S (2014a). Influence of Low Confining Pressure in Modeling of Lateral Pipeline/Soil Interaction in Dense Sand. *Proc. of the ASME 33rd International Conference on Ocean, Offshore and Arctic Engineering*, San Francisco, California, USA, June 8–13, 9 p.
- Roy, K, Hawlader, B, Kenny, S and Moore, I (2014b). Finite element modeling of uplift pipeline/soil interaction in dense sand. *Geohazards6*, Kingston, Ontario, Canada, June 15–18.
- Sørensen SPH, Brødbæk KT, Møller M, Augustesen AH and Ibsen LB (2009). Evaluation of the load–displacement relationships for large-diameter piles in sand. *Proc. of the 12th International Conference on Civil, Structural and Environmental Engineering Computing* (Topping BHV, Costa Neves LF and Barros RC (eds)), Civil-Comp Press, Sterling, UK, Paper 244, 19 p.

- Schanz, T, and Vermeer, PA (1996). Angles of friction and dilatancy of sand. *Géotechnique*, Vol. 46, no. 1, pp. 145–151.
- Smith, TD (1987). Pile horizontal soil modulus values. *Journal of Geotechnical Engineering*, Vol. 113, no. 9, pp. 1040–1044.
- Tatsuoka, F, Sakamoto, M, Kawamura, T, and Fukushima, S (1986). Strength and deformation characteristics of sand in plane strain compression at extremely low pressures. *Soils and Foundations*, Vol. 26, no. 1, pp. 65–84.
- Tatsuoka, F, Siddiquee, MSA, Park, C -S, Sakamoto, M, and Abe, F (1993). Modeling stress-strain relations of sand. *Soils and Foundations*, Vol. 33, no. 2, pp. 60–81.
- Tiwari, B, and Al-Adhadh, AR (2014). Influence of Relative Density on Static Soil–Structure Frictional Resistance of Dry and Saturated Sand. *Geotechnical and Geological Engineering*, Vol. 32, pp. 411–427.
- Tiwari, B, Ajmera, B, and Kaya, G (2010). Shear strength reduction at soil–structure interaction. *GeoFlorida 2010: Advances in Analysis, Modeling & Design*, Orlando, Florida, United States, February 20–24, pp. 1747–1756.
- Vermeer, PA, and deBorst, R (1984). Non-associated plasticity for soils, concrete, and rock. *Heron*, Vol. 29, no. 3, pp. 5–64.
- Wolf, TK, Rasmussen, KL, Hansen, M, Ibsen, LB, and Roesen, HR (2013). Assessment of  $p - y$  curves from numerical methods for a non-slender monopile in cohesionless

soil. Aalborg: Department of Civil Engineering, Aalborg University, DCE Technical Memorandum, no. 24, 10 p.

Zhang, L, Silva, F, and Grismala, R (2005). Ultimate lateral resistance to piles in cohesionless soils. *Journal of Geotechnical and Geoenvironmental Engineering*, Vol. 131, no. 1, pp. 78–83.

## Chapter 5

### Conclusions and Future Recommendations

#### 5.1 Conclusions

The use of suction caissons as a mooring system is spreading worldwide. Also, large-diameter steel piles are being extensively used for supporting offshore wind turbines. Although, both suction caissons and large-diameter monopiles have been proven as viable alternatives to the conventional gravity based anchoring system and long flexible piles, respectively, the current design methodologies and standards still lack proper guidance towards the optimum design. Finite element (FE) modeling is a strong tool in present days to evaluate the soil–caisson and soil–pile interaction under various loading conditions. FE modeling in conjunction with a proper soil constitutive model is a key to the successful simulation of such soil–structure interaction behavior.

In the first part of the present study, FE modeling of suction caisson installed in dense sand under oblique loading has been performed to evaluate the pullout capacity for various loading angles and mooring positions. In the second part, concentration has been given on the estimation of lateral capacity of large-diameter monopile for different loading eccentricities, also installed in dense sand. The FE analyses have been conducted by commercially available FE software package Abaqus/Explicit to reduce the convergence

problem associated with large displacement analysis in Abaqus/Standard.

The behavior of sand is simulated by adopting a modified form of Mohr-Coulomb (MMC) model which enables the stress and strain dependent behavior of dense sand to take into consideration. The variation of mobilized friction angle ( $\phi'$ ) and dilation angle ( $\psi$ ) with mean effective stress and accumulation of plastic strain is incorporated, which is observed in laboratory tests. This modification removes the constant dilation phenomenon of the built-in Mohr-Coulomb (MC) model available in Abaqus. The stress and strain dependency of mobilized friction angle ( $\phi'$ ) and dilation angle ( $\psi$ ) of sand is implemented by user subroutine VUSDFLD written in FORTRAN. In addition to the analyses performed by the MMC model, the MC model is also used to show the comparison between the results obtained by the both models.

The estimation of pullout capacity of suction caisson for various load inclination angles and mooring positions is presented in Chapter 3. A total of 60 analyses have been performed to examine the effects of loading angle, mooring position and aspect ratio on the pullout capacity. The maximum pullout capacity is obtained for 75% mooring position with loading angle of  $0^\circ$ . Higher capacity is obtained for a constant caisson diameter ( $D$ ) with higher aspect ratio ( $L/D$ ). The results obtained by both the MC and MMC models are compared to centrifuge test results available in literature. Although, the results obtained by the MC model matches well with the centrifuge test results, the MMC model has been found to simulate better the soil behavior surrounding the caisson. The MMC model

produces slightly lower pullout capacity than those obtained by the MC model. The possible explanation of this phenomenon is the variation of mobilized  $\phi'$  and  $\psi$  with mean effective stress and accumulated plastic strain. A distinctive shear band is formed which represents the failure surface and the variation of  $\phi'$  and  $\psi$  is clearly observed inside the shear band. In the MC model, this variation of  $\phi'$  and  $\psi$  is not achievable and constant dilation prevails. Hence, it can be concluded that, the MMC model can simulate better the soil behavior and the estimation of pullout capacity.

In Chapter 4, the lateral capacity of large-diameter monopile for supporting offshore wind turbines is investigated. A total of 46 analyses have been conducted to assess the effects of load eccentricity and aspect ratio. Lower the load eccentricity, higher the lateral capacity is obtained for a given aspect ratio ( $L/D$ ). Also, for higher aspect ratio with a constant pile diameter ( $D$ ) and a given load eccentricity, higher capacity is obtained. The simulation results with the MMC model compare well to centrifuge test results available in literature. Based on the FE results, simplified equations are also proposed to estimate the lateral and moment capacities of monopiles for different load eccentricities and aspect ratios, which take into account the allowable rotation under serviceability limit state (SLS) under monotonic load. The simulations with the MC model produce higher lateral capacities than those obtained by the MMC model. The possible reason behind this can be explained by the formation of distinctive shear bands in front of the pile (in loading direction) in case of the MMC model which is not observed in case of the MC model. Also, the magnitudes of mobilized  $\phi'$  and  $\psi$  vary across the shear bands formed which reach to peak at certain lateral

displacement and then reduce to critical state ( $\phi'_c$ ) and  $0^\circ$ , respectively. This variation of  $\phi'$  and  $\psi$  can not be achieved in the case of the MC model, where constant values of  $\phi'$  and  $\psi$  are used. The simulations with the MMC model provide realistic behavior of dense sand as observed in laboratory tests. Hence, the MMC model is a better tool for estimating the capacity of monopiles and simulating the realistic behavior of surrounding dense sand.

## 5.2 Future Recommendations

The current study presents the estimation of inclined loading pullout capacity of suction caisson and lateral capacity of large-diameter monopile in dense sand by employing an advanced soil model (MMC model). The limitations associated with the conventional built-in MC model have been overcome. Although, the MMC model has been used, the simulations have been performed under static loading. Hence, some recommendations for future studies can be made as follows:

- The simulations can be performed under cyclic loading to get a clear picture of degradation of stiffness of soil.
- The consideration of excess pore water pressure generation due to cyclic loading can also be investigated.
- The modulus of elasticity of soil can be varied with in situ mean effective stress in the simulations in conjunction with the MMC model used in this thesis.
- The effect of disturbance of soil during installation and residual loading can be investigated.

## Appendix A

The technical paper in Appendix A is prepared according to the conference format. This part of the research has been published as:

Ahmed, SS, and Hawlader, BC (2014). Finite Element Modeling of Inclined Load Capacity of Suction Caisson in Sand with Abaqus/Explicit. *Proc. of the 24<sup>th</sup> International Ocean and Polar Engineering Conference*, Busan, Korea, June 15-20, pp. 463–469.

Most of the research work presented in this chapter was conducted by the first author. He also prepared the draft manuscript. The second author supervised the research and reviewed the manuscript.

# Finite Element Modeling of Inclined Load Capacity of Suction Caisson in Sand With Abaqus/Explicit

*Sheikh Sharif Ahmed*

Faculty of Engineering and Applied Science, Memorial University  
St. John's, Newfoundland, Canada

*Bipul Chandra Hawlader*

Faculty of Engineering and Applied Science, Memorial University  
St. John's, Newfoundland, Canada

## ABSTRACT

Suction caissons are widely used in mooring systems for deep water oil and gas development projects. The response of a caisson in sand is different from its response in clay under pullout force. In this study, three-dimensional finite element (FE) analyses are conducted to calculate the pullout capacity of a suction caisson subjected to various oblique loadings. The FE modeling is performed using Abaqus FE software. In the mooring systems, the caisson could have a significant movement and rotation before reaching to the maximum pullout force. Therefore, the Arbitrary Lagrangian Eulerian (ALE) method available in the Abaqus/Explicit is used in the present FE analysis to avoid numerical issues due to excessive mesh distortion at large displacements that typically encountered in the FE formulations in the Lagrangian framework. The sand around the caisson is modeled using the Mohr-Coulomb model. The effects of key variables, such as loading angle, mooring position and aspect ratio, on pullout capacity and rotation of the caisson are presented. The comparison between FE and centrifuge test results is also shown.

**KEY WORDS:** Suction caisson; Arbitrary Lagrangian Eulerian (ALE) method; pullout force; sand; loading angle; mooring position.

## INTRODUCTION

Suction caissons (also known as suction anchors, suction piles or suction buckets) are a unique form of foundation/mooring system that have several advantages over traditional pile foundation and anchors. The main advantages include fast installation, elimination of the pile driving process, reduction in material costs and reusability. A suction caisson is a large diameter hollow cylinder, usually made of steel having top end closed and bottom end opened that is installed in soil by applying suction with pumping water out of caisson interior. Suction caissons are now widely being used in offshore industries for anchoring large offshore floating facilities to the seafloor. The pullout capacity of the caisson is one of the main concerns. The caissons are usually connected to the floating structures by a mooring line which is attached to a pad eye on one side of the caisson.

The pullout behavior of suction caissons installed in both sand and clay

is of great interest of many oil and gas development industry. Previous studies mainly focused on caissons in clay. For example, Aubeny et al. (2003) presented a theoretical method to estimate the inclined load capacity of suction caissons based on an upper bound plasticity formulation for clay. Cao et al. (2002a, b & 2003) conducted centrifuge tests and FE analyses for caissons in clay. Similarly, FE analyses have been performed using various soil constitutive models, including Cam Clay and MIT-E3 models, to understand the response of caissons in clay (e.g. Sukumaran et al., 1999; Handayanu et al., 2000; Zdravkovic et al., 2001).

Limited number of research is available in the literature to estimate the pullout capacity of suction caissons in sand. The mechanisms involved in the installation of a caisson in sand is different from that of in clay. In sand, the seepage due to applied suction plays a significant role. The installation issues of suction caisson in sand and sand/silt layers have been described by Houlsby et al. (2005a, b) and Tran et al. (2007). Some centrifuge tests have been conducted in the past to understand the pullout behavior of caisson in sand (e.g. Allersma et al., 2000; Lee et al., 2003; Kim et al., 2005, 2009, 2010; Jones et al. 2007; Bang et al., 2011, Jang and Kim 2013). Bang et al. (2011) reported a series of centrifuge tests at 100g on a model suction caisson in medium dense sand to determine the pullout capacities.

Numerical modeling of suction caisson in sand is very limited. Deng and Carter (2000) conducted FE analyses of suction caisson in sand assuming axisymmetric loading conditions using the AFENA FE software package and Mohr-Coulomb soil model. Iftekhazzaman and Hawlader (2012) conducted three-dimensional FE analysis using Abaqus/Standard FE software, where they encountered some mesh distortion issues at large displacement.

This paper presents three-dimensional FE modeling of suction caisson in sand subjected to pullout loading at different inclination angles and mooring line attachment positions to evaluate the pullout capacities. A total of 60 cases are analyzed to determine the pullout capacity of the caisson. A parametric study is also conducted to evaluate the effects of length/diameter ratio on pullout capacity. The finite element results are compared with centrifuge test results.

## PROBLEM DEFINITION

A suction caisson of length  $L$  and diameter  $D$  installed in dense sand is simulated in this study. During the installation, the soil in the vicinity of the suction caisson can be disturbed. However, the effects of disturbance on capacity are not considered in this study, instead the simulations are performed for a wished-in-place suction caisson. The caisson is loaded at the five pad eye locations shown in Fig. 1 (a) at different angle  $\theta$  with the horizontal (Fig. 1b). The sign convention used for displacement and rotation of the caisson is shown in Fig. 1(c).

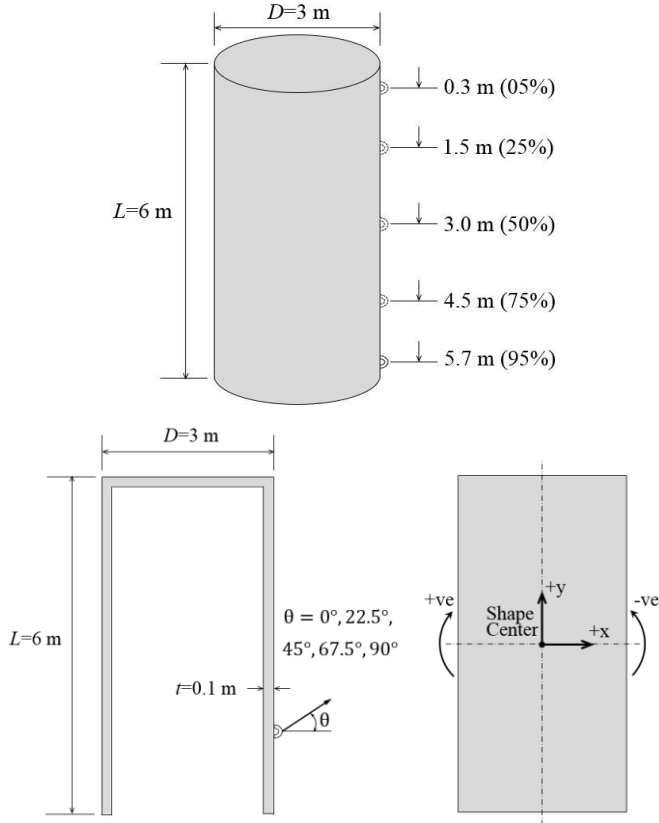


Fig. 1. Problem definition: a) pad eye position, b) loading angle, c) sign convention for displacement and rotation

## FINITE ELEMENT MODEL

The FE analyses are performed using the commercially available finite element software Abaqus/Explicit 6.10-EF-1. Taking the advantage of symmetry, a half-circular soil domain of diameter 22 m and depth 20 m is modeled as shown in Fig. 2. The size of the soil domain is large enough compared to the size of the caisson, and therefore, significant boundary effects are not expected on calculated load, displacement and deformation mechanism.

In the FE model (Fig. 2), the vertical plane of symmetry is restrained from any displacement perpendicular to it, while the other sides of the soil domain are restrained from any lateral displacement using roller supports at the nodes. The bottom boundary is restrained from any vertical displacement, while the top boundary is free to displace.

The soil is modeled using the C3D8R solid homogeneous elements available in Abaqus/Explicit element library, which is an 8-noded linear brick element with reduced integration and hourglass control. The mooring line is modeled as 3D wire using T3D2 element (a 2-node linear 3-D truss) with no interaction with soil domain. Typical FE mesh used in this study is shown in Fig. 2.

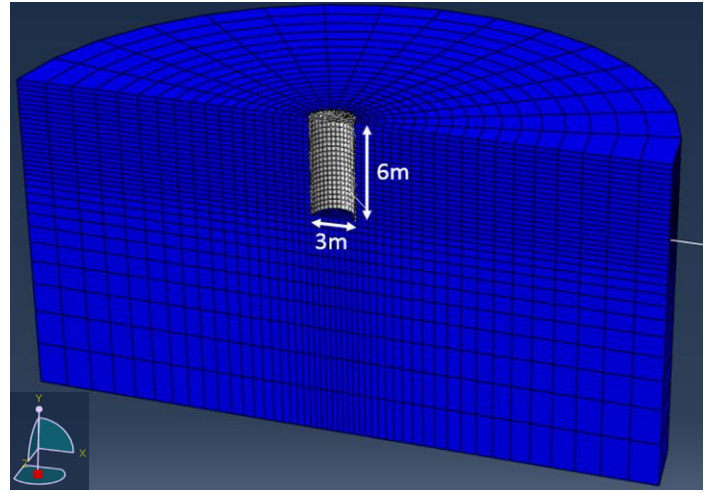


Fig. 2. Finite element mesh used in analysis

## Modeling of Suction Caisson

A caisson of 6 m length and 3 m diameter with 100 mm wall thickness is modeled first. This geometry is referred as “base case” in the following sections. Analyses are also performed for different length and diameter to show the effects of aspect ratio. In the following sections, the results of base case are presented first. Modeling the caisson as elastic-perfectly plastic material and also as rigid body, it is found that the pullout capacity and rotation do not vary significantly with these modeling techniques. However, the FE model with the caisson as a rigid body is computationally very efficient. Therefore, the caisson is considered as a rigid body in the FE analyses presented in the following sections.

## Modeling of Mooring Line

A wire of 50 m length representing the mooring line connected to the suction caisson is modeled using truss element with material properties of steel. The interface friction between the mooring line and soil is assumed to be zero. The pullout force is applied by a displacement boundary condition at the far end.

## Modeling of Sand

The sand is modeled by the Mohr-Coulomb model available in the Abaqus FE software. The submerged unit weight of sand of 8.2 kN/m<sup>3</sup> is used. The geometry and mechanical properties used in the analysis are shown in Table 1. It is to be mentioned that the geometry and soil parameters stated in Table 1 are very similar to Bang et al. (2011), because the FE results are compared with their centrifuge test results to show the performance of the present FE model.

The soil/caisson interaction is modeled using Coulomb friction model, which defines the friction coefficient ( $\mu$ ) as  $\mu = \tan(\phi_\mu)$ , where  $\phi_\mu$  is the soil/caisson interface friction angle. The value of  $\phi_\mu$  is assumed to be equal to  $0.6\phi'_p$  in this analysis.

The effects of loading position and angle of loading are investigated for the base case parameters listed in Table 1. The loads are applied at 5%, 25%, 50%, 75% and 95% mooring positions from the top of the caisson. The inclination angle of the load ( $\theta$ ) is varied as 0°, 22.5°, 45°, 67.5° and 90° for each mooring position. That means a total of 25 analyses are conducted for the base case to evaluate the effects of

mooring position and load inclination angle.

Table 1. Geometry and mechanical properties in FE modeling

Suction Caisson	Diameter ( $D$ )	3 m
	Length ( $L$ )	6 m
Mooring Line	Modulus of elasticity ( $E_s$ )	$2.08 \times 10^8$ kN/m <sup>2</sup>
	Poisson's ratio ( $\nu_p$ )	0.29
Sand	Angle of internal friction ( $\phi'_p$ )	$39^\circ$
	Angle of dilation ( $\psi$ )	$9^\circ$
	Modulus of elasticity ( $E_s$ )	60,000 kN/m <sup>2</sup>
	Poisson's ratio ( $\nu_s$ )	0.30
	Cohesion ( $c'$ ) <sup>1</sup>	0.10 kN/m <sup>2</sup>
	Submerged unit weight ( $\gamma'$ )	8.2 kN/m <sup>3</sup>

<sup>1</sup>Cohesion is required to be defined in Abaqus FE analysis. For sand in this study a very small value of  $c'=0.10$  kN/m<sup>2</sup> is used.

## RESULTS

### Mesh Sensitivity Analysis

In general, smaller FE mesh yields more accurate results but computationally expensive. For efficient modeling, small elements are used near the caisson. The size of the elements is increased with increase in radial distance from caisson as shown in Fig. 2. Similarly, the element size is increased with distance from the bottom of the caisson. To select the optimum mesh, several trial analyses are conducted with different mesh sizes. The force-displacement curves for three different sizes of mesh are shown Fig. 3 for 50% mooring position and loading angle,  $\theta=0^\circ$ . As shown in Fig. 3 that the calculated pullout force is smaller with fine mesh than that of with coarse mesh. In this study, the medium dense mesh is selected to perform the analyses as it is computationally faster, although it is recognized that it gives slightly higher pullout force than that of with fine mesh.

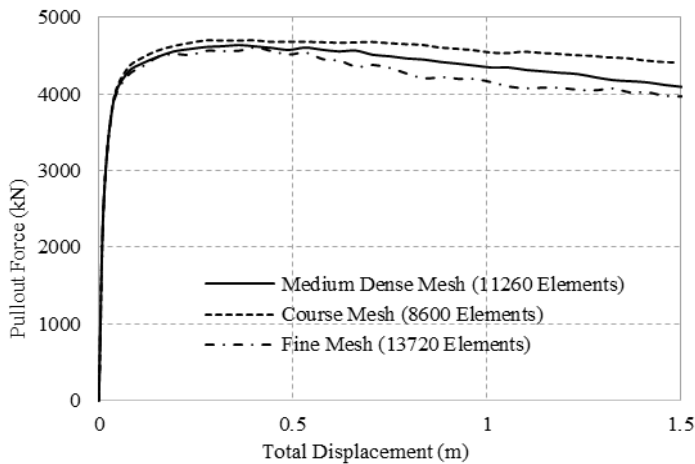


Fig. 3. Mesh Sensitivity Analysis

### Force-displacement Curves

Typical variation of pullout force with total displacement along the direction of pulling is shown in Fig. 4. The pullout force is obtained from the axial force in the wire (truss element in this case). As Abaqus/Explicit is used, a large displacement could be applied without numerical issues. In this study, a total displacement of 1.5 m is applied.

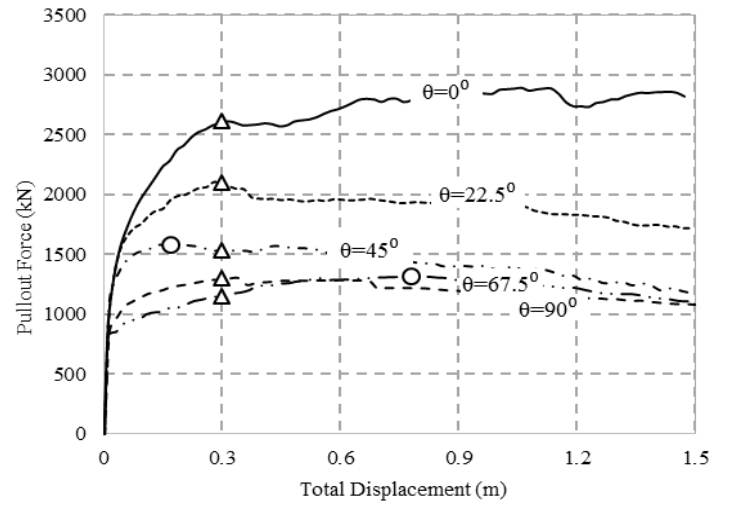


Fig. 4. Typical force-displacement curve (mooring position 5% from the top)

Several methods are available in the literature to estimate the maximum resistance or capacity of pipelines, anchors or pile foundations from force-displacement curves. As shown in Fig. 4, mainly four types of force-displacement curves are obtained from the present FE analyses. Firstly, the force-displacement curve does not show any clear peak as shown for  $\theta=0^\circ$  in Fig. 4. Two out of 25 cases analyzed show this type of behavior. In this cases, the pullout force at 0.3 m ( $=0.1D$ ) displacement is considered as the pullout capacity as shown by the open triangle in Fig. 4. The second type of force-displacement curve shows a clear peak at about  $0.1D$  displacement as shown in Fig. 4 for  $\theta=22.5^\circ$ . In the third type of force-displacement curves, a clear peak is formed before  $0.1D$  displacement as shown in Fig. 4 for  $\theta=45^\circ$  with an open circle. Finally, in the fourth type the peak force is developed at displacements more than  $0.1D$ . However, it is found in all third and fourth type of force-displacement curves that the difference between the peak forces (circles) and the force at  $0.1D$  displacement is very small. Therefore, in this study the force at  $0.1D$  displacement is considered as the pullout force.

The decrease in pullout force at large displacement is mainly because of significant upward movement and rotation of the caisson at large displacement.

### Pullout Capacity

The pullout capacities for different loading angles and mooring positions are shown in Fig. 5. The solid lines in this figure show the FE results while the data point of same symbol show the centrifuge test results (Bang et al., 2011) of similar conditions. The pullout capacities obtained from the present FE analysis follow the same trend as obtained in the centrifuge tests (Bang et al, 2011). For a given mooring position, the maximum pullout capacity is obtained for lateral loading ( $\theta=0^\circ$ ), while the minimum pullout capacity is obtained for  $\theta=90^\circ$ . The difference between the pullout capacity for  $\theta=90^\circ$  and  $\theta=67.5^\circ$  is very small for mooring position up to 75%, because in both cases the caisson moves almost vertically. Note that, even at  $\theta=90^\circ$  the caisson does not move pure vertically as the pad eye is located on one side of the caisson and therefore some counterclockwise rotation is occurred. The maximum pullout capacity is developed at approximately 75% mooring position for  $\theta \leq 45^\circ$ .

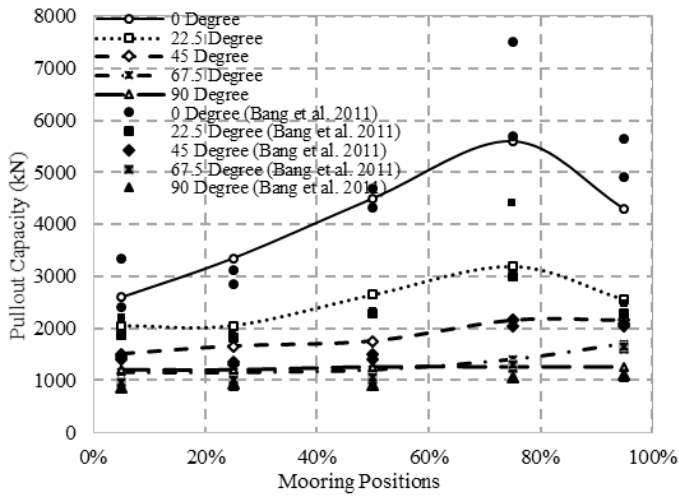


Fig. 5. Comparison of pullout capacity between FE and centrifuge tests

### Rotation

The rotation of the caisson has a significant effect on force-displacement behavior. The rotation of the caisson about the geometric center with total displacement is plotted in Fig. 6 for 25% mooring positions and different load inclination angles. The sign convention used for rotations is shown in Fig. 1(c) in which positive value represents clockwise rotation. As shown, the caisson rotate clockwise for  $\theta=0^\circ$ ,  $22.5^\circ$  and  $45^\circ$ . However, for  $\theta=90^\circ$  counterclockwise rotation is occurred. For  $\theta=67.5^\circ$ , very small rotation of the caisson is occurred. It is to be noted here that although the rotation varies almost linearly with displacement in this case, it is not true for all the cases analyzed.

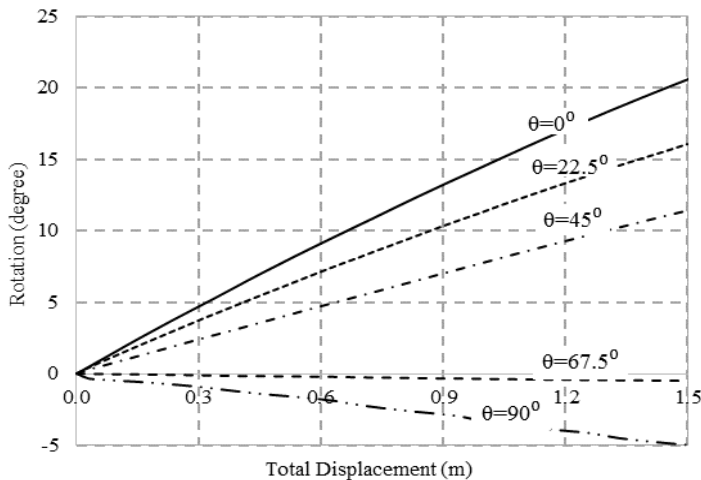


Fig. 6. Typical rotation of caisson (mooring position 25% from the top)

The rotation of the caisson at the pullout capacity ( $0.1D$  displacement) is shown in Fig. 7 for different mooring positions and load inclination angles. The clockwise positive rotation is occurred for 5%, 25% and 50% mooring positions for  $\theta=0^\circ$ ,  $22.5^\circ$  and  $45^\circ$ . The maximum positive rotation is occurred for 50% mooring position at  $\theta=0^\circ$ . On the other hand counterclockwise (negative) rotation is occurred for 75% and 95% mooring positions. Very small rotation is calculated for large values of  $\theta$  ( $=67.5^\circ$  &  $90^\circ$ ), which is also almost independent of mooring position. This is one of the reasons of calculating similar pullout capacity at these loading angles as shown in Fig. 5. The rotation is almost independent of mooring positions for  $90^\circ$  loading angle, and therefore

almost same pullout capacity is obtained for different mooring positions for this value of  $\theta$  as shown in Fig. 5.

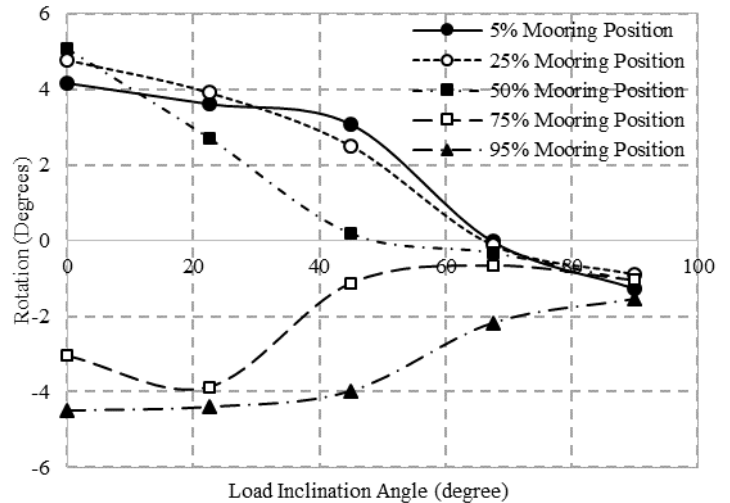


Fig. 7. Rotation of caisson at pullout capacity

### Lateral Displacement

Figure 8 shows the lateral displacement of the geometric centerline of the caisson with depth for different mooring positions at  $\theta=0^\circ$  at the pullout capacity ( $0.1D$  displacement). The lateral displacements for loading at 5%, 25% and 50% mooring positions are opposite to that of 75% and 95% mooring positions. The minimum lateral displacement and rotation of the caisson are occurred for loading at  $\theta=0^\circ$  and 75% mooring position.

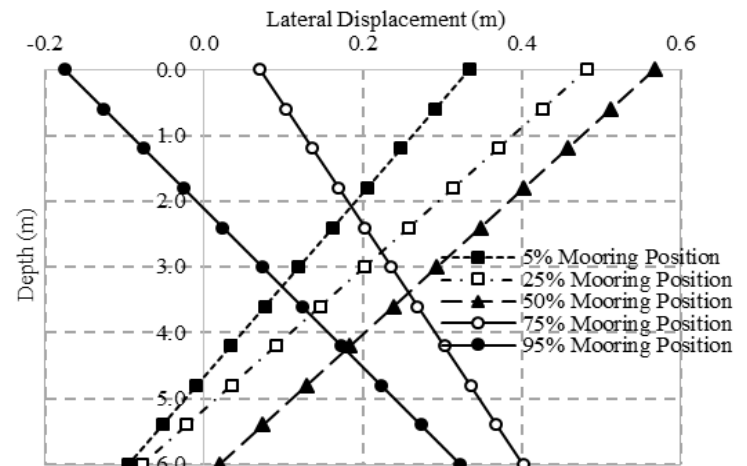


Fig. 8. Lateral displacement of caisson for  $\theta=0^\circ$

### Shape of Soil Failure Wedge

The shape of failure wedge of soil due to inclined loading applied on the caisson is dependent on mooring position and loading angle. The maximum principal plastic strain and the magnitude of total displacements for loading at 25% and 75% mooring positions at  $\theta=0^\circ$  are shown in Fig. 9 and Fig. 10, respectively. As shown in Fig. 9(a) that significant plastic strain is developed in a narrow zone in the right side of the caisson, and a wedge of soil is pushed upward forming heave at the right side of the caisson. The plastic strain inside the wedge is not

very significant. The movement of this wedge is governed by the passive resistance of the soil. In the left side, a gap is formed near the bottom of the caisson and a wedge of soil moves downward resulting in settlement at the seabed. The failure of this soil wedge is mainly governed by the active failure condition.

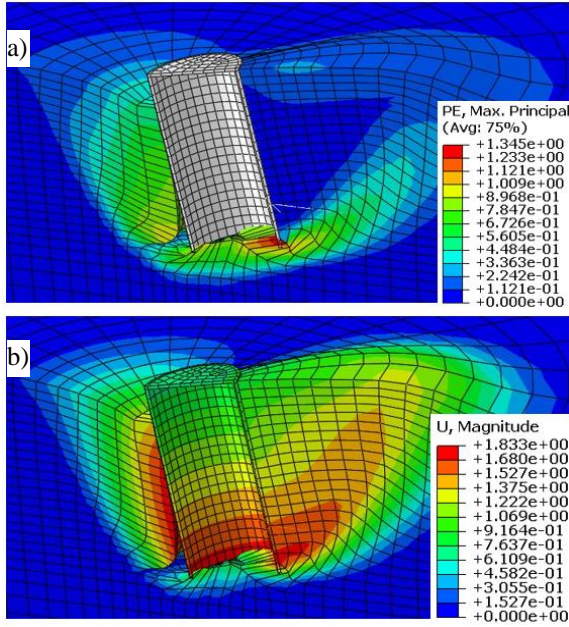


Fig. 9. Maximum principal plastic strain and total displacement profile for 75% mooring position and 1.5 m displacement at  $\theta=0^\circ$

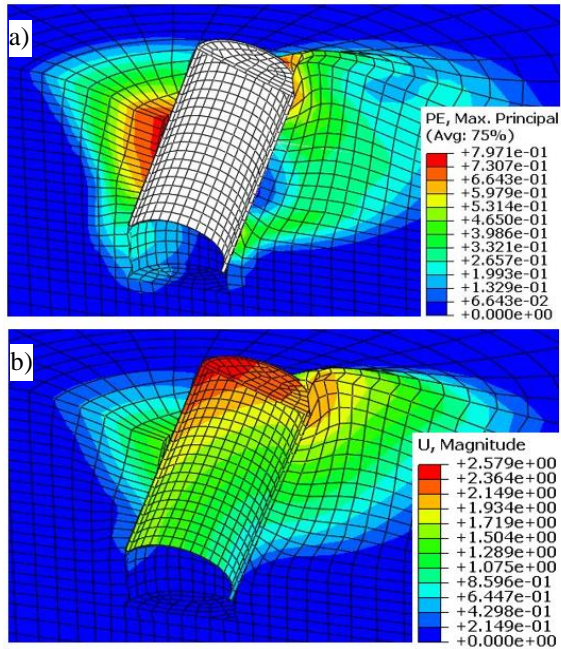


Fig. 10. Maximum principal plastic strain and total displacement profile for 25% mooring position and 1.5 m displacement at  $\theta=0^\circ$

When the caisson is loaded at 25% mooring position, the rotation is in the opposite direction of the rotation for 75% mooring position. Therefore, the soil failure pattern is different as shown in Fig. 10.

The formation of failure wedge in the  $xy$  plane for different mooring positions and loading angles obtained from the present FE analyses are

shown schematically in Figs. 11 and 12. When the caisson is loaded at  $\theta=67.5^\circ$  and  $\theta=90^\circ$  the caisson rotates counterclockwise and failure wedges as shown in Fig. 11 is formed irrespective of the mooring positions. On the other hand, when the caisson is loaded at  $\theta=0^\circ$ ,  $22.5^\circ$  and  $45^\circ$ , the failure pattern is depends on mooring position because of the rotation of the caisson in different direction (Fig. 12). When the caisson is loaded at 5%, 25% and 50% mooring positions, the failure wedge shown in Fig. 12(a) is formed. However, when it is loaded at 75% and 95% mooring position a larger passive wedge is formed as shown in Fig. 12(b). This important phenomenon should be considered in the calculation of the pullout capacity of the caisson.

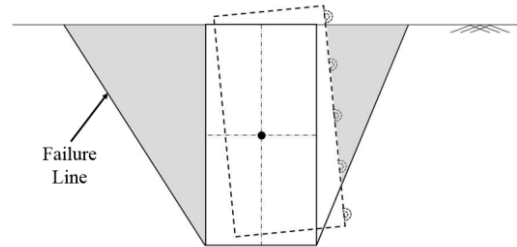


Fig. 11. Failure wedge for  $\theta=67.5^\circ$  and  $90^\circ$  and all mooring positions

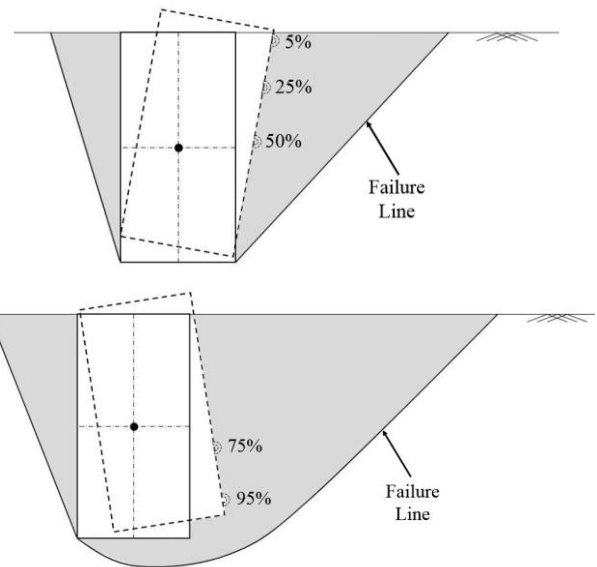


Fig. 12. Failure wedge for  $\theta=0^\circ$ ,  $22.5^\circ$  and  $45^\circ$ : (a) mooring position 5%, 25% and 50%, (b) mooring position 75% and 95%

#### EFFECT OF ASPECT RATIO ( $L/D$ )

The results presented in the previous sections are for the base case where length  $L=6$  m and diameter  $D=3$  m is used. In this section, the pullout capacity for different  $L/D$  ratio is presented. A total of 35 additional analyses are performed to investigate the effect of  $L/D$  ratio on pullout capacity. The geometric parameters are listed in Table 2 which are used for the analyses. All the analyses are conducted for 5%, 25%, 50%, 75% and 95% mooring positions. Only one value of  $\theta$  ( $=0^\circ$ ) is used and the results are compared with the centrifuge tests results by Jang and Kim (2013) where the applied load was in the lateral direction. The soil parameters used in the analysis are listed in Table 1. A typical force-displacement curve for 50% mooring position with different  $L/D$  ratio is shown in Fig. 13. For better comparison, the pullout force and displacement are normalized by diameter in this case

as the diameter is varied. Here,  $\sigma'_v$  is the initial vertical effective stress at the bottom of the caisson. As shown the normalized pullout capacity increases with increase in  $L/D$  ratio.

Table 2. Geometric parameters for different aspect ratios

$L/D$	$L$ (m)	$D$ (m)	$L$ (m)	$D$ (m)
1.5	9	6	6	4
2.0	9	4.5	6	3
2.5	9	3.6	6	2.4
3.0	9	3	6	2

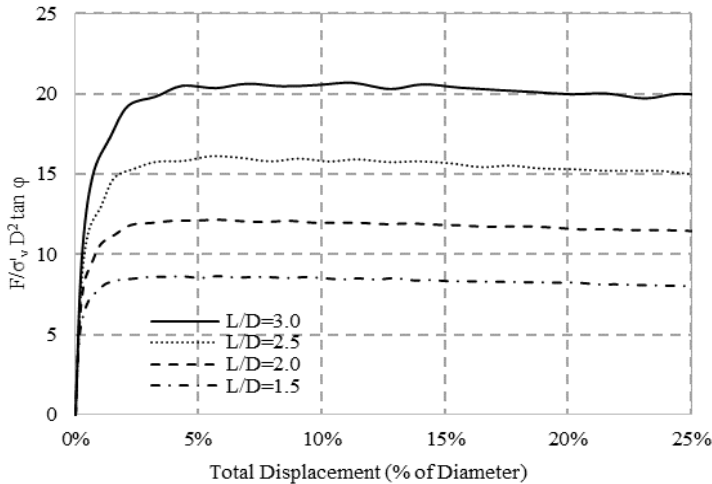


Fig. 13. Force-displacement curves for 50% mooring position

The pullout capacity for different mooring position is shown in Fig. 14. In all four  $L/D$ , the maximum pullout force is obtained for 75% mooring position. Although limited, the centrifuge test results of Jang and Kim (2013) is also shown in Fig. 14. The FE results compare reasonably with the centrifuge test results.

## CONCLUSION

Finite element analyses are conducted to investigate the response of suction caissons in dense sand under large displacement. Abaqus/Explicit FE software package is used in order to overcome the difficulties involved in Abaqus/Standard for large displacement analysis. The caisson is moved 50% of its diameter i.e., 1.5 m and force-displacement curves over a large displacement condition is obtained. The results obtained from the present FE analyses compare reasonably with available centrifuge test results.

The uplift capacity is examined based on three key factors: mooring position, load inclination angle and  $L/D$  ratio. The maximum uplift capacity obtained for 75% mooring position at  $0^\circ$  inclination angle of loading. The rotation of the caisson plays a key role in the pullout capacity. Moreover, the normalized capacity of the caisson increases with increase in  $L/D$  ratio.

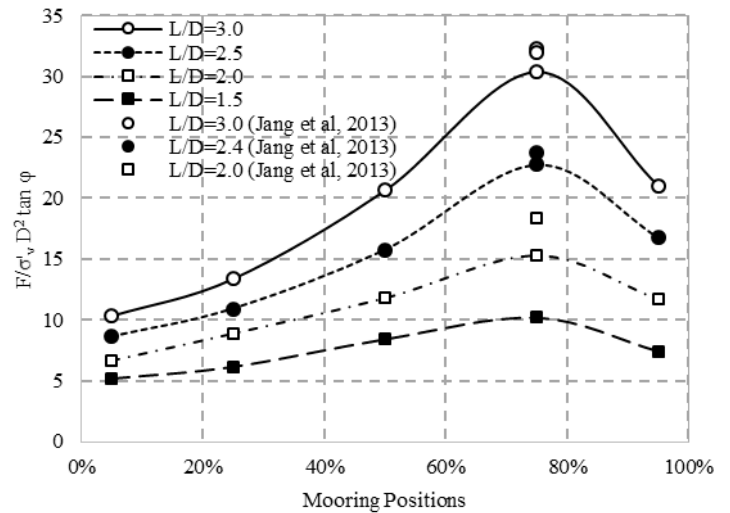


Fig. 14. Pullout capacity for  $\theta=0^\circ$  for different mooring positions

## ACKNOWLEDGEMENTS

The work presented in this paper has been funded by NSERC Discovery grant, MITACS and Petroleum Research Newfoundland & Labrador. The first author expresses his sincerest thank to Md. Iftekharuzzaman, a former graduate student at Memorial University, for his help with initial development of finite element models.

## REFERENCES

- Allersma, HGB, Brinkgreve, RBJ, Simon, T and Kirstein, AA (2000). "Centrifuge and Numerical Modelling of Horizontally Loaded Suction Piles," *International Journal of Offshore and Polar Engineering*, Vol. 10, No. 3, pp. 222-228.
- Aubeny, CP, Han SW and Murff, JD (2003). "Inclined load capacity of suction caissons," *International Journal for Numerical and Analytical Methods in Geomechanics*, Vol. 27, pp. 1235-1254.
- Bang, S, Jones, KD, Kim, KO, Kim, YS and Cho, Y (2011). "Inclined loading capacity of suction piles in sand," *Journal of Ocean Engineering*, Vol. 38, pp. 915-924.
- Cao, J, Phillips, R, Popescu, R, Al-Khafaji, Z, and Audibert, JME (2002a). "Penetration resistance of suction caissons in clay," *Proceedings of the 12th International Offshore and Polar Engineering Conference*, Kitakyushu, May 26-31, pp. 800-806.
- Cao, J, Phillips, R, Audibert, JME and Al-Khafaji, Z (2002b). "Numerical analysis of the behavior of suction caissons in clay," *Proceedings of the 12th International Offshore and Polar Engineering Conference*, Kitakyushu, Japan, May 26-31, pp. 795-799.
- Cao, J, Phillips, R, Popescu, R, Audibert, JME and Al-Khafaji, Z (2003). "Numerical analysis of the behavior of suction caissons in clay," *International Journal of Offshore and Polar Engineering*, Vol. 13, No. 2, pp. 154-159.
- Deng, W, and Carter, JP (2000). "Inclined uplift capacity of suction caissons in sand," *Offshore Technology Conference*, Houston, Texas, OTC 12196, pp. 809-820.
- Handayanu, Swamidasa ASJ, Booton M (2000). "Ultimate strength of offshore tension foundations under vertical and inclined loads," *Proc. of the International Conference on Offshore Mechanics and Arctic Engineering*, New Orleans, Louisiana, Vol. 2, pp. 95-100.
- Houlsby, GT and Byrne BW (2005) "Design procedures for installation of suction caissons in sand," *Proc. ICE - Geotechnical Engineering*, Vol. 158, No 3, pp. 135-144.

- Houlsby, GT and Byrne, BW (2005a). "Calculation procedures for installation of suction caissons in sand," *Proc ICE - Geotechnical Engineering*, Vol. 158, No 3, pp. 135-144.
- Houlsby, GT and Byrne, BW (2005b). "Calculation procedures for installation of suction caissons in clay and other soils," *Proc ICE - Geotechnical Engineering*, Vol. 158, No 2, pp. 75-82.
- Iftekharuzzaman, Md and Hawlader, B (2012). "Numerical modeling of pullout capacity of a suction pile in sand under oblique load," *Second International Conference on Geotechnique, Construction Materials and Environment*, Kuala Lumpur, Malaysia, Nov. pp. 14-16.
- Jang, YS and Kim, YS (2013). "Centrifugal Model Behavior of Laterally Loaded Suction Pile in Sand," *KSCE Journal of Civil Engineering*, Vol. 17, No. 5, pp. 980-988.
- Jones, KD, Bang, S and Cho, Y (2007). "Pullout capacity of embedded suction anchors in sand," *Journal of Ocean Engineering*, Vol. 34, Issue 16, pp. 2107-2114.
- Kim, KO, Kim, YS, Cho, Y, Bang, S and Jones, K (2009). "Centrifuge Model Tests on Suction Piles in Sand under Inclined Loading," *Proceedings of the Nineteenth International Offshore and Polar Engineering Conference*, Osaka, Japan, June 21-26, Vol. II, pp.191-196.
- Kim, Y, Kim, K, Cho, Y and Bang, S (2010). "Centrifuge model tests on suction pile pullout loading capacity in sand," *Int. Conf. on Physical Modelling in Geomechanics*, Vol. 2, pp. 787-792.
- Kim, YS, Kim, KO, Cho, Y, Bang, S and Jones, K (2005). "Centrifuge Model Tests on Embedded Suction Anchors," *Proceedings of the Fifteenth International Offshore and Polar Engineering Conference*, Seoul, Korea, June 19-24, Vol. II, pp.431-435.
- Lee, SH, Cho, Y, Kim, KO, Kim, YS, Lee, TH, and Kwag, DJ (2003). "Centrifuge model tests on embedded suction anchor loading capacities," *Proceedings of The Thirteenth International Offshore and Polar Engineering Conference*, Honolulu, Hawaii, USA, May 25-30, Vol. II, pp. 789-793.
- Sukumaran, B, McCarron, WO, Jeanjean, P and Abouseeda, H (1999). "Efficient finite element techniques for limit analysis of suction caissons under lateral loads," *Computers and Geotechnics*, Vol. 24, pp. 89-107.
- Tran, MN, Randolph, MF and Airey, DW (2007). "Installation of suction caissons in sand with silt layers," *Journal of Geotechnical and Geoenvironmental Engineering*, Vol. 133, No. 10, pp. 1183-1191.
- Zdravkovic, L, Potts, DM, and Jardine, RJ (2001). "A parametric study of the pull-out capacity of bucket foundations in soft clay," *Geotechnique*, Vol. 51, No. 1, pp. 55-67.

## Appendix B

The technical paper in Appendix B is prepared according to the conference format. This part of the research has been published as:

Ahmed, SS, Hawlader, BC, and Roy, KS (2014). Finite Element Modeling of Large Diameter Monopiles in Dense Sand for Offshore Wind Turbine Foundations. *Proc. of the ASME 2015 34<sup>th</sup> International Conference on Ocean, Offshore and Arctic Engineering*, St. John's, Newfoundland, Canada, May 31-June 5, OMAE2015-42218, 7 p.

Most of the research work presented in this chapter was conducted by the first author. He also prepared the draft manuscript. The second author supervised the research and reviewed the manuscript. The third author helped the first author to prepare the draft manuscript.

# FINITE ELEMENT MODELING OF LARGE DIAMETER MONOPILES IN DENSE SAND FOR OFFSHORE WIND TURBINE FOUNDATIONS

**Sheikh Sharif Ahmed**

MEng Candidate

Memorial University of Newfoundland

St. John's, NL, Canada

Email: ssa725@mun.ca

**Bipul Hawlader**

Associate Professor

Memorial University of Newfoundland

St. John's, NL, Canada

**Kshama Roy**

PhD Candidate

Memorial University of Newfoundland

St. John's, NL, Canada

## ABSTRACT

With increasing demand of energy, attention to the alternative sources of sustainable energy is getting priority over the last decades. Offshore wind turbine is one of them. The most widely used foundation system for the wind turbine is the monopile, which is a large diameter single pile. In the present study, three-dimensional finite element (FE) analyses are performed to evaluate the capacity of large diameter monopiles in dense sand using the Arbitrary Lagrangian-Eulerian (ALE) approach available in Abaqus/Explicit FE software. The behavior of sand is modeled using the Mohr-Coulomb (MC) and a modified Mohr-Coulomb (MMC) model where the pre-peak hardening, post-peak softening and the effects of mean effective stress and relative density on stress-strain behavior of dense sand are considered. Comparison with physical model test results shows that the MMC model can simulate better the load-displacement response than that with the MC model. The mechanisms involved in soil deformation are also explained using FE results.

**Keywords:** monopiles; finite element methods; dense sand; offshore wind turbine.

## INTRODUCTION

The quest for renewable and sustainable energy system is one of utmost priorities in today's world. Wind energy is one of the most promising renewable energy sources through which electricity can be produced by using large wind turbines. The use of wind turbines in offshore is now growing because more electricity could be generated using larger structures in offshore.

The possible options (Fig. 1) that can be used as foundation for offshore wind turbines are: gravity based foundation, monopile, mono-caisson, multi-pile and multi-caisson [1]. At shallow water depths (<35 m), monopiles are the most popular foundation option. For example, by the end of 2013, monopiles cover 76% of all the foundation types for wind turbines [2].

While being used as foundations to support offshore wind turbines, monopiles encounter large overturning moment and horizontal load compared to vertical load. The aim of the present study is to model numerically the combined effects of horizontal and moment loading (because of load eccentricity) on monopile. While authors understand that cyclic loading due to wave and wind actions on the pile is equally important, the focus of this study is to simulate the behavior of monopile under static loading.

The most widely used current design method for monopiles is the  $p-y$  curve method [3]. Another alternative design method is the strain wedge method developed by Norris [4] and Ashour and Norris [5]. Although the  $p-y$  curve method has been used in the design of piles for offshore oil and gas platforms, it has originally been developed from field tests on long and flexible piles with small load eccentricity and having relatively small diameters ranging between 0.5 and 2.0 m ([6], [7]). Since the anticipated loads on offshore wind turbine supporting monopiles include a large moment as well as horizontal load, the design of these large diameter monopiles based on the  $p-y$  curve method requires significant extrapolation.

The behavior of monopiles as a foundation system for offshore wind turbines is still under research. The primary focus of most of the research is on the initial stiffness and the ultimate

capacity for the  $p$ - $y$  curves (e.g., [8], [9], [10], [11], [12], [13]). A few field test results and centrifuge test results on monopiles have also been reported in the literature. For example, Hokmabadi et al. [14] reported a full-scale test on monopiles in the Pars Special Economic Energy Zone in southern Iran. Dickin and Nazir [15] conducted centrifuge tests on short rigid piles to evaluate moment carrying capacity. Klinkvort et al. [16] reported centrifuge tests to evaluate the performance of piles under cyclic lateral loading. Klinkvort and Hededal [17] reported centrifuge test results of monopiles under static combined loading and cyclic loading in sand. In a recent study, Klinkvort and Hededal [18] conducted centrifuge tests to examine the effects of load eccentricity on load-displacement behavior and proposed a modified hyperbolic equation for the  $p$ - $y$  curves.

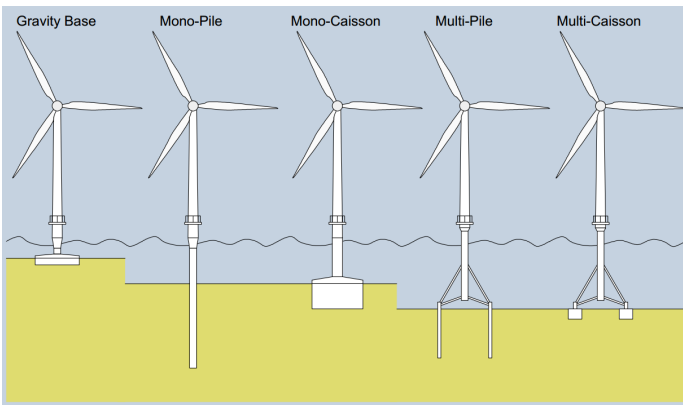


**Figure 1:** Foundation options for offshore wind turbine (after Byrne [1])

Limited attempts have been undertaken to simulate the behavior of eccentrically loaded monopiles using FE methods. Numerical modeling of monopiles and suction caissons in sand has been performed by Rahman and Achmus [19] and they reported the effects of  $L/D$  ratio on stiffness of foundation as well as horizontal displacement and rotation. Wolf et al. [20] performed numerical analysis of a laterally loaded monopile in sand and compared the  $p$ - $y$  curves with a full-scale test results and API method.

In the present study, three-dimensional FE analyses are performed to evaluate the response of a monopile in dense sand subjected to lateral load at different eccentricities using Abaqus/Explicit FE software. Recognizing the need of an appropriate constitutive model for dense sand, a modified form of Mohr-Coulomb model is employed. Analyses are also performed using the built-in Mohr-Coulomb model. The FE results are compared with centrifuge test results.

## PROBLEM DEFINITION

A monopile of length  $L$  and diameter  $D$  installed in dense sand is simulated in this study. During the installation, the soil in the vicinity of the monopile can be disturbed. However, the effects of disturbance on capacity are not considered in this study,

instead the simulations are performed for a wished-in-place monopile. The monopile is horizontally loaded for two different load eccentricities shown in Fig. 2. The sign convention used for displacement of the monopile is also shown in this figure.

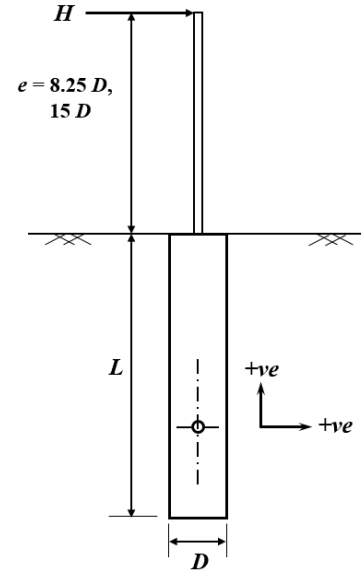


**Figure 2:** The schematic of the model monopile

## FINITE ELEMENT MODEL

Numerical analyses are performed using the commercially available FE software package Abaqus/Explicit 6.13-1. Taking the advantage of symmetry, a half-circular soil domain of diameter 45 m ( $=15D$ ) and depth 30 m ( $=1.67L$ ) is modeled as shown in Fig. 3. The size of the soil domain is selected based on preliminary analyses conducted with different dimensions. The size of the domain is large enough compared to the size of the monopile considered and therefore significant boundary effects are not observed on calculated load, displacement and deformation mechanisms.

In the FE model (Fig. 3), the vertical plane of symmetry is restrained from any displacement perpendicular to it, while the other sides of the soil domain are restrained from any lateral displacement using roller supports at the nodes. The bottom boundary is restrained from any vertical displacement, while the top boundary is free to displace. The soil and the pile are modeled using the C3D8R solid homogeneous elements available in Abaqus/Explicit element library, which is an 8-noded linear brick element with reduced integration and hourglass control. The monopile is modeled as a rigid body with a reference point at a distance  $e$  above the pile head, where, displacement is applied along the  $x$  direction. This creates horizontal load  $H$  and moment  $M = H \times e$  at the pile head.

## MODELING OF MONOPILE

Klinkvort and Hededal [18] conducted a number of centrifuge tests to understand the response of monopiles in dense sand

subjected to eccentric lateral loading. Two of their tests (T6 and T9) are simulated in this study to show the performance of the present FE modeling. In these tests a monopile of 18 m length and 3 m diameter in prototype scale was installed in saturated dense sand ( $D_r \approx 90\%$ ). The pile was then subjected to lateral loading at an eccentricity ( $e$ ) of  $8.25D$  and  $15D$  in test T6 and T9, respectively (Fig. 2). Although monopiles are typically hollow, Klinkvort and Hededal [18] conducted tests using solid steel piles and therefore the rigidity might be different. In order to check this effect, first the analysis is performed with a hollow steel pile of 100 mm wall thickness where the pile is modeled as elastic-perfectly plastic material. In the second step, analysis is performed assuming the pile as a rigid body. No significant difference between these two analyses is found. Therefore, all the analyses presented in the following sections, the pile is considered as a rigid body because it saves the computational time significantly.

### MODELING OF SAND

The Mohr-Coulomb (MC) model is one of the most widely used soil constitutive model which can reasonably simulate the behavior of sand. This model has been used earlier to evaluate the combined loading behavior of monopile as well as to simulate the deformation characteristics of surrounding sands ([19], [20]). However, the Mohr-Coulomb model has some inherent limitations. Once the soil reaches the yield surface, constant dilation is employed which implies that soil will continue to dilate indefinitely if shearing is continued, whereas realistically the soil reaches the critical state as found from laboratory tests. In the present study, this limitation is overcome by employing a modified form of Mohr-Coulomb (MMC) model proposed by Roy et al. [21] which takes into account the effects of pre-peak hardening, post-peak softening, density and confining pressure on angle of internal friction ( $\phi'$ ) and dilation angle ( $\psi$ ) of dense sand. A summary of the constitutive relationships of the MMC is shown in Table 1.

The peak friction angle of sand increases with the increase in relative density ( $D_r$ ) and decreases with the increase in confining pressure, which is a well-recognized phenomena observed in both triaxial tests and direct simple shear tests. The variation of mobilized friction angle and dilation angle with accumulated plastic strain can be expressed as functions of relative density and confining pressure ([22], [23]). Hsu and Liao [22] and Hsu [23] proposed some relationships among mobilized friction angle, dilation angle, relative density, confining pressure and accumulated plastic shear strain. They also implemented these relationships in FLAC to evaluate the uplift behavior of anchors in sand. More recently, Roy et al. [21] further improved the relationships (MMC model) and successfully employed in Abaqus to simulate the behavior of buried pipeline in dense sand.

In this paper, both MC and MMC models for dense sand are used to evaluate the capacity of monopiles for eccentric loading and to capture the deformation behavior of surrounding sand and

then compared to the available test results. In the MMC model, the mobilized friction angle and dilation angle of dense sand is varied with accumulated plastic strain as well as confining pressure via user subroutine written in FORTRAN.

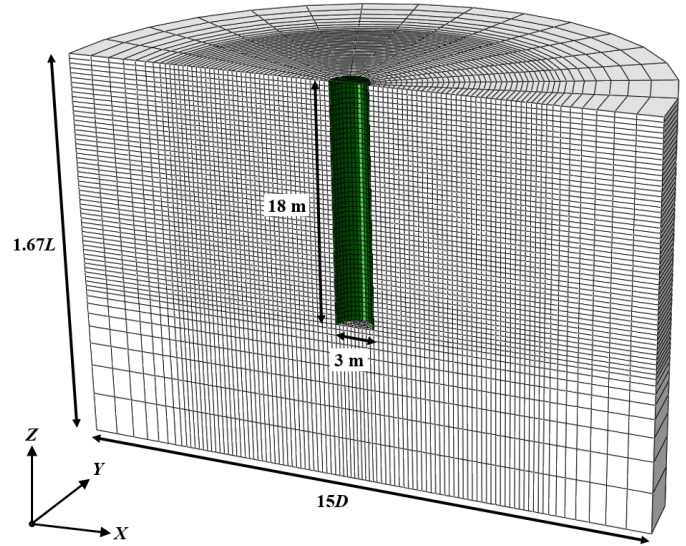


**Figure 3:** Finite element mesh used in the study

The soil parameters used in FE analysis are listed in Table 2. Details of these soil parameters are available in Roy et al. [21]. However, two parameters  $A_\psi$  and  $k_\psi$  need to be discussed further. Based on experimental results, Bolton [24] recommended  $A_\psi=5$  and  $k_\psi=0.8$  for plane strain condition and  $A_\psi=3$  and  $k_\psi=0.5$  for triaxial condition. In a recent study, Chakraborty and Salgado [25] showed that  $A_\psi=3.8$  and  $k_\psi=0.6$  is valid for both triaxial and plane strain condition for Toyoura sand. Note that, the soil around the pile under loading is not only in triaxial or plane strain condition but varies in a wide range of stress conditions. Therefore, in this study  $A_\psi=3.8$  and  $k_\psi=0.6$  is used for simplicity. In addition, the parameter  $Q$  is varied as  $Q = 7.4 + 0.6 \ln(\sigma'_c)$  [25] with  $7.4 \leq Q \leq 10$ , where  $\sigma'_c$  is the initial confining pressure which is calculated from in-situ stresses.

As the variation of  $\phi'$  and  $\psi$  with plastic strain and confining pressure is not considered in the Mohr-Coulomb model, the estimation of representative values for constant  $\phi'$  and  $\psi$  is challenging. Based on American Petroleum Institute ([26]),  $\phi'$  (in degree) can be estimated as  $\phi' = 16D_r^2 + 0.17D_r + 28.4$ . Now using the relationship proposed by Bolton [24], the  $\psi = (\phi' - \phi'_c)/0.8$  can be calculated. In this study,  $\phi' = 41.5^\circ$  and  $\psi = 12.5^\circ$  for  $D_r=90\%$  and  $\phi'_c = 31^\circ$ . It is to be noted here that,  $\phi' = 41.5^\circ$  and  $\psi = 12.5^\circ$  are used while conducting the analyses with the MC model.

The soil/pile interaction is modeled using the Coulomb friction model, which defines the friction coefficient ( $\mu$ ) as  $\mu = \tan(\phi_\mu)$ , where  $\phi_\mu$  is the soil/pile interface friction angle. A value of  $\mu=0.5$  is used in this study.

**Table 1:** Equations for Modified Mohr-Coulomb Model (MMC) (summarized from Roy et al. [21], [28] )

Description	Constitutive Equation	Soil Parameters
Relative density index	$I_R = I_D(Q - \ln p') - R$	$I_D = \frac{D_r(\%) }{100}$ , $R = 1$ [24], $Q = 7.4 + 0.6 \ln(\sigma'_c)$ & $7.4 \leq Q \leq 10$ [25], $\sigma'_c = p' \left( 1 - \frac{2 \sin \phi'_c}{3 - \sin \phi'_c} \right)$
Peak friction angle	$\phi'_p = \phi'_c + A_\psi I_R$	$\phi'_c, A_\psi$
Peak dilation angle	$\psi_p = \left( \frac{\phi'_p - \phi'_c}{k_\psi} \right)$	$k_\psi$
Strain softening parameter	$\gamma_c^p = C_1 + C_2 I_D$	$C_1, C_2$
Plastic strain at $\phi'_p$	$\gamma_p^p = \gamma_c^p \left( \frac{p'}{p'_a} \right)^m$	$p'_a, m$
Mobilized friction angle at zone-II	$\phi' = \phi'_{in} + \sin^{-1} \left[ \left( \frac{2\sqrt{\gamma^p \gamma_p^p}}{\gamma^p + \gamma_p^p} \right) \sin(\phi'_p - \phi'_{in}) \right]$	
Mobilized dilation angle at Zone-II	$\psi = \sin^{-1} \left[ \left( \frac{2\sqrt{\gamma^p \gamma_p^p}}{\gamma^p + \gamma_p^p} \right) \sin(\psi_p) \right]$	
Mobilized friction angle at zone-III	$\phi' = \phi'_c + \exp \left[ - \left( \frac{\gamma^p - \gamma_p^p}{\gamma_c^p} \right)^2 \right] (\phi'_p - \phi'_c)$	
Mobilized dilation angle at Zone-III	$\psi = \exp \left[ - \left( \frac{\gamma^p - \gamma_p^p}{\gamma_c^p} \right)^2 \right] \psi_p$	
<p><b>Symbols:</b> <math>A_\psi</math>: slope of <math>(\phi'_p - \phi'_c)</math> vs. <math>I_R</math>; <math>m, C_1, C_2</math>: soil parameters; <math>I_R</math>: relative density index; <math>k_\psi</math>: slope of <math>(\phi'_p - \phi'_c)</math> vs. <math>\psi_p</math>; <math>\phi'_{in}</math>: <math>\phi'</math> at the start of plastic deformation; <math>\phi'_c</math>: critical state friction angle; <math>\gamma^p</math>: engineering plastic shear strain</p>		

The Young's modulus of sand ( $E_s$ ) can be expressed as a function of mean effective stress ( $p'$ ) as,  $E_s = K p_{atm} (p'/p_{atm})^n$  [27]; where,  $K$  and  $n$  are soil parameters and  $p_{atm}$  is the atmospheric pressure. However, in this study, no attempt has been taken to vary  $E_s$  with  $p'$  during loading; rather, a constant value of  $E_s=90$  MPa is used which is a reasonable value for a dense sand having  $D_r=90\%$ .

## RESULTS

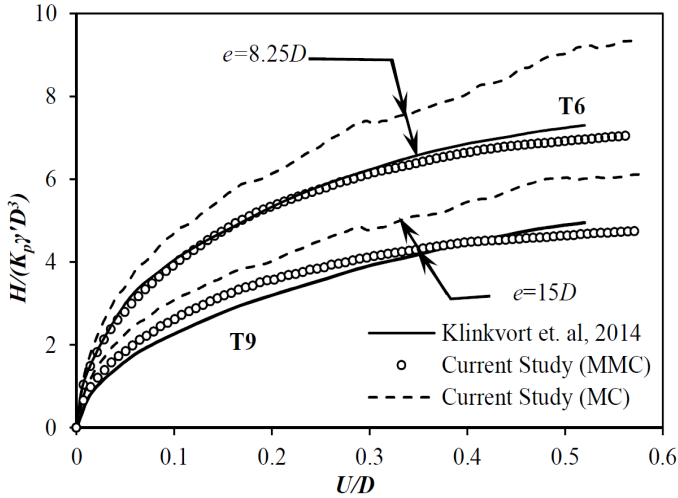
### Load-Displacement Behavior

Figure 4 shows the normalized load-displacement curves for the two centrifuge tests simulated in this study. Similar to Klinkvort et al. [18], the horizontal load ( $H$ ) is normalized as  $H/K_p \gamma' D^3$ , where  $K_p$  is the Rankin's passive earth pressure

coefficient. The horizontal displacement of the pile head ( $U$ ) is normalized by diameter. The load-displacement curves obtained from centrifuge tests [18] are also plotted in this figure. As shown in Fig. 4, the FE results with the MMC model match very well with test results.

The dashed lines in Fig. 4 show the FE results with the built-in Mohr-Coulomb model in ABAQUS. For both  $e = 8.25D$  and  $e = 15D$ , the MC model calculates higher normalized resistance than test results. This is because of two reasons—at low  $U/D$ , the mean stress in front of the pile is low and very few elements reach the post-peak softening state. These factors increase mobilized  $\phi'$  and  $\psi'$ . In contrast, at large displacements, the mean stress and the number of elements in the post-peak softening state increase (shown later), which reduce  $\phi'$  and  $\psi'$ ,

causing the reduction of the stiffness of the force-displacement curve. This trend is very similar to the centrifuge test results. As these factors are not considered in the MC model, the reduction of stiffness with  $U/D$  cannot be simulated.



**Figure 4:** Comparison of normalized load displacement curve with centrifuge test results

**Table 2:** Parameters used in FE analyses

Parameters	Value
External diameter of monopile, $D$ (m)	3
Length of the monopile, $L$ (m)	18
Poisson's ratio of soil, $\nu_{soil}$	0.3
$A_\psi$	3.8
$k_\psi$	0.6
$\phi'_{in}$	29°
$C_1$	0.22
$C_2$	0.11
$m$	0.25
Critical state friction angle, $\phi'_c$	31°
Relative density of sand, $D_r$ (%)	90
Submerged unit weight, $\gamma'$ (kN/m <sup>3</sup> )	10.2
Interface friction co-efficient, $\mu$	0.5
<sup>1</sup> Cohesion, $c'$ (kN/m <sup>3</sup> )	0.10

### SOIL FAILURE MECHANISM

The mechanisms involved in force-displacement behavior can be further explained using plastic deformation of soil and formation of shear bands (plastic shear strain concentrated zones). Figure 5 shows the development of plastic shear strains for the simulation of test T9 for three different values of  $U/D$  ( $=0.03, 0.2$  and  $0.6$ ) with  $D=3$  m. The left column of Fig. 5 (a-c) shows the simulation using the MMC model. Figure 5(a) shows that at small  $U/D=0.03$ , the plastic shear strains develop in the soil mainly near the pile head. Because of eccentric lateral loading, an inclined downward shear band  $f_1$  is formed in front of the pile (right side) from the pile head. At this stage,

another inclined upward shear band  $f_2$  is also formed. These shear bands created a failure wedge. Very small or negligible plastic shear strains develop in the soil elements inside the wedge. With increase in lateral displacement, the plastic shear strains inside and around the shear bands mainly increase. At  $U/D=0.2$ , another shear band  $f_3$  is formed (Fig. 5b). The process is continued as shown in Figs. 5(a) to 5(c).

The formation of plastic shear zones in the soil around the pile with the Mohr-Coulomb (MC) model (right column of Fig. 5) is different from the simulation with the MMC model. For the MC model, the shear band formation is not very clear because post-peak softening is not considered in this model. The plastic shear strains are distributed over a large area in front of the pile. In other words, the soil failure mechanisms with the Mohr-Coulomb model are different from that of with the modified Mohr-Coulomb model.

### CONCLUSIONS

In this study, FE modeling is carried out to simulate the response of large diameter monopiles in dense sand which are widely used to support offshore wind turbines. Recognizing the fact that constitutive model of sand influences the load carrying capacity, two models of sand are employed in the present FE simulations. It is shown that if the mobilized friction angle and dilation angle are modeled as function of plastic strain, density, and mean effective stress as the proposed modified Mohr-Coulomb model, the simulation of load-displacement response improves as compared to the simulations with the Mohr-Coulomb model where constant friction angle and dilation angle are used. The failure mechanisms are also different in the simulations with the Mohr-Coulomb and modified Mohr-Coulomb models.

### ACKNOWLEDGMENTS

The work presented in this paper is funded by MITACS, PRNL and NSERC.

### REFERENCES

- [1] Byrne, B.W. 2011, "Foundation Design for Offshore Wind Turbines", *Géotechnique Lecture 2011*, British Geotechnical Association, Institution of Civil Engineers, 9th November 2011.
- [2] EWEA. 2014. *The European offshore wind industry - key trends and statistics 2013*, European Wind Energy Association.
- [3] API. 2011. *ANSI/API recommended practice, 2GEO 1st ed., Part 4*, American Petroleum Institute.
- [4] Norris, G. 1986, "Theoretically based BEF laterally loaded pile analysis", *3rd International Conference on Numerical Methods in Offshore Piling*, Nantes, France, pp. 361-386.
- [5] Ashour, M., & Norris, G. 1998, "Lateral loading of a pile in layered soil using the strain wedge model", *Journal of*

**Modified Mohr-Coulomb (MMC) model**

**Mohr-Coulomb (MC) model**

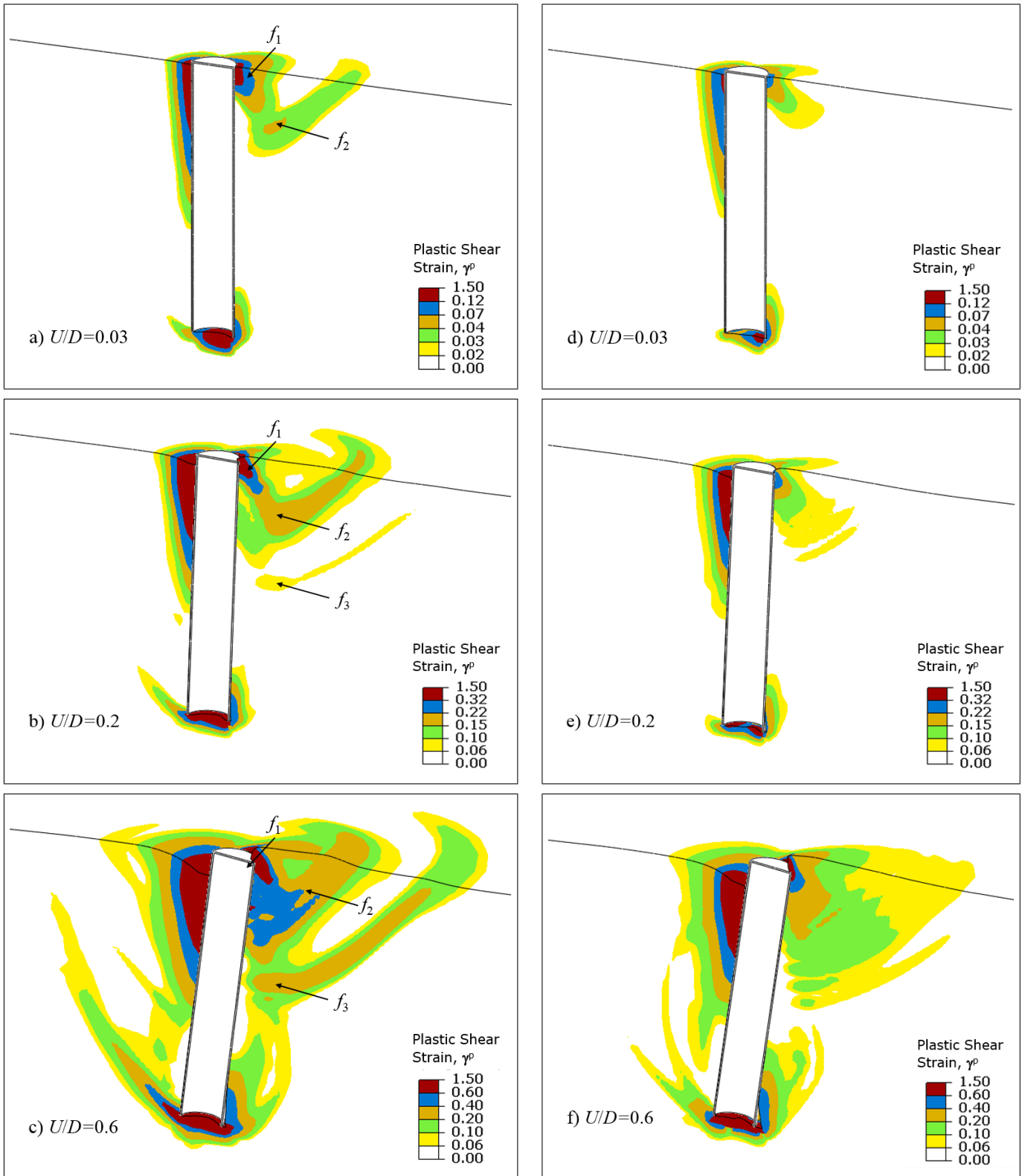


**Figure 5:** Development of plastic shear zone with the MMC and MC model

- Geotechnical and Geoenvironmental Engineering*, vol. 124, no. 4, pp. 303-315.
- [6] Reese, L.C., & Matlock, H. 1956. "Non-dimensional solutions for laterally-loaded piles with soil modulus assumed proportional to depth", *Proceedings of the Eighth Texas Conference on Soil Mechanics and Foundation Engineering*.
- [7] McClelland, B., & Focht, J.J.A. 1956. "Soil modulus for laterally loaded piles", *Journal of the Soil Mechanics and Foundations Division*, ASCE, vol. 82, no. 4, pp. 1-22.
- [8] Ashford, S.A., & Juimarongrit, T. 2003. "Evaluation of pile diameter effect on initial modulus of subgrade reaction", *Journal of Geotechnical and Geoenvironmental Engineering*, vol. 129, no. 3, pp. 234-242.
- [9] Fan, C., & Long, J.H. 2005. "Assessment of existing methods for predicting soil response of laterally loaded piles in sand", *Computers and Geotechnics*, vol. 32, no. 4, pp. 274-289.
- [10] Zhang, L., Silva, F., & Grismala, R. 2005. "Ultimate lateral resistance to piles in cohesionless soils", *Journal of Geotechnical and Geoenvironmental Engineering*, vol. 131, no. 1, pp. 78-83.
- [11] Lesny, K., & Wiemann, J. 2006. "Finite element modelling of large diameter monopiles for offshore wind energy converters", *Proceedings of GeoCongress 2006: Geotechnical Engineering in the Information Technology Age*, vol. 2006, pp. 1-6.
- [12] Pender, M.J., Carter, D.P., & Pranjoto, S. 2007. "Diameter effects on pile head lateral stiffness and site investigation requirements for pile foundation design", *Journal of Earthquake Engineering*, vol. 11, no. 1, pp. 1-12.
- [13] Hald, T., Mørch, C., Jensen, L., Bakmar, C.L., & Ahle, K. 2009. "Revisiting monopile design using  $p - y$  curves: Results from full scale measurements on Horns Rev", *Proceedings of the European Offshore Wind 2009 Conference*.
- [14] Hokmabadi, A.S., Fakher, A. & Fatahi, B. 2012, "Full scale lateral behaviour of monopiles in granular marine soils", *Marine Structures*, vol. 29, pp. 198-210.
- [15] Dickin, E.A., & Nazir, R.B. 1999. "Moment-Carrying capacity of short pile foundations in cohesionless soil", *Journal of Geotechnical and Geoenvironmental Engineering*, vol. 125, no. 1, pp. 1-10.
- [16] Klinkvort, R.T., Leth C.T., & Hededal, O. 2010. "Centrifuge modelling of a laterally cyclic loaded pile", *Physical Modelling in Geotechnics (Springman, S, Laue, J and Seward, L (eds.))*, CRC Press, London, UK, pp. 959-964.
- [17] Klinkvort, R.T., & Hededal, O. 2011. "Centrifuge modelling of offshore monopile foundation", *Frontiers in Offshore Geotechnics II*, ed. 1, Taylor & Francis, pp. 581-586.
- [18] Klinkvort, R.T., & Hededal, O. 2014. "Effect of load eccentricity and stress level on monopile support for offshore wind turbines", *Canadian Geotechnical Journal*, vol. 51, no. 9, pp. 966-974.
- [19] Rahman, K.A., & Achmus, M. 2006. "Behaviour of monopile and suction bucket foundation systems for offshore wind energy plants", *5th International Engineering Conference*, Sharm El-Sheikh, Egypt, 2006.
- [20] Wolf, T.K., Rasmussen, K.L., Hansen, M., Ibsen, L.B., & Roesen, H.R. 2013. "Assessment of p-y curves from numerical methods for a non-slender monopile in cohesionless soil", *Aalborg: Department of Civil Engineering, Aalborg University*, DCE Technical Memorandum, no. 24.
- [21] Roy, K.S., Hawlader B.C. & Kenny, S. 2014, "Influence of Low Confining Pressure on Lateral Soil/Pipeline Interaction in Dense Sand", *33rd International Conference on Ocean, Offshore and Arctic Engineering (OMAE2014)*, San Francisco, California, USA, June 8-13, 2014.
- [22] Hsu, S.T., & Liao, H.J. 1998. "Uplift behaviour of cylindrical anchors in sand", *Canadian Geotechnical Journal*, vol. 34, pp. 70-80.
- [23] Hsu, S.T. 2005. "A constitutive model for the uplift behavior of anchors in cohesionless soils", *Journal of the Chinese Institute of Engineers*, vol. 28, no. 2, pp. 305-317.
- [24] Bolton, M.D. 1986. "The strength and dilatancy of sand", *Géotechnique*, vol. 36, No. 1, pp. 65-78.
- [25] Chakraborty, T., & Salgado, R. 2010. "Dilatancy and shear strength of sand at low confining pressures", *Journal of Geotechnical and Geoenvironmental Engineering*, Vol. 136, No. 3, pp. 527-532.
- [26] API. 1987. "Recommended practice for planning, designing and constructing fixed offshore platforms", *API Recommended practice 2A (RP 2A)*, 17th ed., American Petroleum Institute.
- [27] Janbu, N. 1963. "Soil compressibility as determined by oedometer and triaxial test", *Proceedings of 3rd European Conference on Soil Mechanics and Foundation Engineering*, Wiesbaden, Germany, vol. 1, pp. 19-25.
- [28] Roy, K.S., Hawlader, B.C., Kenny, S. & Moore, I. 2014, "Finite Element Modeling of Uplift Pipeline/Soil Interaction in Dense Sand", *Geohazards6*, Kingston, Ontario, Canada, June 15-18.